A MATHEMATICAL MODEL OF THE STRETCH REFLEX IN HUMAN MUSCLE SYSTEMS

by

JAMES CHARLES HOUK, JR.

B.S., Michigan College of Mining and Technology
(1961)

SUBMITTED IN PARTIAL FULFILLMENT OF THE
REQUIREMENTS FOR THE DEGREE OF
MASTER OF SCIENCE

at the

MASSACHUSETTS INSTITUTE OF TECHNOLOGY
May, 1963

Signature of Author _____
Department of Electrical Engineering, May 17, 1963

Certified by _____
Thesis Supervisor

Accepted by _____
Chairman, Departmental Committee on Graduate Students

A MATHEMATICAL MODEL OF THE STRETCH REFLEX IN HUMAN MUSCLE SYSTEMS

by

JAMES CHARLES HOUK, JR.

Submitted to the Department of Electrical Engineering on May 17, 1963 in partial fulfillment of the requirements for the degree of Master of Science.

ABSTRACT

The stretch reflex, a biological feedback control system, is studied in the wrist-rotation muscular system of man by first examining the performance of its isolated components. Mathematical models of these components are then assembled according to their known topology to form an integrated model of the system. This model has the advantage of being generally applicable to any studies which might be conducted on the system.

Experimental studies on human subjects, along with theoretical considerations, justify the simplification to a linear model with situation-varying parameters. Transient responses of the model are studied on an analog computer and correlation is achieved with responses of human subjects. The comparisons indicate that adaptive behavior under the control of the central nervous system is present. The model is then used to clarify certain related studies.

Thesis Supervisor: Dr. Lawrence Stark

Title: Research Associate, Biology Department

ACKNOWLEDGEMENT

I wish to thank Dr. L. Stark, Dr. Y. Okabe, Dr. J. Elkind, and P.A. Willis for introducing me to man's motor coordination system and for the direction, advice, and encouragement which they made available to me throughout the course of this research. Special acknowledgement is given Dr. Stark who served as Thesis Advisor without whose many suggestions and constant encouragement this study could never have been completed. I also thank Professor L.Gould for discussing some of the control problems with me and for making available to me the REAC analog computer in the Electronic Systems Laboratory which was used to simulate the model. Acknowledgement is due to the Computations Center at M.I.T. Initially the model was simulated on their IBM 709 and IBM 7090 digital computers. Thanks are also given to Mr. B. Zuber for his assistance in conducting the experiments.

The personnel in the Publications Office and Drafting Room of the Electronic Systems Laboratory are acknowledged for their assistance in preparing this thesis.

This work was partially supported by the Office of Naval Research under Contract ONR-1841(70) and by the United States Public Health Service under Grant NB 3055-3.

Appreciation is extended to International Business Machines Company for their generous fellowship aid which supported the author during his studies this past year.

TABLE OF CONTENTS

TABLE OF CONTENTS (continued)

TABLE OF CONTENTS (Continued)

LIST OF FIGURES

LIST OF FIGURES (Continued)

CHAPTER I

MUSCULAR CONTROL SYSTEMS - AN INTRODUCTION

This thesis examines the functional properties of the more peripheral components of muscular control systems. These properties are exhibited as a mathematical model of the stretch reflex. Finally, the insights which this model lends to the problems of voluntary control and servo-analysis of the stretch reflex are exploited. A brief review of past work on human muscular control systems is now given.

A. ANALYZING MUSCULAR CONTROL - A REVIEW

The motor coordination system of man is a highly complex feedback control system which, with appropriate simplifications, may be analyzed by feedback control techniques. Motor activities have been analyzed by many investigators [1, 2, 3, 4*] to determine the transfer characteristics of man performing some specific task. These investigations have generally treated man as a black box for which a transfer function is to be found. This transfer function allows prediction of the response of the human to an input included in the family of inputs for which this transfer function was obtained. Beside being quite limited in application, this representation reveals little about the physiological contents of the system.

With the purpose of obtaining a better understanding of motor coordination other researchers have begun to investigate the contents of this black box. Merton[5] defined the organization of the pathways that might be involved in the servo-control of movement. Adolph[6] has looked at what physiologists know about the peripheral components of motor activity

---

* Superscripts refer to numbered items in the Bibliography.

and some of the simpler spinal reflexes through which feedback control is accomplished. He has formulated a theoretical model involving these feedback loops and has demonstrated stability of this part of the system. Partridge and Glaser[7] conducted a frequency analysis of the stretch reflex of a single muscle in decerebrate cats; no Bode plots of their results were published however. Instead they made a few verbal comparisons between conventional servomechanisms and the cat's stretch reflex. Hammond[8] advanced this servo approach by laying out a block diagram of a one-muscle system and calculating its frequency response. Johnson[9] was the first to consider the more general problem of two muscles pulling against each other, thus controlling coordinated movements. He found justification for considering one muscle which pushes and pulls, rather than two muscles pulling against each other, when he briefly developed a theoretical model of the stretch reflex. Most of his work was devoted to an experimental determination of the transfer characteristics of the stretch reflex path. He concluded that the stretch reflex acts predominantly as a spring to load disturbances.

Stark[10] saw the need for a general model of motor coordination to tie together previous work and to direct future investigations in this area. Working with Atwood and King (unpublished) he defined the basic characteristics of the components involved in the stretch reflex, organized them into a model which included conscious as well as reflex paths, and began digital simulation studies at the Computation Center of M.I.T. The work of this thesis proceeds from this point.

B. INTRODUCTION TO THIS STUDY

The heart of a muscular control system is striated muscle, a unidirectional, force generating mechanism. Small groups of muscles, innervated by alpha motor neurons in the spinal cord, work together and against each other to provide fine control of position, velocity, and force in a limb of man. Several sensory mechanisms report back to the central nervous system the progress that is being made in carrying out the desired motor activity. The transmission paths of these sensors vary in complexity from the simple spinal stretch reflex, which is instrumental to maintenance of posture, to extremely involved, decision-making pathways characteristic of visual feedback (see Fig. 1.1).

The physiological components of a muscular control system may be classified under four major categories.

1. Muscle - a unidirectional force generating device.
2. Sensory Organs - transducers which monitor system performance.
3. Neural Ganglion - processors composed of hundreds of neurons which transform sensory signals into purposive commands to muscle.
4. Nerve Fibers - the active transmission lines of the nervous system.

The above classification is at a level which has physical significance in that the resulting components are autonomous, physiological, noninteracting entities which are entirely analogous to physical components of an engineering control system. Moreover, characterization of these components at this level may be readily accomplished by employing techniques of physiological research which are in current practice. In most cases

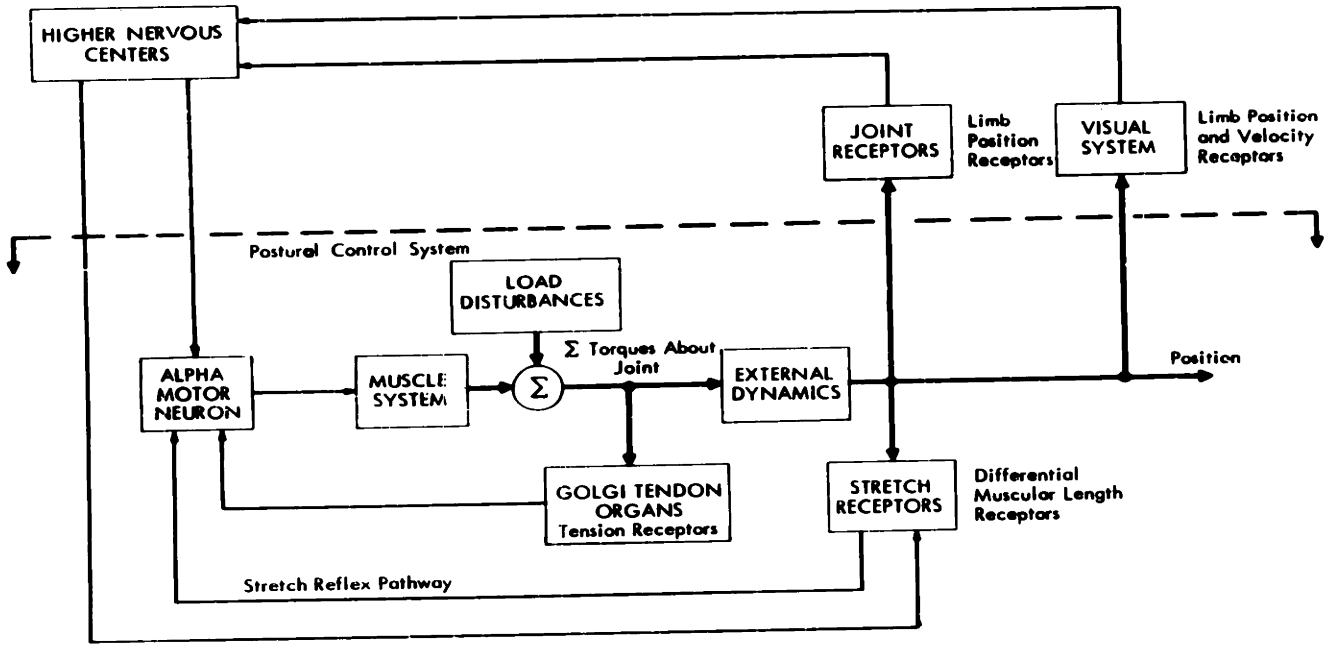

Fig. 1-1 THE ORGANIZATION OF MUSCULAR CONTROL. Heavy lines indicate mechanical connections; light lines indicate nural connections. The postural control system (PCS), which is the topic of investigation in this thesis, has been sectioned off with a heavy dotted line.

enough information is available from the literature to construct a general model of a component; the values of certain parameters of this general model which pertain to a particular system may then be determined by selected experiments on this system.

A model of the system may then be constructed by interconnecting the models of its components. This representation is more revealing than the black-box type representation because each variable which appears is an output from a real physiological component and serves as an input to another. Therefore we may observe performance of models of components during execution of a simulated control task just as we might observe performance of the actual physiological components during a subject's execution of a control task. The latter is usually rather difficult and often impossible.

The limitations in overall performance imposed by individual components may be located and studied. Compensation for weaknesses of some components provided by other components may be discovered. Experiments crucial to understanding the system are often suggested from simulations with the system model. Certainly we are attempting to understand the system at a level which renders our simulations living and our conclusions real.

C. THE POSTUAL CONTROL SYSTEM AND ITS MODEL

The subsystem inclosed in dotted lines of Fig. 1.1 was chosen for study because:

1. Present physiological knowledge was adequate for the construction of simple, general models of its components.
2. It's operation in response to short transient disturbances was thought to be independent of the

complex and less understood higher centers, thus rendering the problem and interpretation of the results reasonably simple.

This part of the muscular control system will be referred to as the postural control system, abbreviated PCS.

The block diagram of the model of the PCS is shown in Fig. 1.2. Here the muscles causing motion in one direction have been called the agonists, those opposing this motion are called antagonists. The nonlinearities associated with this pull-pull arrangement of unilateral muscles are included in this model. Note also that the tendon receptors have been deleted. This is a simplification which will be discussed and justified in Chapter II.

Implicit in this model are the following assumptions:

1. A muscular system may be adequately represented by two equivalent muscles working against each other (see Chapter II).
2. Everywhere in the model an average over all microscopic units (e.g., nerve fibers, muscle fibers, neurons) acting towards the same macroscopic effect will be used as the continuous signal from one component to another. For example, the nerve signal of the model will represent the ensemble-average instantaneous frequency over all the nerve fibers subserving a common function.
3. Physiological data from vertebrates other than man will also be used to develop the model. This is justified since the PCS includes only simple spinal reflex pathways for which, it has been found, a certain amount of consistency prevails throughout the vertebrates.

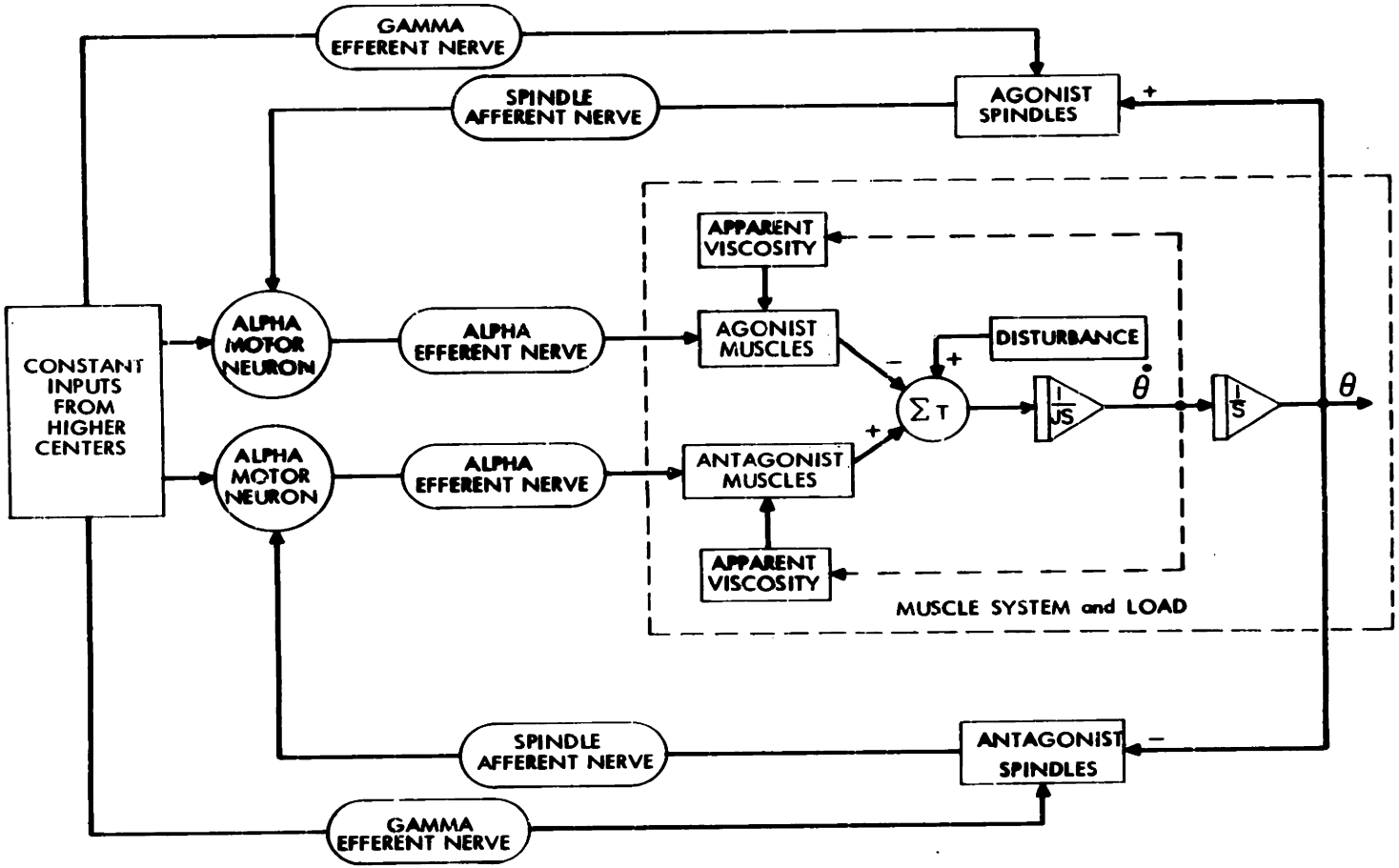

Fig. 1-2 A BLOCK DIAGRAM OF THE MODEL OF THE POSTURAL CONTROL SYSTEM. The stretch reflex pathways provide negative feedback around both sets of muscles. Torques are summed about the joint, integrated and divided by inertia to compute velocity, and integrated again to compute position.

Much of the work of this thesis will be generally applicable to any physiological muscular control system. However, when comparisons are to be made with experimental results on human subjects, the parameters of the model which relate it to a particular muscular system will be those of wrist and forearm rotation. This system was choosen because an apparatus was available on which to conduct experiments with human subjects (termed "experiments" in this thesis; studies on the model will be referred to as "simulations"). Units of rotational motion (e.g., torque, angular velocity) are most convenient for describing this system.

In Chapters II, III, and IV models of each of the physiological components (blocks of Fig. 1.2) will be developed from physiological literature and experiments by this author. These models will then be interconnected in Chapter V according to Fig. 1.2, thus forming the PCS model. Chapter VI describes electromyographic and transient disturbance experiments on the PCS. In Chapter VII justification is given for reducing the nonlinear model of Chapter V to a simplified linear model with parameters which vary with the experimental situation. Correspondence is achieved with the experiments obtained in Chapter VI. A summary, conclusions, and implications of the model are presented in Chapter VIII.

The author suggests that the serious reader supplement this thesis with Hammond, Merton, and Sutton's excellent review of the physiology of motor coordination[18] and, if a knowledge of feedback control theory is lacking, Chestnut and Mayer's book on this subject.[38]

CHAPTER II

A MODEL OF MUSCLE

The characteristics of striated muscle have been investigated quite thoroughly by A.V. Hill,[11, 12] Douglas Wilkie,[13] and many other physiologists.[14, 15, 16, 17] They have found that general characteristics prevail in all vertebrate striated muscle, only the values of certain parameters vary among muscles belonging to this class. In this chapter these general characteristics will be reviewed during the development of a generalized model of muscle. Experiments will be presented which allow approximation of the necessary parameters pertaining to the muscles which effect wrist rotation. The dynamic equations necessary for using this model as a component in the PCS model will also be developed.

A. CHARACTERIZATION OF MUSCLE - A GENERALIZED MODEL

1. Apparent Viscosity

Consider the following experiment which has been performed on many samples of striated muscle. The muscle is supported by one tendon; on the other tendon is fastened a weight causing a downward force, F_L. Upward velocity of the weight is recorded as a function of time as the muscle is maximally stimulated. In a few tenths of a second the velocity, v(t), reaches a steady value, V (Fig. 2.1). If the load is changed, and the experiment is repeated; v(t) reaches a different steady state. At this steady-state value of v(t) the force produced by

CHAPTER II

A MODEL OF MUSCLE

The characteristics of striated muscle have been investigated quite thoroughly by A.V. Hill,[11, 12] Douglas Wilkie,[13] and many other physiologists.[14, 15, 16, 17] They have found that general characteristics prevail in all vertebrate striated muscle, only the values of certain parameters vary among muscles belonging to this class. In this chapter these general characteristics will be reviewed during the development of a generalized model of muscle. Experiments will be presented which allow approximation of the necessary parameters pertaining to the muscles which effect wrist rotation. The dynamic equations necessary for using this model as a component in the PCS model will also be developed.

A. CHARACTERIZATION OF MUSCLE - A GENERALIZED MODEL

1. Apparent Viscosity

Consider the following experiment which has been performed on many samples of striated muscle. The muscle is supported by one tendon; on the other tendon is fastened a weight causing a downward force, F_L. Upward velocity of the weight is recorded as a function of time as the muscle is maximally stimulated. In a few tenths of a second the velocity, v(t), reaches a steady value, V (Fig. 2.1). If the load is changed, and the experiment is repeated; v(t) reaches a different steady state. At this steady-state value of v(t) the force produced by

the muscle must be identical to the load force since acceleration has diminished to zero, thus eliminating the force due to inertia. Therefore the maximum force the muscle is capable of producing while moving at a velocity V is merely F_L (i.e., $F_L = F_m$). A plot of $F_m = F_L$ as a function of $v = V$ (Fig. 2.2) may now be applied to find the muscular force produced by the maximally stimulated muscle at any velocity, V.

These results immediately suggest that muscle be modeled as a force generator producing a force, $F_{isometric}$, in parallel with a viscous element, B, whose value depends on the velocity of the load (Fig. 2.3). The equation of motion for this model is

$$F_m = F_{iso.} - B\left[v(t)\right] v(t) = F_L + M \frac{dv(t)}{dt} \qquad (2.1)$$

where the value of B for a given v may be calculated from the force-velocity curve (FIg. 2.2).

Hill[11, 12] has fit the force velocity curve with the equation

$$(F_m + a)\ (v + b) = \text{Const.}$$

and has related the constants to measured thermodynamic properties of the muscle. The linear approximation shown by the dotted line in Fig. 2.2 was judged sufficiently accurate for these purposes, and has therefore been adopted to simplify simulation (note that B becomes a constant, independent of velocity).

2. Less Than Maximal Stimulation

Hundreds of muscle fibers act in parallel to produce the maximum force of a single muscle. In the intact animal gradations of muscular tone are accomplished by varying the number of active fibers in a muscle.[18]

Fig. 2-1 VELOCITY OF A LOAD ACCELERATED BY MAXIMALLY STIMULATED MUSCLE PLOTTED AS A FUNCTION OF TIME FOR THREE DIFFERENT LOADS. In each case the velocity reaches a steady value which depends on the load.

Fig. 2-2 A TYPICAL FORCE-VELOCITY CURVE FOR STRIATED MUSCLE. This curve gives the force produced by the maximally stimulated muscle for each load velocity. The straight dotted line gives the approximation to this curve resulting when B is assumed constant.

Fig. 2-3 PRELIMINARY MODEL OF MUSCLE ACTING ON A WEIGHT.

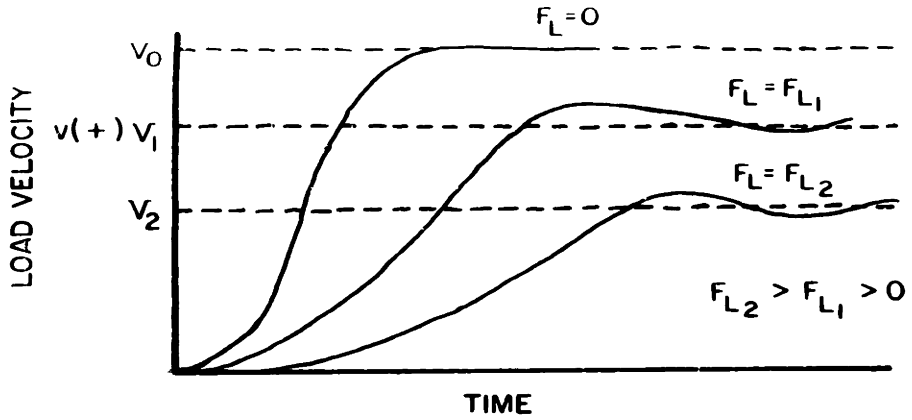

Fig. 2-1

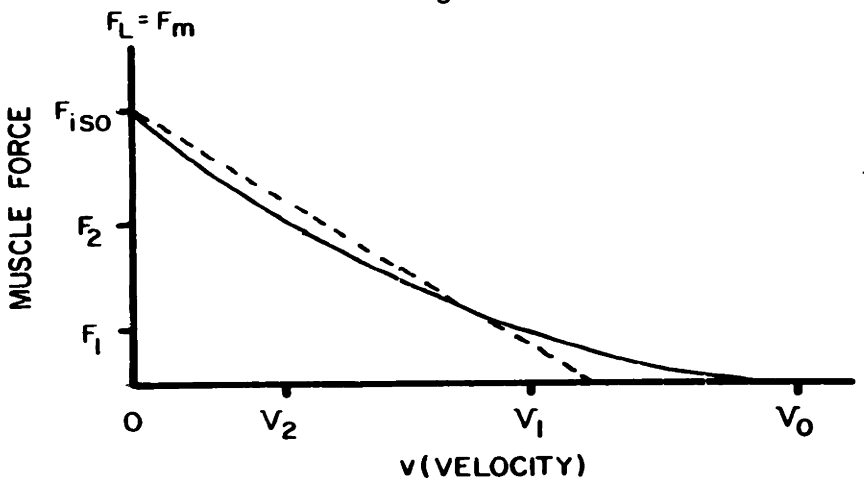

Fig. 2-2

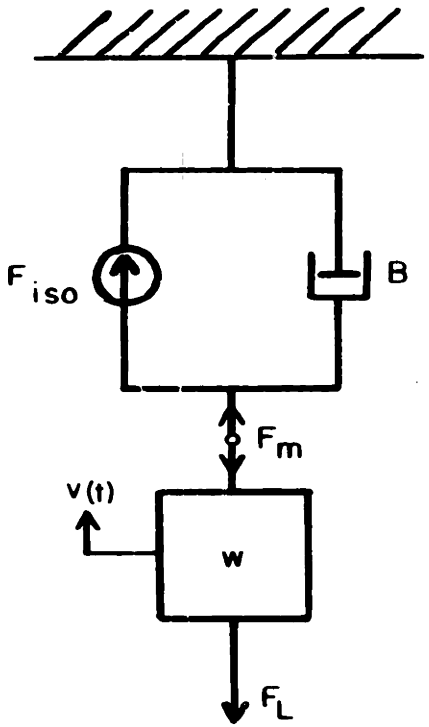

Fig. 2-3

The hypothesis that the isometric force produced by a muscle is directly proportional to the number of active fibers is suggested by the above statements and supported in a paper by Lippold.[16]

Moreover, Bigland and Lippold[17] have obtained force-velocity relationships for several different levels of muscular excitation. These results show a family of curves all of which pass through the same point for no load conditions (V_o of Fig. 2.2); the slopes of the curves at a given velocity decrease with decreased excitation; and, as mentioned previously, the isometric force is directly proportional to the excitation. A signal, $a(t)$, which is allowed to vary between zero and unity, is defined to be the normalized neural signal initiating muscular contraction. (This representation will be used for neural signals throughout.) A mathematical expression for muscular force as a function of neural signal and load velocity which demonstrates all of the characteristics outlined above may be written

$$F_m = a(t) \quad [F_{iso} - B\,v(t)] \quad . \tag{2.2}$$

3. Lengthening Muscle

Thus far, only shortening muscle has been considered. If $F_L > F_{iso}$, the muscle will be forced to lengthen. Katz[15] seems to be the only person who has studied lengthening muscle. In the isolated sartorius muscle of a frog he discovered that the muscular force increased very rapidly as the velocity of lengthening increased. At a very small velocity of lengthening the force becomes great enough to permanently damage the muscle. This certainly is not the physiological condition present in the intact animal; here the Golgi tendon organ, although it has a fairly

high threshold, would sense this dangerous tension and instruct the muscle to exert less force. This function of tendon organs is quite apparent and is the only function attributed to them in this thesis. (The possibility that their signals are employed in control tasks is unlikely but has not been disproven.)

4. Series Elasticity

Closer inspection of experimental curves of $F_m(t)$, $v(t)$, etc. reveal that both series and parallel elastic elements must be included in a model of muscle to explain the more subtle irregularities of these time curves.[11, 13] The parallel element is rather small and would have a negligible effect on system performance. The series element, however, is not stiff enough to neglect and will be approximated later in this chapter.

5. Constancy of Isometric Force

Wilkie[13] has shown that the isometric force produced by the muscle system causing flexion of the arm remains nearly constant over the operating range of the arm. If this were not the case, it would be necessary to insure that all points on a force-velocity curve corresponded to the same muscular length, and the curve would not be valid for other muscle lengths.

B. EQUIVALENT TORQUE PRODUCING MUSCLES AND AN EXPERIMENTAL DETERMINATION OF THEIR PARAMETERS

The model of muscle for which all parameters must now be determined is shown in Fig. 2.4. All the muscles tending to produce pronation will be treated collectively as a single torque producing muscle causing pronation. The same will be done with the supinator muscles. The justification for postulating equivalent muscles is the consistency of the

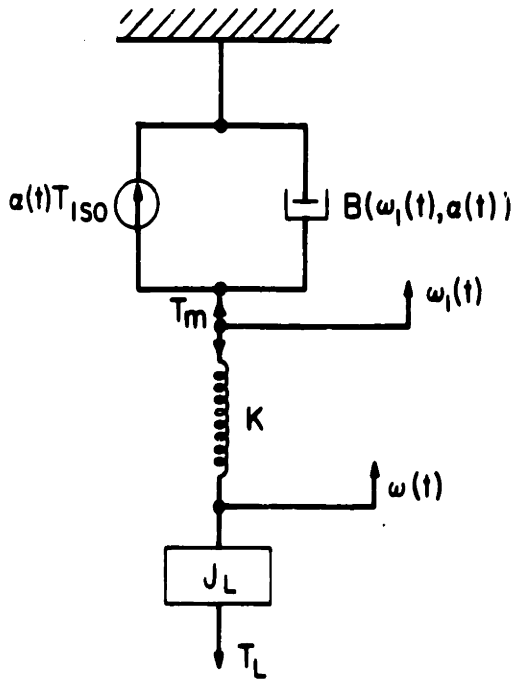

Fig. 2-4 MODEL OF AN EQUIVALENT TORQUE PRODUCING MUSCLE. T's are torques; ω's are angular velocities; and J_L is load inertia.

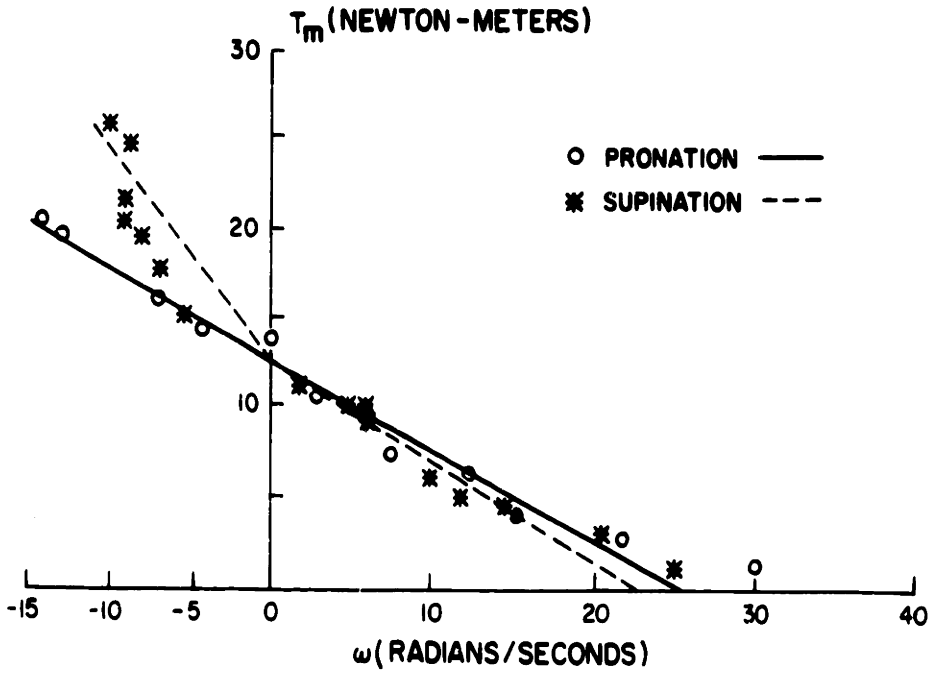

Fig. 2-5 TORQUE-ANGULAR VELOCITY CURVE FOR THE EQUIVALENT SUPINATOR AND PRONATOR MUSCLES. The straight line approximations for the quasi-linear models are superimposed.

forthcoming experimental results as interpreted in terms of this model. Although the parameters and variables are now in angular units (i.e., torque, angular velocity, torsional spring constant, etc.), a rectilinear display will be used for clarity of illustration. The equations which will evolve are exactly analogous.

1. Apparent Viscosity

A handle was welded to a shaft supported by two pillow block bearings. Weights were hung from a 10" diameter pulley which was attached to the shaft between the pillow blocks. The weights effected a constant torque, T_L, plus an inertia on the axis of the shaft. The subject was instructed to grasp the handle and exert almost maximum effort against T_L. (The command, "exert maximum effort," caused rapid fatiguing and led to inconsistent results.)

Records of angular velocity is a function of time (Fig. 2.6) were obtained by differentiating the voltage across a linear potentiometer which recorded the angular position of the shaft. The maximum velocity attained in a single experiment provided one point for the torque-velocity curve (Fig. 2.5).

As T_L was increased beyond T_{iso} (forcing the muscle to lengthen), results similar to those for shortening muscle were obtained, as shown in Fig. 2.6(b). However, when T_L was increased to a value greater than about twice T_{iso} no leveling off of the velocity curve occurred (Fig. 2.6(c)). Careful observation of (Fig. 2.6(c)) reveals that the "viscous" force, that force proportional to velocity, is increasing as the velocity increases, thus causing the acceleration to decrease a little. Estimating the acceleration at the end of the record, and solving the equation of motion,

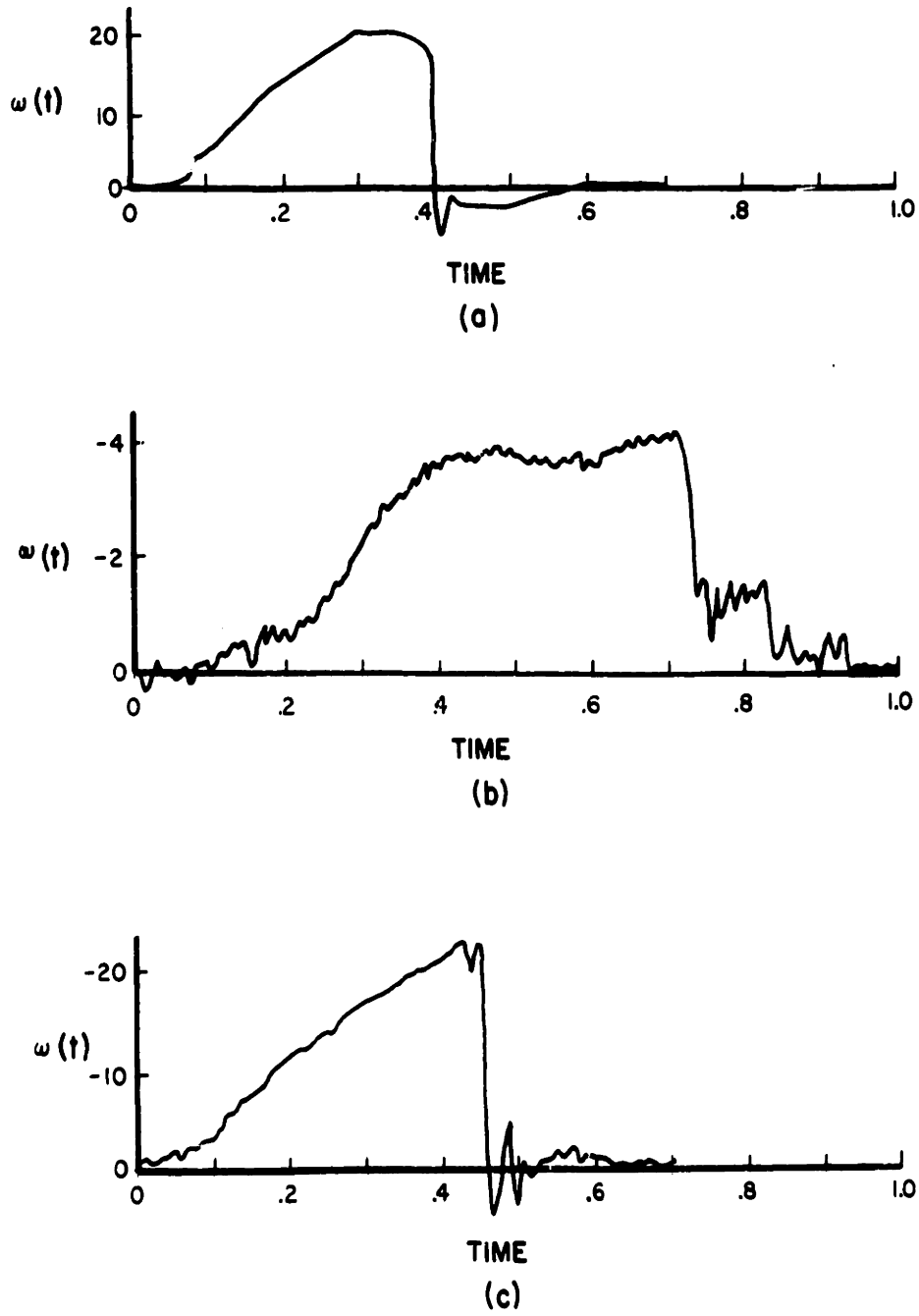

Fig. 2-6 SAMPLE RECORDS OF $\omega(t)$ USED IN DETERMINING THE APPARENT VISCOSITY. ω is in radians/sec.; time in seconds. a) Shortening muscle, T_L = 2.6 N-m. b) Lengthening muscle, T_L = 15 N-m. c) Saturation, T_L = 23 N-m. Subject effort is approximately 3/4 maximum effort. All records are for the pronator muscle.

$$T_L - T_m = J \frac{d\omega}{dt}$$

for T_m yields approximately ten Newton-meters as the force the muscle is producing.

Probably the Golgi tendon organ has detected dangerously high tensions in the muscles and instructed the muscles to relax, as the theory that its function is that of a safety valve would predict. A more positive statement concerning this phenomena could be made from a longer record which, however, is not obtainable since we have conducted the above experiment over the full range of wrist rotation. We are certain, though, that the muscular force does not exceed $2 F_{iso}$. This requirement will be employed in the model.

The linear approximations in the two regions (shortening and lengthening) have been drawn over the experimental points of the T-(torque-velocity) curves in Fig. 2.5. This is the T-ω curve for almost maximal excitation. Inspection of Eq. 2.2 reveals that, according to our model, multiplication of this single T-ω curve by a neural activity factor, a, will yield the T-ω curve for all values of excitation. The value of T_{iso} for maximal effort was used to obtain the T-ω plots of Fig. 2.7 from those for almost maximum effort (Fig. 2.5). The maximum torque for lengthening muscle is represented by the saturation for large negative velocities. Since a muscle is incapable of pushing against a load causing it to shorten, a saturation at $T_m = 0$ is also necessary in the model. The T-ω curve for half effort ($a = \frac{1}{2}$) was calculated and is also shown in Fig. 2.7.

Inertia and series elasticity have not entered into these experiments since all measurements have been taken in the steady-state where inertia

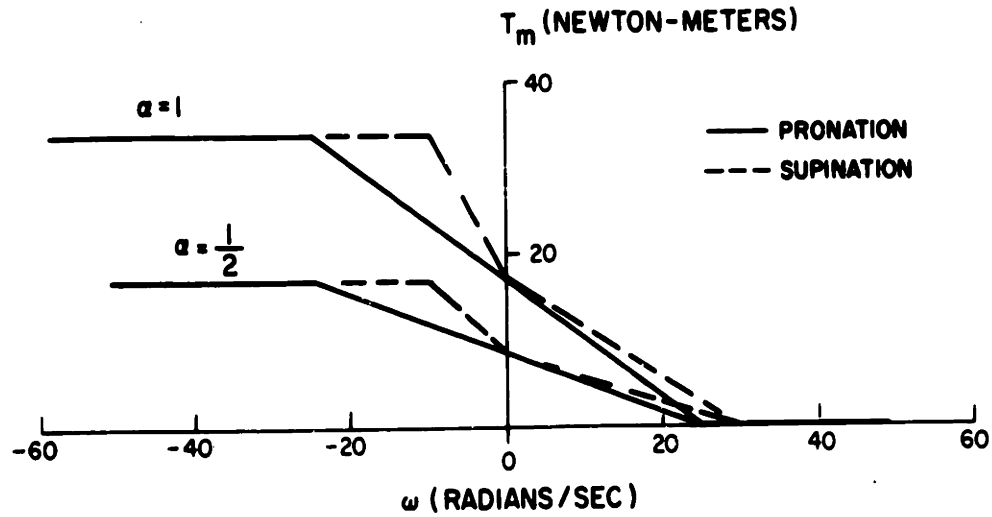

Fig. 2-7 QUASI-LINEAR MODEL OF THE APPARENT VISCOSITY FOR THE EQUIVALENT SUPINATOR AND PRONATOR MUSCLES under conditions of maximum effort, $a = 1$, and half-maximum effort, $a = 1/2$.

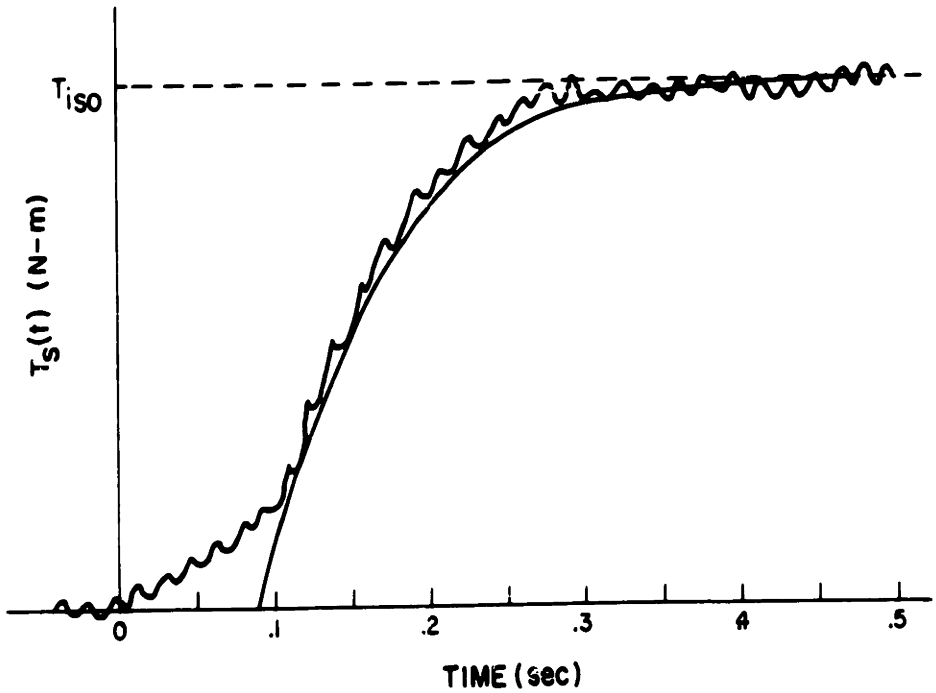

Fig. 2-8 EXPERIMENTAL RISE OF ISOMETRIC TORQUE IN THE EQUIVALENT SUPINATOR MUSCLE. The record shows 60 cps noise which was present in an amplifier. Superimposed on this is an exponentially rising curve with a 70 m sec time constant. This represents the approximate fit employed in determining the series elasticity, K; and it is also the simulated response of the model.

is no longer being accelerated, and the spring has reached a steady length. To complete the model we must now measure the values of these energy storage elements.

2. Series Elasticity

Measurement of the rise of isometric torque was selected as a method of estimating the series elastic component of the equivalent muscle which effects wrist rotation. (Wilkie used the same method on an arm flexion system.)[13] A pair of Alnico foil strain gauges were laid down at right angles to each other and 45° off the axis of the half inch steel shaft of the apparatus used to measure the viscous element in muscle. The shaft was clamped behind the strain gauges fixing the handle in a vertical position. Torsion which was introduced by the subject trying with maximal effort to rotate the handle was indicated by the unbalanced voltage across a Wheatstone bridge, the strain gauges comprising two opposite arms of the bridge. This voltage was amplified with a Philbrick operational amplifier and recorded on a portable Sanborn heat recorder. A record is shown in Fig. 2.8.

Consider the equations describing the rise of isometric torque in the model of Fig. 2.4. Since the mechanical node represented by the inertia of the arm and load has been clamped, $\omega(t) = 0$ throughout the experiment. A torque, $T_m(t)$ causing the spring to stretch is given by

$$T_m(t) = K \int_0^t \omega_1(t)\, dt$$

where K_1, the torsional spring constant, has been assumed constant. Using

the value of the viscous element inherent in shortening muscle which was determined in the previous section, $T_m(t)$ may be expressed as

$$T_m(t) = T_{iso} U_{-1}(t) - B \omega_1(t)$$

$T_m(t)$ is also identically equal to $T_S(t)$, the torque applied to the shaft and the variable which is being measured. If $T_S(t)$ is substituted for $T_m(t)$ in both equations, the first equation differentiated, the second solved for $\omega(t)$ and substituted back into the first, which is then solved for T_{iso}, the following expression is obtained

$$T_{iso} U_{-1}(t) = T_S(t) + \frac{B}{K} \frac{d}{dt} T_S(t)$$

which may be solved for $T_S(t)$,

$$T_S(t) = T_{iso} \left(1 - e^{-\frac{K}{B} t} \right) U_{-1}(t)$$

Indeed, a rising exponential with a 70 msec. time constant fits the main part of the experimental $T_S(t)$ curve (Fig. 2.8). The slowly rising initial part of the curve has been attributed to initial compression of tissue of the hand which is grasping the handle. Since B is known to be 0.7 N-m-sec -rad^{-1}, constraining the time constant to 70 msec. allows the calculation of K = 10 N-m-rad^{-1}. The same value was found for both supination and pronation.

3. Load Inertia

The inertia of the forearm has been found to be negligible in comparison to the inertia of the loaded machine on which some experiments in this thesis have been performed.[36] The inertia of the machine was determined by observing the frequency of slightly damped oscillations of

the machine about an angle θ_o when a torsional spring of known spring constant was attached to it. In such a system,

$$J \simeq \frac{K}{\omega^2}$$

and the inertia of the machine was

$$J_l = 10^{-2} \text{ Newton-meter-sec}^2\text{-rad}^{-1}$$

Similarly the inertia of the unloaded machine was calculated to be:

$$J_U = 2 \times 10^{-4} \text{ N-m-sec}^2\text{-rad}^{-1}$$

The moment of inertia of the hand and forearm was approximated by assuming them to be a solid cylinder, 30 cm. long, 6 cm in diameter, and 1 g/cm^3 density (the average density of living tissue).

$$J_h \simeq 4 \times 10^{-4} \text{ N-m-sec}^2\text{-rad}^{-1}$$

4. Variation of T_{iso} with Position

Isometric torque under conditions of maximum effort was measured at different wrist positions (Fig. 2.9). It was found that the maximum force capable of being produced by the supinator muscle decreases for wrist angles greater than $\theta = 0°$, the center position. (Figure 6.1 shows a subject in center position.) Similarly, the maximum force capable of being produced by the pronator muscle decreases for angles less than 10°.

There are three possible reasons for this decrease in capability: 1) there are fewer muscle fibers available for contraction in the regions of decreased capability; 2) those fibers available have shortened to the point where their individual capabilities for producing force are beginning to decrease; and 3) the mechanical advantage of the available

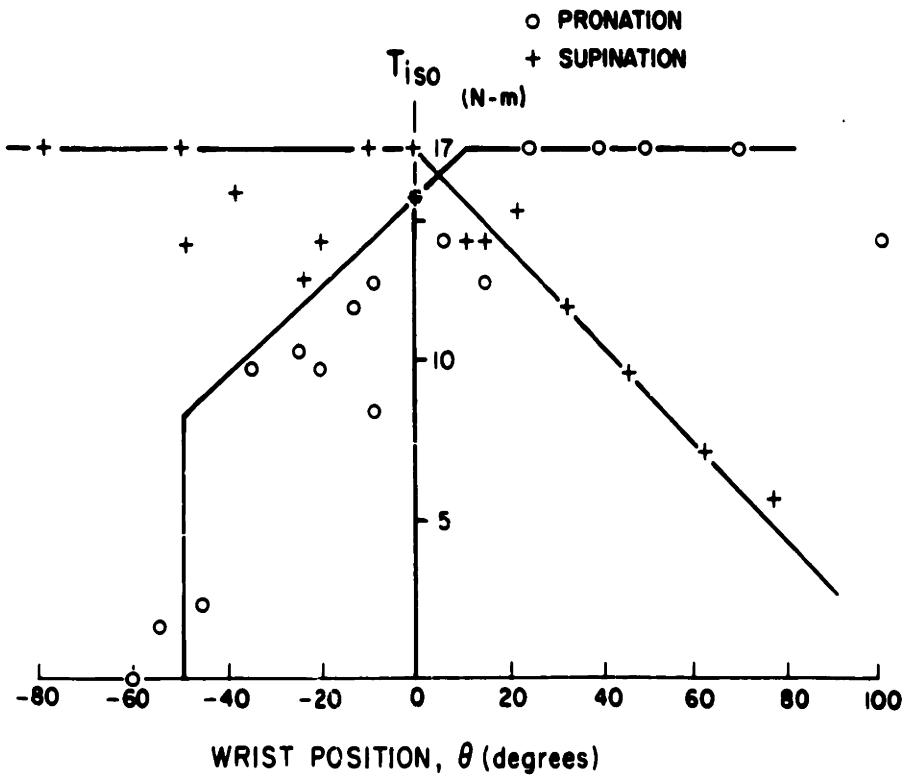

Fig. 2-9 THE VARIATION OF MAXIMUM ISOMETRIC TENSION WITH WRIST POSITION.

fibers has decreased due to rotation of the forearm. Probably all three factors are together responsible for the decrease.

The validity of the experimental determination of the apparent viscosity must now be challenged. If the velocity saturation evidenced in the $\omega(t)$ curves of Fig. 2.6 occurred in the regions of decreased capability, then the saturation was in part caused by this decreasing capability. Some sort of adjustment would be required of the corresponding points on the T-ω curve. Fortunately, for all experiments except those using very small loads (small T_L) velocity saturation occurred before the regions of decreasing capability were reached. Furthermore, the T-ω points corresponding to small T_L's were ignored in the straight-line approximation to the curve. Therefore the model of apparent viscosity has been maintained without adjustment.

C. FORMULATION OF THE SIMULATION MODEL

The PCS model requires a supinator muscle system acting on an inertial load in opposition to a pronator muscle system (Fig. 1.2). A node for delivering mechanical disturbances to the load must also be provided. A model of this muscular system has been constructed in Fig. 2.10 by allowing two of the muscle models (Fig. 2.4) to exert opposite torques on an inertial load. T_L represents a disturbance to the load.

The equations of motion for this model are given below:

$$T_L - T_a + T_b = J_L \frac{d\omega}{dt} \tag{2.3}$$

$$T_a = a_1 T_{iso_1} - B_1^* \omega_1 \tag{2.4}$$

$$T_b = a_2 T_{iso_2} - B_2^* \omega_2 \tag{2.5}$$

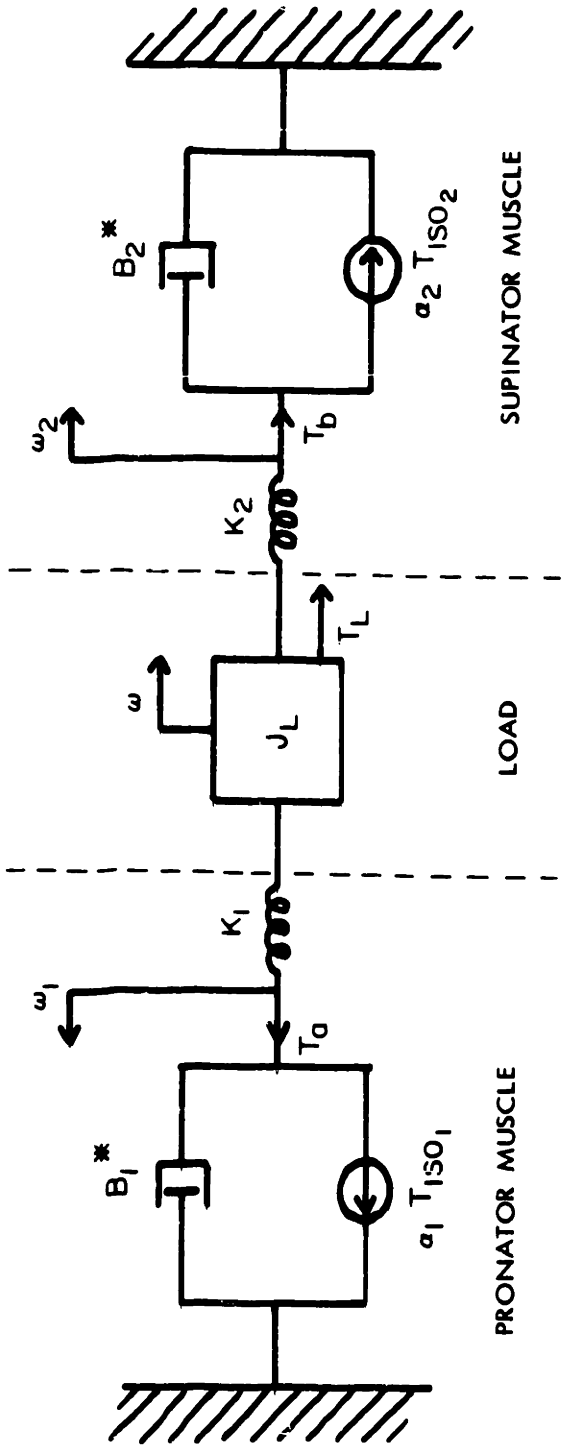

Fig. 2-10 DIAGRAMATIC MODEL OF THE PRONATOR-SUPINATOR MUSCULAR SYSTEM OF WRIST ROTATION. Inputs are the normalized nerve signals to the muscle, a_1 and a_2, and external disturbances, T_L; outputs are angular velocities, ω, ω_1, and ω_2. B_j^* is denoted with an asterisk as a reminder that it is a function of a_1 and ω_1.

$$\frac{1}{K_1}\ \frac{dT_a}{dt} = \omega_1 + \omega \tag{2.6}$$

$$\frac{1}{K_2}\ \frac{dT_b}{dt} = \omega_2 - \omega \tag{2.7}$$

where the variables are those defined in Fig. 2.10. A solution is desired for the angular velocity of the system in terms of its three inputs, neural signals, α_1 and α_2, and disturbances, T_L. A solution by superposition is invalid because of the nonlinear viscosities. Nevertheless, the equations may be represented by a feedback block diagram which may then be simulated to obtain a solution.

As defined in this model, B_1^* and B_2^* do not possess inverses. Therefore Eqs. 2.4 and 2.5 may not be used to compute ω_1 and ω_2 (this solution necessitates using the inverses of B_1^* and B_2^*). Equations 2.6 and 2.7 must be used instead, thus demanding that the operators $\frac{1}{K_1}\ \frac{dT_a}{dt}$ and $\frac{1}{K_2}\ \frac{dT_b}{dt}$ be simulated. Care must therefore be exercised to insure that the simulation of differentiation does not lead to noise problems.

The flow diagram used to solve these equations is shown in Fig. 2.11 S is the Laplace operator. Each of the variables is represented by a node. A single equation is used to solve for a single node in terms of transmissions from other nodes.[19] For example, Eq. 2.4 defines the transmissions from α_1 and ω_1 which serve as inputs to the node T_a. The $T_{iso}(\theta)$ curves determine how T_{iso} varies with position.

The parameters which were determined in the previous sections (using the author as the subject) are tabulated below for the reader's convenience.

$$\frac{1}{K_1}\ \frac{dT_a}{dt} = \omega_1 + \omega \tag{2.6}$$

$$\frac{1}{K_2}\ \frac{dT_b}{dt} = \omega_2 - \omega \tag{2.7}$$

where the variables are those defined in Fig. 2.10. A solution is desired for the angular velocity of the system in terms of its three inputs, neural signals, α_1 and α_2, and disturbances, T_L. A solution by superposition is invalid because of the nonlinear viscosities. Nevertheless, the equations may be represented by a feedback block diagram which may then be simulated to obtain a solution.

As defined in this model, B_1^* and B_2^* do not possess inverses. Therefore Eqs. 2.4 and 2.5 may not be used to compute ω_1 and ω_2 (this solution necessitates using the inverses of B_1^* and B_2^*). Equations 2.6 and 2.7 must be used instead, thus demanding that the operators $\frac{1}{K_1}\ \frac{dT_a}{dt}$ and $\frac{1}{K_2}\ \frac{dT_b}{dt}$ be simulated. Care must therefore be exercised to insure that the simulation of differentiation does not lead to noise problems.

The flow diagram used to solve these equations is shown in Fig. 2.11 S is the Laplace operator. Each of the variables is represented by a node. A single equation is used to solve for a single node in terms of transmissions from other nodes.[19] For example, Eq. 2.4 defines the transmissions from α_1 and ω_1 which serve as inputs to the node T_a. The $T_{iso}(\theta)$ curves determine how T_{iso} varies with position.

The parameters which were determined in the previous sections (using the author as the subject) are tabulated below for the reader's convenience.

J_ℓ (inertia of loaded machine) = 10^{-2} $\frac{\text{N-m-sec}^2}{\text{rad}}$

J_u (inertia of unloaded machine) = 2×10^{-4} $\frac{\text{N-m-sec}^2}{\text{rad.}}$

J_h (inertia of hand and forearm) = 4×10^{-4} $\frac{\text{N-m-sec}^2}{\text{rad.}}$

For the pronator muscle (muslce 1):

B_S (apparent viscosity in shortening) = 0.7 $\frac{\text{N-m-sec}^2}{\text{rad.}}$

B_L (apparent viscosity in lengthening) = 0.7 $\frac{\text{N-m-sec}^2}{\text{rad.}}$

K (series elasticity) = 10 $\frac{\text{N-m}}{\text{rad.}}$

T_{iso} (maximum isotric torque) = 17 N-m

For the supinator muscle (muscle 2):

$B_S = 0.6 \ \frac{\text{N-m-sec}^2}{\text{rad.}}$

$B_L = 1.7 \ \frac{\text{N-m-sec}^2}{\text{rad.}}$

$K = 10 \ \frac{\text{N-m}}{\text{rad.}}$

$T_{iso} = 17$ N-m

D. SUMMARY AND DISCUSSION

This chapter has been concerned with the problem of mathematically characterizing muscle in terms of physically meaningful parameters. From a review of the general characteristics of muscle it was concluded that muscle fiber is a device which, upon stimulation, produces a force which is dependent on its velocity of motion. This dependance on velocity is analogous to that which would be due to mechanical viscosity. Although this analogy is quite satisfactory for the purposes of this thesis, it should be kept in mind that this apparent viscosity is due to biochemical factors which

are not clearly understood and are explained by a number of theories.[20]

Several other factors influence the dynamic performance of muscle. The effects of a series elasticity, which is present in muscle fiber, are great enough to demand the inclusion of this element in the model. Isometric torque varies rather radically with position; this function must be included in the model. Parallel elasticity, which is known to be present,[11] has minor effects on muscle dynamics and may be neglected. Any dynamics which might be associated with the force generator have been neglected (justification is discussed in Chapter VI).

It was desirable to see how the model behaved when it was used to simulate some of the experiments which were used to determine the parameters of the equivalent muscles. The nonlinear model of Fig. 2.11 was programmed for digital simulation using **BIOSIM** (described in Appendix A), a program which permits the operator to address the IBM 7090* with either analog or digital instructions. Figure 2.12 compares an experimental $\omega(t)$ curve, with the simulated curve for the same task. Correspondence was excellent. The simulated $T_{iso}(t)$ curve is superimposed on the experimental curve in Fig. 2.8. It follows identically the exponential fit to the experimental curve used to determine K, as is dictated by the model.

This lumped parameter model of the muscular system provides a vehicle for understanding interactions and nonlinearities present in the PCS. It will be presented as is in Chapter V, but will be simplified to a

---

* Computations Center, Massachusetts Institute of Technology, Cambridge 39, Massachusetts

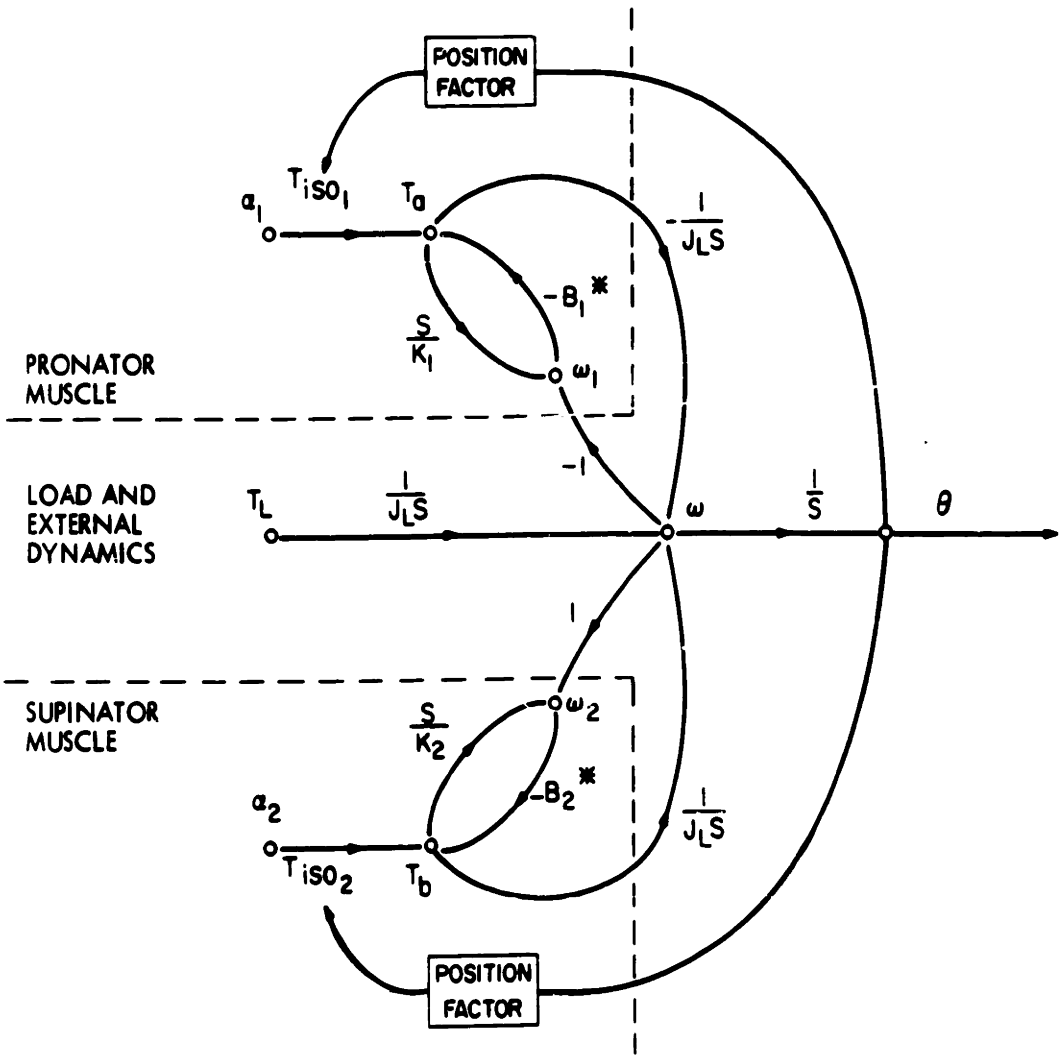

Fig. 2-11 FLOW GRAPH OF THE MODEL OF THE PRONATOR-SUPINATOR MUSCULAR SYSTEM SHOWN IN FIGURE 10.

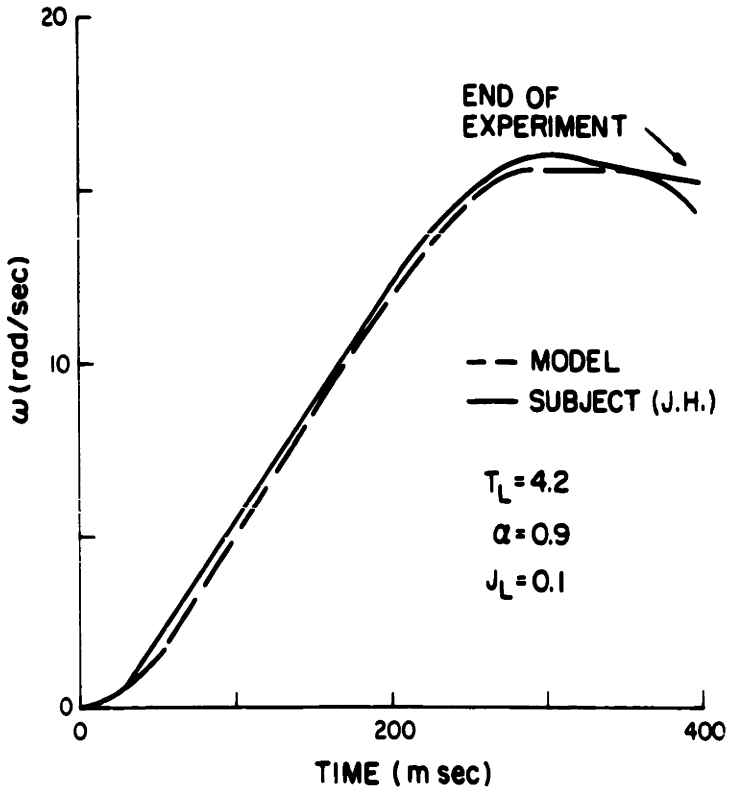

Fig. 2-12 COMPARISON OF EXPERIMENTAL AND SIMULATED $\omega(t)$ CURVES. The experimental curves were used to measure apparent viscosity.

linear approximation with time varying parameters when it is used as a component in a simplified model of the PCS in Chapter VII.

CHAPTER III

MODEL OF MUSCLE SPINDLE RECEPTOR

The muscle spindle receptors supply the central nervous system and in particular the alpha motor neurons with signals related to the position and velocity of the muscle in which they are located. The purpose of this chapter is to develop an adequate model of the spindle receptor organ for use in the integrated model.

A. ANATOMY OF MUSCLE SPINDLE RECEPTORS

A detailed anatomy of muscle spindles has been provided by Barker;[21, 22] a much simplified picture, which nevertheless illustrates the primary functional features of this receptor, will be presented here.

In parallel[30] with the main fibers (extrafusal fibers) of a muscle are a few fibers (intrafusal fibers) whose innervation may be regulated by the central nervous system independently of the former. In Fig. 3.1(a) a bundle of these fibers has been exaggerated and displaced from their normal position among extrafusal fibers to clearly illustrate their in-parallel arrangement and separate innervation. An enlarged section filled with lymphatic fluid, the nuclear bag, receives no efferent innervation, i.e., it is passive.

The afferent innervation of the receptor includes two types of endings, primary or annulo-spiral endings and secondary or flower spray endings (Fig. 3.1(a)). The functional aspects of these two types of endings have been reviewed by Granit.[23] The primary endings are sensitive mainly

CHAPTER III

MODEL OF MUSCLE SPINDLE RECEPTOR

The muscle spindle receptors supply the central nervous system and in particular the alpha motor neurons with signals related to the position and velocity of the muscle in which they are located. The purpose of this chapter is to develop an adequate model of the spindle receptor organ for use in the integrated model.

A. ANATOMY OF MUSCLE SPINDLE RECEPTORS

A detailed anatomy of muscle spindles has been provided by Barker;[21,22] a much simplified picture, which nevertheless illustrates the primary functional features of this receptor, will be presented here.

In parallel[30] with the main fibers (extrafusal fibers) of a muscle are a few fibers (intrafusal fibers) whose innervation may be regulated by the central nervous system independently of the former. In Fig. 3.1(a) a bundle of these fibers has been exaggerated and displaced from their normal position among extrafusal fibers to clearly illustrate their in-parallel arrangement and separate innervation. An enlarged section filled with lymphatic fluid, the nuclear bag, receives no efferent innervation, i.e., it is passive.

The afferent innervation of the receptor includes two types of endings, primary or annulo-spiral endings and secondary or flower spray endings (Fig. 3.1(a)). The functional aspects of these two types of endings have been reviewed by Granit.[23] The primary endings are sensitive mainly

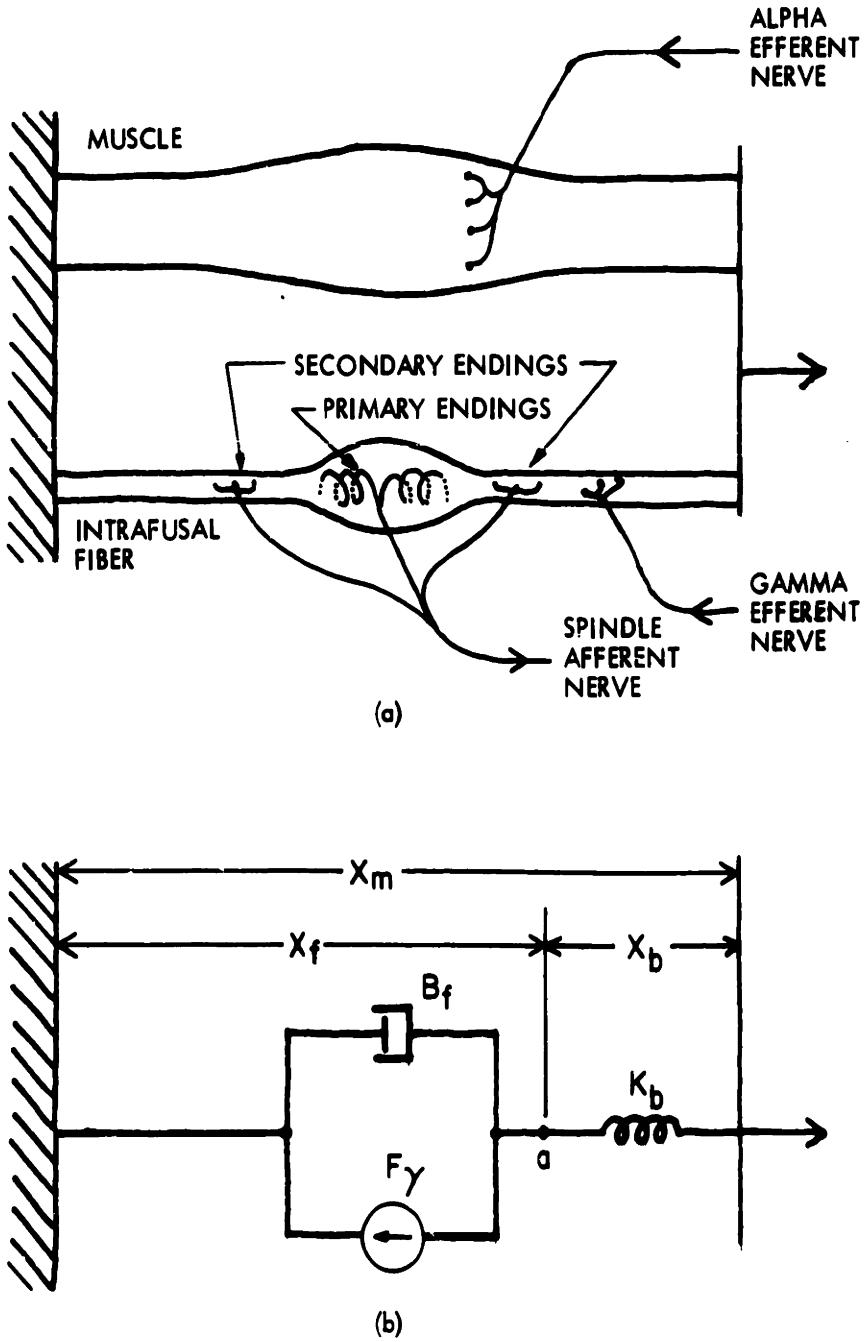

Fig. 3-1 A SCHEMATIC DIAGRAM OF SPINDLE RECEPTOR (a) AND ITS MECHANICAL MODEL (b).

to rate-of-change of muscle length, while the secondary endings are sensitive mainly to muscle length; there is some overlap in this apparent separation of sensitivity. The secondary endings are less abundant than the primaries, and the nerve fibers which relay their messages to the spinal cord are a bit slower.

B. SMALL-SIGNAL CHARACTERIZATION AS A LEAD FILTER

A qualitative examination of the response of a spindle to a step increase of muscle length, X_m, reveals that this transducer behaves like a lead filter. The average instantaneous frequency of sensory nerve pulses, e_A, rises very rapidly at the onset of stretch. It then decays exponentially toward a constant frequency greater than that present before stretch occurred. This steady-state response continues indefinitely. (e.g., 24, 25) (see Fig. 3.2)

The qualitative response verbally described above is quantitatively described by the transfer function

$$\frac{e_A(s)}{X_m(s)} = C\left(\frac{\eta T s+1}{Ts+1}\right) \tag{3.1}$$

where s is the Laplace operator, T is a time constant parameter, and η, a dimensionless parameter, is greater than unity. Letting $X_m(s) = \frac{1}{s}$ (corresponding to $X_m(t) = u_{-1}(t)$, a unit step) we find

$$e_A(s) = \frac{C}{s}\ \frac{\eta T s+1}{Ts+1}$$

which, upon transformation into the time domain, becomes

$$e_A(t) = C\left\{1 + (\eta - 1)\, e^{-\frac{t}{T}}\right\}\ u_{-1}(t) \tag{3.2}$$

An example of the response $e_A(t)$ is shown in Fig. 3.2 superimposed upon an experimental step response from Lippold, Nicholls, and Redfearn.[24] Values of C, η, and T have been choosen to obtain a good fit.

The parameters have a definite interpretation. Inspection of Eqs. 3.1 and 3.2 reveals that C is the d-c or steady-state gain of the transducer; T is the time constant of exponential decay to C; and $\eta \times 100$ is the percent overshoot immediately following the step input. With this information the lead filter model may be easily fitted to experimental step responses of spindles.

C. EXPERIMENTAL SINUSOIDAL ANALYSIS

An experimental sinusoidal analysis of spindle was undertaken in Dr. Jose del Castillo's laboratory at the University of Puerto Rico, School of Tropical Medicine.[26] The purpose was to determine the adequacy of the above model, primarily with regard to the linearity assumption which is made whenever one writes a transfer function (Eq. 3.1).

A toe muscle of the frog, the extensor longitus digitus IV, was used for the study. This preparation contains 3-7 spindle bags with as many as 3 occurring on a single intrafusal fiber. No attempt was made to obtain single-unit responses; rather the average response of all the units associated with this unifunctional muscle were judged to be more useful for justifying a model of this transducer which is suitable for simulating the postural control system.

The preparation was stretched sinusoidally in position about a dc level that was chosen to eliminate saturations at either maximum frequency of

nerve pulses or a minimum frequency of no pulses. The peak-to-peak stretch was 0.4 mm which should correspond to a small signal input to this 17-mm long muscle. The nerve impulses triggered a linear sweep circuit; a trace whose length was proportional to the pulse interval resulted. The record was calibrated in pulses per second so that the results might be evaluated in terms of instantaneous rate of firing. A sample record is shown in Fig. 3.3.

Figure 3.4 shows that the phase vs. frequency plot is only roughly proportional to the slope of the amplitude vs. frequency plot, an exact proportionality being required of a linear system. Figure 3.5 shows a step response of this preparation. As another check on linearity it was desired to compare this step response with that predicted from the sinusoidal analysis. The break frequencies of rough asymptotes drawn on the gain plot of Fig. 3.4 were used to form the transfer function

$$H(s) = \frac{K(30\,s+1)}{(5\,s+1)\,(0.35\,s+1)}$$

K was evaluated from the lowest frequency point of Fig. 3.4 to be K = 27 (pps/mm stretch). The unit step response was calculated

$$S(t) = 27 + 143\,e^{-0.2t} - 170\,e^{-3t}$$

and is superimposed on the record in Fig. 3.5. The rise time is rather slow, but decay is approximately correct.

Since the analysis was conducted with only two preparations and since the range of frequencies was barely sufficient for characterization, we are prevented from drawing any strong conclusions. Nevertheless, these studies indicate that the nonlinearities present in the transducer do not influence the small signal characteristics too radically; the step response

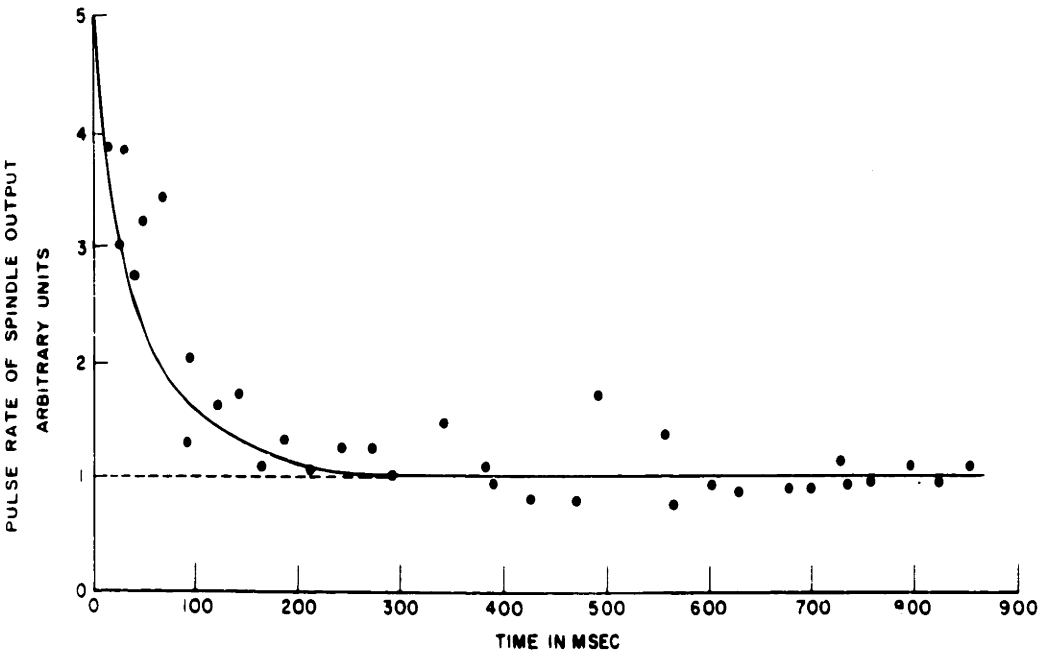

Fig. 3-2 STEP RESPONSE OF A SPINDLE RECEPTOR. Dots show data points taken from Reference 24. Continuous curve shows step response of a lead filter which has been matched to these data.

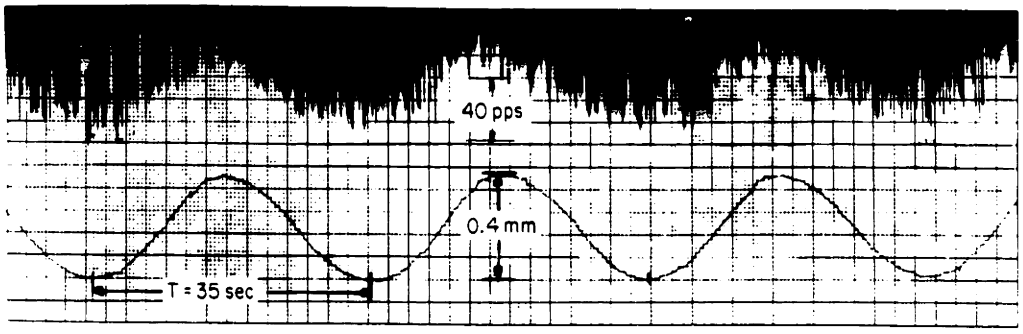

Fig. 3-3 RESPONSE OF SPINDLE RECEPTOR TO SINUSOIDAL INPUT. Length of vertical lines in top record is proportional to the interval between successive nerve pulses from the spindle; the peak-to-peak change in instantaneous frequency is about 40 pps. Bottom trace shows the sinusoidal component of the input, spindle stretch.

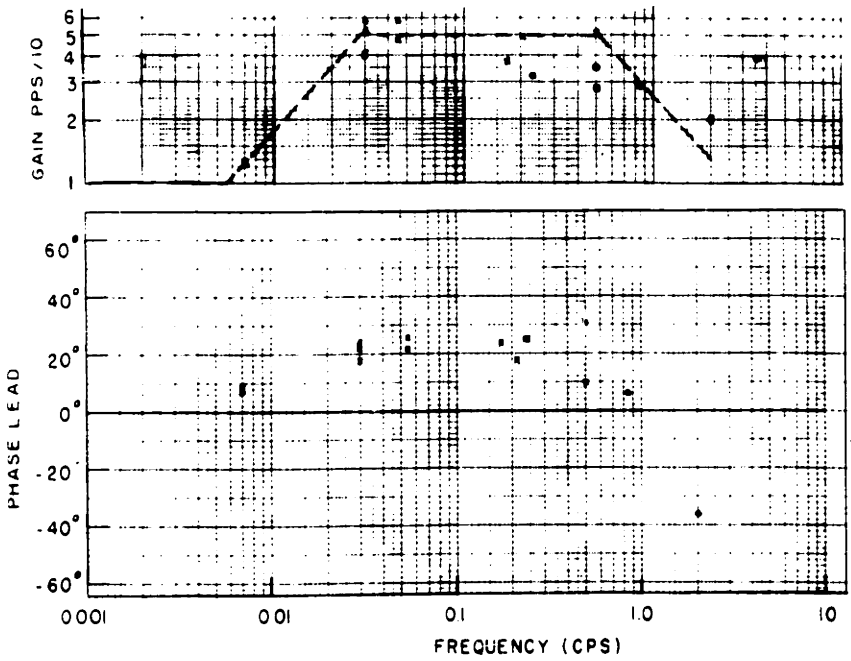

Fig. 3-4 FREQUENCY RESPONSE OF A FROG SPINDLE RECEPTOR. Rough asymptotes have been drawn on the gain curve.

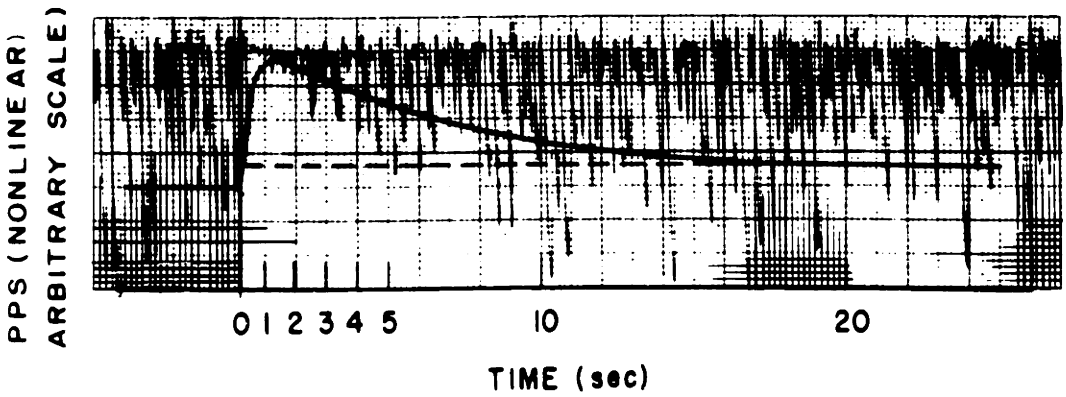

Fig. 3-5 STEP RESPONSE OF A FROG SPINDLE RECEPTOR. The step response predicted from the frequency response data is shown by the solid line.

can be approximately predicted from the sinusoidal responses, thus indicating approximate validity of superposition. A system in which superposition is valid is defined to be linear.

D. ANATOMICAL CONSIDERATIONS

There are three main transformations that occur as the spindle changes muscle length into nerve pulses (Fig. 3.6). Transformation A evolves from the interaction of the mechanical properties of the various tissues of which spindle receptors are composed. Transformation B is due to a biochemical process which produces continuous generator potentials proportional to the distortion of nerve endings caused by A. Transformation C is due to a membrane break-down process found in all nerve cells. Dynamic and nonlinear characteristics in the responses of spindle receptors must be accounted for by a cascade combination of these three transformations.

Katz[41] and Lippold[24] have shown that C is a linear, no-memory transformation which can be characterized by a gain factor.

The dynamic (referred to as "phasic" in physiological literature) chacteristics have been attributed to A by Lippold[24] and by Harvey and Matthews,[27] and to B by Granit.[23] The former hypothesis is more fully described, and therefore easier to model. The hypothesis here is then:

1. Dynamic characteristics are due to A, a linear, memory transformation.
2. Nonlinear characteristics are due to B, a nonlinear, no-memory transformation.

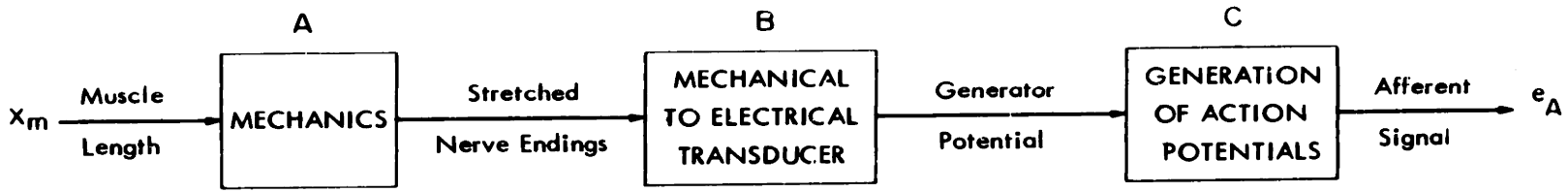

Fig. 3-6 TRANSFORMATIONS INHERENT IN THE SPINDLE PROCESSES WHICH CHANGE MUSCLE LENGTH TO AFFERENT PULSES.

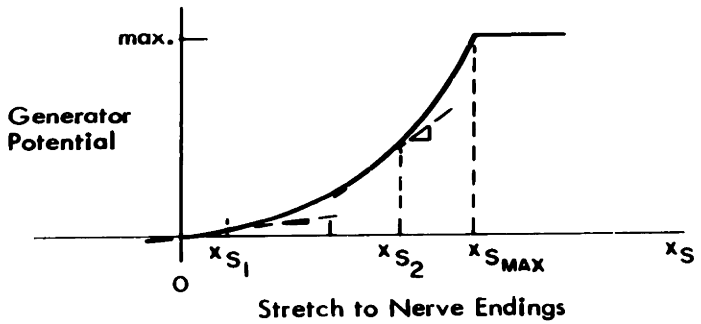

Fig. 3-7 INPUT-OUTPUT CHARACTERISTICS OF TRANSFORMATION B
Note the increased incremental gain with increased d-c levels of X_S.

E. A DYNAMIC MODEL FOR TRANSFORMATION A

A linear model of transformation A which accounts for the observed dynamic characteristics of spindle readily suggests itself from physical considerations. From Chapter II we recall that muscle fiber may be represented by a force generator in parallel with a viscous element, all in series with an elastic element. Moreover, the elastic element is rather stiff and limits only high frequency response. Now, let us hypothesize that the nuclear bag is mainly an elastic element, possessing little viscosity, and that its spring constant is much smaller than the series elasticity of the intrafusal fiber. The intrafusal fiber may then be approximated by a force generator in parallel with a viscous element. The mass of the constituents is small and may be neglected.

This model is shown in Fig. 3.1(b). Comparison should be made with the anatomical drawing (Fig. 3.1(a)). The two regions of intrafusal fiber have been lumped into one. X_f is intrafusal fiber length, the input to the secondary nerve endings. Nuclear bag length is X_b, the input to the primary endings. Inputs are muscle length, X_m, and force due to efferent stimulation of intrafusal fibers, F_γ.

We desire expressions for X_f and X_b in terms of X_m, F_γ and the mechanical parameters. The force in both directions from node a is identical:

$$K_b X_b(s) = F_\gamma(s) + s B_f X_f(s) \tag{3.3}$$

where the Laplace transformation of the time domain equation has already been taken. Also,

$$X_m(s) = X_b(s) + X_f(s) \tag{3.4}$$

Eliminating X_b from Eqs. 3.3 and 3.4 yields:

$$X_f(s) = \frac{K_b}{s B_f + K_b} X_m(s) - \frac{F_\gamma(s)}{s B_f + K_b} \tag{3.5}$$

and eliminating X_f from the same equations yields:

$$X_b(s) = \frac{s B_f}{s B_f + K_b} X_m(s) + \frac{F_\gamma(s)}{s B_f + K_b} \tag{3.6}$$

If we now let "a" represent the number of primary nerve endings stretched by X_b, and "b" represent the number of secondary endings stretched by X_f, we may then write an expression for X_s, the total stretch to nerve endings.

$$X_s(s) = a X_b(s) + b X_f(s) \tag{3.7}$$

Substitution of Eqs. 3.5 and 3.6 yields:

$$X_s(s) = b \frac{s \frac{a}{b}\left(\frac{B_f}{K_b} + 1\right)}{s \frac{B_f}{K_b} + 1} X_m(s) + \frac{\frac{b}{K_b}\left(\frac{a}{b} - 1\right)}{s \frac{B_f}{K_b} + 1} F_\gamma(s)$$

This expression will serve as the output from transformation A.

Further interpretation can now be given to some of the parameters. Consider the contribution to X_s due to the input X_m, $F_\gamma = 0$:

$$\frac{X_s(s)}{X_m(s)} = b \frac{s \frac{a}{b} \frac{B_f}{K_b} + 1}{s \frac{B_f}{K_b} + 1} \tag{3.9}$$

Comparison with Eq. 3.1, the small signal characteristics of spindle, reveals that:

$$T = \frac{B_f}{K_b} \; ; \; \eta = \frac{a}{b} \; ; \; C = b \tag{3.10}$$

Granite[23] has noted that there are more primary endings than secondary endings, i.e., $a > b$, thus insuring $\eta > 1$ as we required in Section B. $a > b$ also insures that the coefficient of the F_γ term of Eq. 3.8 is positive. Thus the well known increase in spindle discharge resulting from increases in gamma efferent activity is also present in the model. The time constant of decay is interpreted to be given by the ratio of the apparent viscosity of the intrafusal fiber to the spring constant of the nuclear bag. The steady-state gain of the spindle is interpreted as the number of secondary nerve endings in the spindle.

The mechanical model of spindle anatomy which was assumed (Fig. 3.1(b)) neglected many elements which were considered relatively unimportant. It is interesting to investigate the consequences of including some of these in the model.

Inclusion of small nuclear-bag viscosity or large intrafusal-fiber series elasticity would add another pole to the transfer function of Eq. 3.9. This pole would have a high frequency break point and would therefore decrease the high frequency response of the model. This effect was evident in the sinusoidal analysis (Fig. 3.4). Inclusion of small mass elements would accentuate this effect.

In the absence of gamma innervation ($F_\gamma = 0$), a decrease of muscle length would probably lead to a sagging spindle; i.e., K_b in pushing against B_f would probably cause buckling of the spindle rather than shortening of X_f. The weak spring in parallel with B_f (discussed in Chapter II, Section A) would help overcome this buckling. These effects are evident in the negative step responses of Jansen and Mathews.[28]

In Chapter II it was found that the apparent viscosity was proportional to the state of muscle fiber activity. According to this model, then, as gamma innervation increases, B_F would also increase. This would increase T, the time constant of decay to step inputs. This result is somewhat contradictory to the results which will be presented in Chapter VII.

In spite of these deficiencies of the model, it was judged to be quite adequate for the simulation of the PCS in this thesis.

F. NONLINEARITIES IN TRANSFORMATION B

There are certain nonlinearities which are known to exist and are probably caused by transformation B. The spindle cannot produce fewer pulses per second than zero. There is also a maximum frequency of firing at which further stretch elicits no increase in rate of firing. It is not known how abruptly these saturations occur.

Two pieces of experimental evidence by Granit[25] suggest that a power relationship exists between the input and output of B. He has found that the steady-state frequency of pulses does not increase linearly with stretch, but, instead, with some power of stretch. The relationship is approximately that of a squarer. He also found that the gain of the spindle increased with an increase in gamma bias in an approximately linear way. Both of these effects are seen only in the normal operating range of the spindle where saturation effects which were discussed above are not present.

All of the above phenomena can be explained by the nonlinear, no-memory model for transformation B which is shown in Fig. 3.7. The saturations have been assumed to be abrupt; the output increases as the square of the

input; and the small-signal gain at X_{s_2} is greater than that at X_{s_1}, where $X_{s_2} > X_{s_1}$. Since nothing is known about the process which causes transformation B, it will not be possible to relate these results to a biochemical process.

G. ASSEMBLY OF THE MODEL OF SPINDLE

Models of each of the processes which contribute to the spindle's ability to change position and gamma innervation into related nerve impulses have been developed. These models have been assembled into the composite model of spindle receptor shown in block diagram form in Fig. 3.8. This model accounts for the observed dynamic characteristics as well as the major nonlinearities of muscle spindle receptors.

The values of the parameters C_1, C_2, C_3, η, and T must be determined for the particular spindle which one is considering. It was not possible to conduct experiments on human muscle spindles to obtain them. Instead they will be treated as parameters in the model of the PCS which will be adjusted to obtain correspondence between experiments on subjects and simulations of the PCS model. The plausibility of the resulting values will then be discussed.

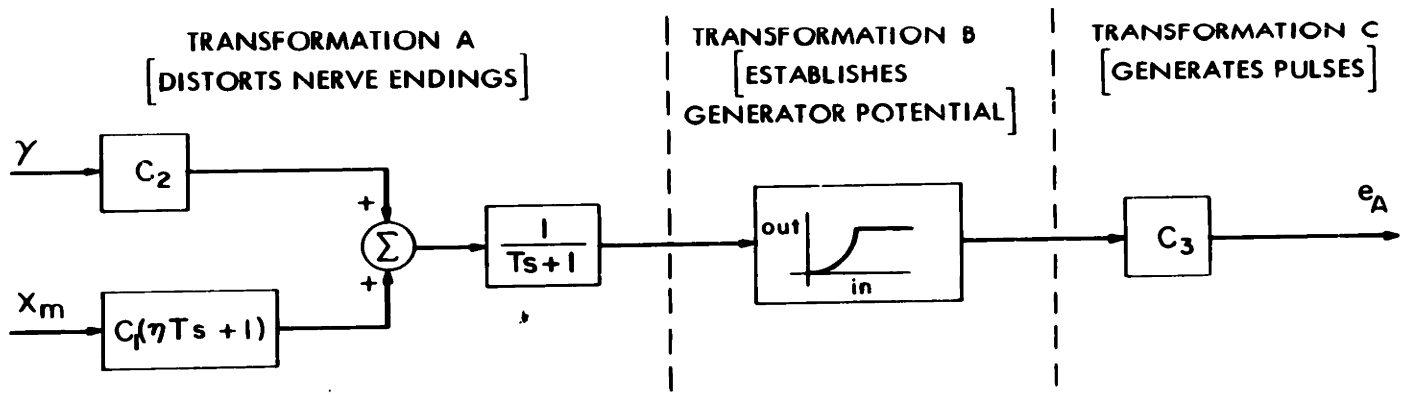

Fig. 3-8 SPINDLE RECEPTOR MODEL. C_1, C_2, and C_3 are constants, S is the Laplace operator, and η is the overshoot factor and T the time constant of decay to a small step input. Inputs are gamma activity and muscle length; the output is instantaneous pulse rate.

CHAPTER IV

NERVE FIBERS AND NEURONS

Nerve fibers, the active transmission lines of the human body, conduct meaningful patterns of nerve impulses which have originated in one part of the body to another site where they may be used either as initiators of muscular activity or as inputs to neurons, the data processors of the central nervous system. The single pool of motor neurons which appear in the PCS represent these data processors in their simplest form. This chapter will discuss some of the properties of these two components. Models of the same suitable for simulation of the PCS model will also be presented.

A. NERVE FIBER

It is generally acknowledged (e.g., 29, 30) that the particular form of a nerve pulse has no meaning to the nervous system. Rather, the position of the pulse in time contains all the information which is transmitted along nerve fibers. Investigators who have postulated that the code of these neural pathways is the instantaneous frequency of pulses have usually found stong correlation between sensory inputs to receptors and the frequency of pulses carried by their afferent fibers (Ref. 30, Chapter III). Only in electrical activity of the brain itself has lack of correlation been evident. (e.g., 31) Let us therefore follow this hypothesis and now consider the flow of instantaneous pulse frequency, i.p.f., through nerve fibers and neurons.

Brindley[29] notes that the distortion to i.p.f. as it is being transmitted by nerve fibers is very slight. It is very rare that a pulse initiated at one end of a nerve fiber does not reach the other end; equally rare is the spontaneous generation of pulses. Moreover, except for a very slight tendency to average intervals of pulses which are close neighbors in time, nerve fiber does not alter the time interval between pulses. We may consider nerve fiber as a distortionless transmission line for i.p.f.

The time delay due to transmission along a nerve fiber is directly proportional to fiber length and inversely proportional to fiber diameter (Chapter III of Ref. 32). The time delay along the spindle afferent nerve and along the alpha efferent nerve may be estimated from the geometry. The length of nerve fiber between the spinal cord and muscles of pronation and supination is about 50 cm. The primary spindle afferents (about 20 μ in diameter) conduct at a velocity of 100 m/sec while the alpha efferents (about 12 μ in diameter) conduct at a velocity of 60 m/sec. The corresponding time delays may be calculated.

t_A (afferent delay) $\simeq$ 5 m sec

t_E (efferent delay) $\simeq$ 9 m sec

B. NEURONS

Motor neurons in the spinal chord have been reported (Chapter V of Ref. 32) to transmit somewhat of a replica of the algebraic sum of its input i.p.f.'s, subject to the following modifications:

1. delayed 0.5-0.9 m sec (synaptic delay)
2. attenuation factor which is somewhat dependent on the past history of inputs (post-tetanic potentiation)
3. some evidence of a rate response to inputs and some evidence for an integrative response to inputs.

Boyle[33] has incorporated some of these characteristics in his analog model of a neuron:

$$f_o(s) = \sum_{i=1}^{N} f_i(s) \frac{K_i}{(s T_{m_i} + 1)} - m \frac{\theta_s}{s} \qquad (4.1)$$

where s is the Laplace operator, f_i is the input i.p.f., f_o is the output i.p.f., and $m\theta_o$ is the threshold cell potential; K_i is the attenuation factor and T_{m_i} is time constant associated with the ith synaptic input to the neuron.

This is a theoretical model based only qualitatively on neuron responses; no values of T_{m_i} were given. Since time and facilities did not allow the experimental determination of typical values of the time constants of mammalian motor neurons, and since experimental records in the literature were inadequate, it will be assumed that $T_{m_i} < 0.01$ sec. in which case neuron dynamics would have a negligible effect on the simulated responses in Chapter VII. Incremental changes of output frequency is the variable of interest, thus allowing us to neglect the threshold term and write:

$$f_o(t) = \sum_{i=1}^{N} K_i f_i(t) \qquad (4.2)$$

which is the time domain representation of Boyle's model with the above mentioned simplifications. The synaptic delay which Boyle did not consider adds a pure delay of about one millisecond to this model.

C. SUMMARY

1. Nerve fiber has been modeled as a distortionless delay line to instantaneous pulse frequency, the continuous neural signal in the PCS model.

2. The motor neuron has been modeled as a summer with a millisecond synaptic delay associated with each input.

CHAPTER V

ASSEMBLING A MODEL OF THE POSTURAL CONTROL SYSTEM

The PCS (Fig. 1.2) which is to be experimented upon, modeled, simulated, and discussed, is a positional feedback control system. Its purpose is to maintain the orientation of a limb in opposition to gravity, mechanical disturbances, and fatigue. It accomplishes its purpose by monitoring muscle position and using this information to alter the instructions to the actuators of the limbs. It depends on the central nervous system for basic orientation and the fixed instructions which are modified by its action. This control system is oriented by biasing the output of the position transducers via the gamma pathway. The fixed instructions are probably given via both the alpha and gamma pathways depending on the peculiarities of the position maintaining task.

In this chapter the models of the PCS components will be assembled according to the arrangement dictated by the topology of the PCS (Figs. 1.2, 5.1).

A. SPINDLE INPUT

The parallel arrangement of intrafusal fibers with respect to main muscle fibers establishes muscle position as the input to the spindle receptors. Nevertheless, as Johnson pointed out,[9] Adolph[6] has used muscle tension as his input to spindal receptor. Among the other investigators who have modeled muscular control systems (e.g., 5, 9, 10) most have considered load position as the variable which is monitored by the spindle. Only Hammond[8] has judged that muscle position is different from load position.

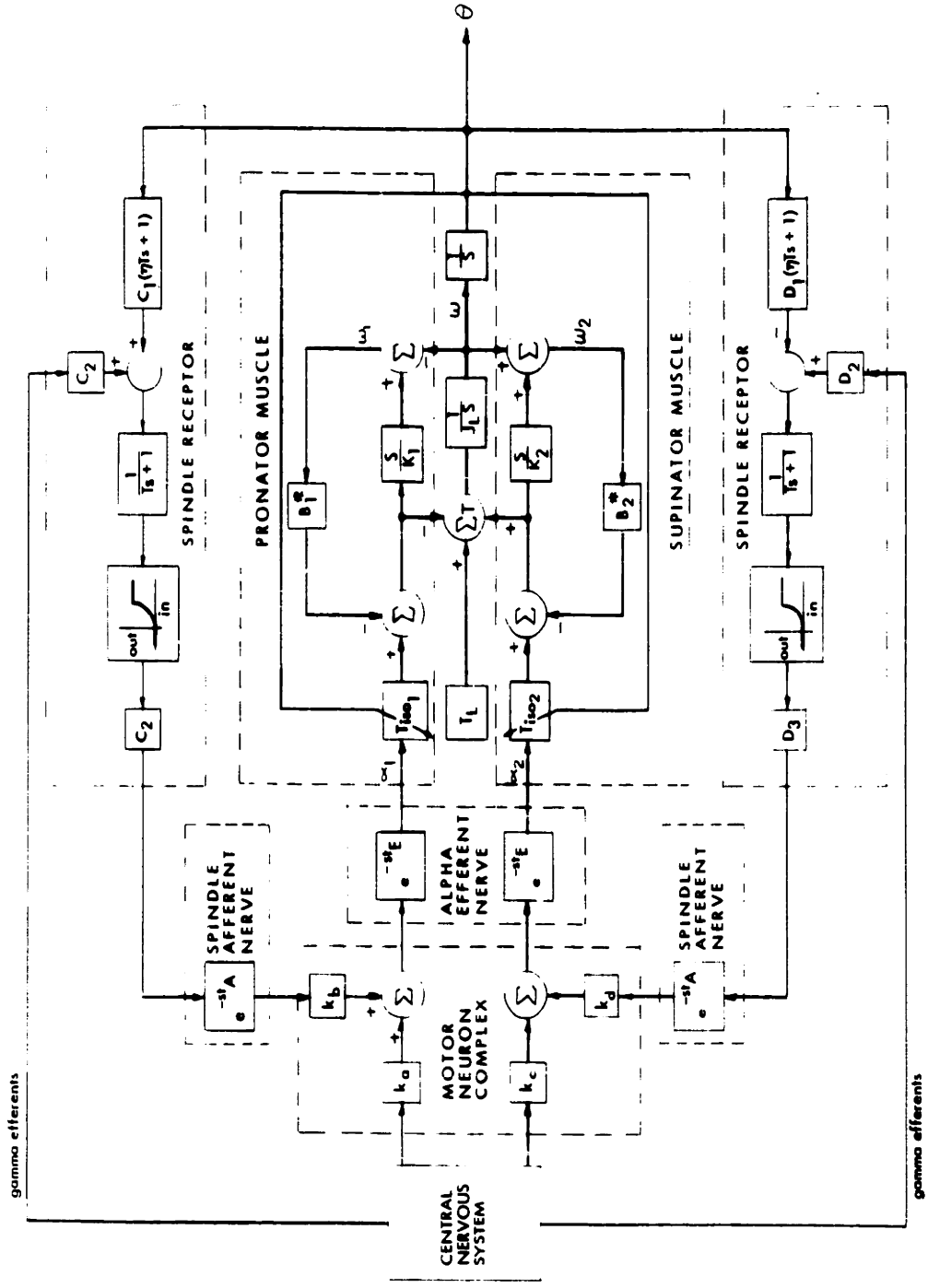

Fig. 5-1 THE INTEGRATED MODEL OF THE PCS

Figure 5.2 demonstrates that the presence of series elasticity due to tendon attachments admits the possibility that variations of muscle position, X_m, will not follow variations of load position, X_L. The rise of isometric torque experiments described in Chapter II fail to differentiate between the two possible origins of series elasticity. Rather, they allow the calculation of the series combination of K_T, the spring constant due to tendonous tissue common to all the muscle fibers, and K, the spring constant due to the series elasticity which is distributed along each individual muscle fiber. Note that the spindle represents only a small fraction of the number of fibers constituting a muscle. It has negligible loading effects (i.e., $K_B << K$) and is merely constrained to follow the variations of X_m.

Hill[34] remarks that K_T varies greatly depending on the function of the muscle. For example, the frog's gastrocnemius muscle has a rather long tendon and consequently a rather small K_T. This allows the frog to move his hind limb faster than the maximum velocity of the contractile elements would allow. This phenomena which is due to stored energy in K_T is important to the frog in jumping.

Most of the muscles employed in wrist rotation, however, have relatively short tendonous attachments; and, although no quantitative estimates are available, most of the series compliance is probably due to K. It has been postulated, therefore, that K_T is large in comparison to K, and thus negligible. In this situation $X_m = X_L$ for a single muscle, and for our equivalent torque producing muscle $\theta_m = \theta_L = \theta$. The input to spindle is θ.

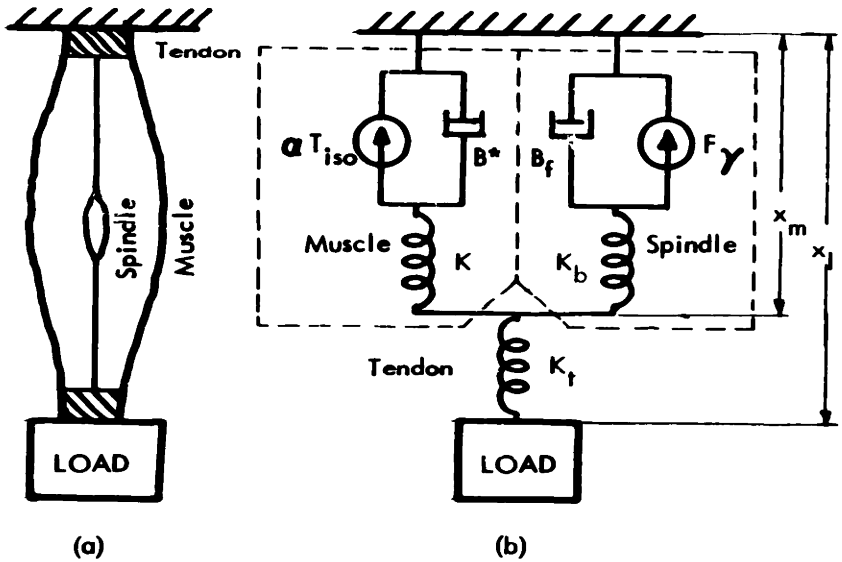

Fig. 5-2 THE MECHANICAL TOPOLOGY OF MUSCLE, SPINDLE, AND TENDON.

If $K_T >> K >> K_b$, $X_m \simeq X_\ell$

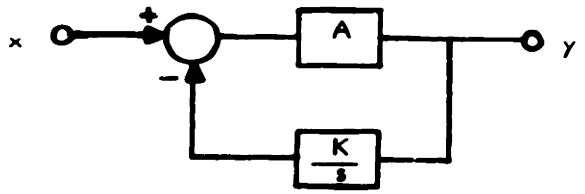

Fig. 5-3 AN ANALOG APPROXIMATION FOR DIFFERENTIATION.

B. THE PROPRIOCEPTIVE NEURAL LOOP

Neural pulses from the spindle model go directly into the spindle afferent nerve (Chapter IV) where they are transmitted with a delay t_A to motor neurons. The primary endings of the spindle are known to encounter only the alpha motor neuron in their transit through the spinal cord. The secondary endings, however, may encounter one or two interneurons before they synapse with the alpha motor neuron, and the signals that they are carrying are thus subject to one or two milliseconds more delay than those signals carried by the primary endings. For the simulations in this thesis this additional delay may be neglected. All signals are therefore subject to 1m sec. synaptic delay in the spinal cord. This delay will be included in t_A. The efferent nerve contributes an additional delay, t_E, before the signals reach the muscles.

The pathway spindle to afferent nerve to motor neuron to efferent nerve to muscle is termed the proprioceptive loop.

C. FORCE GENERATOR INPUT

The signals in the efferent nerve terminate at the neuro-muscular junction. This junction is similar to the synaptic junction of neurons.[35] There is about a millisecond delay between the arrival of an efferent pulse and the initiation of muscle potentials. An additional delay may exist between the establishment of muscle potentials and the production of force. In homeothermic mammals where the body temperature is maintained at 37°C this delay is quite short, of the order of two milliseconds. Hammond[8] has estimated that this delay is 15 milliseconds, but this is the value given for amphibian muscle at rather low temperatures.

Wilkie[13] has shown that the exponential rise of isometric tension in muscle is primarily due to the series elasticity rather than a limited

frequency response of the force generator. In terms of the PCS model this means that a step input to the force generator delivers a very rapidly rising increase in force (of the order of ten milliseconds time constant) which we may assume to be instantaneous in the model. Experimental electromyographic records which will be presented in the next chapter provide support for this conclusion.

The additional pure delays considered above will be added to t_E.

D. SIMULATION OF THE PCS MODEL

The model of the PCS (Fig. 5.1) is now complete except for the values of some of the spindle parameters and neuron attenuation factors. The impracticality of determining these values from experiments which isolate spindle and motor neuron of the human subject was anticipated. Instead, it was proposed that these parameters and gain factors be treated as variables which may be adjusted to obtain correspondence between experiments on the entire PCS and simulations of the same. It was therefore necessary to prepare the PCS model for simulation.

Originally it was hoped that a simulation of the entire nonlinear model could be carried out on the IBM 7090 digital computer. BIOSIM, a program which accepts both digital and analog instructions, had been written with this purpose in mind (see Appendix A). Pure time delays and no-memory nonlinearities are easily programmed with digital instructions. In addition, the integrating subroutines in BIOSIM facilitate rapid programing of linear, memory transfer functions. The only major difficulty is that of simulating pure differentiation which is required in the muscle model.

The approximate differentiator shown in Fig. 5.3 may be employed if the gain factor, A, is not made too large. The transfer function for this system is:

$$\frac{y(s)}{x(s)} = \frac{\frac{1}{K}s}{\frac{1}{AK}s + 1}$$

It satisfactorily differentiates frequencies up to ω_c = AK radians/second. Above this crossover frequency it acts like a pure gain, A. Increasing A therefore increases the bandwidth over which it differentiates. However, if this system forms part of a feedback loop, as it does in the muscle model, and the simulation is conducted for discrete time intervals, as it is done in digital simulation, large values of A lead to an unstable loop. It was found that if $AK \leq \frac{1}{2T}$, where T is the discrete sampling interval for the simulation, the muscle model remained stable. From Chapter II, K, the series elasticity is 10 N-m-rad^{-1}. A sampling interval of one millisecond demanded that $A \leq 50$, this provided differentiation of frequencies up to about five hundred radians/sec and was satisfactory for this study.

The feasibility of the simulation was thus ascertained; however, after the PCS model was programmed, the usefulness of this simulation was challenged on two other accounts. The 7090 was not available for on-line use, but, rather, programs were submitted to the Computations Center and returned one half to two days later. The successful adjustment of one parameter might occupy a week's time. Also, it was found that the model was too complex to facilitate the acquisition of an engineering "feeling" for its behavior. It was therefore decided that the model should be simplified to allow both analytical work and analog simulation. After the parameters had been selected and the behavior of the model was more fully understood, it would be possible to return to the more complete BIOSIM model for further, and more accurate,

studies. The reduced, linear model which will be presented in Chapter VII resulted.

CHAPTER VI

EXPERIMENTS ON THE POSTURAL CONTROL SYSTEM

Chapter V presented a model of that part of the human muscular control system which participates in the stretch reflex. Some of the parameters which appear in this PCS model have been measured for the wrist and forearm rotating system of the subject J.H. In this chapter three e.m.g (electromyographic) experiments which help to verify certain aspects of the model will be presented. The response of the PCS to impulsive load disturbances will also be measured. Correspondence with these responses will form the primary criterion in selecting values for the unmeasured parameters in the model (Chapter VII).

A. EXPERIMENTAL APPARATUS

1. EMG Records

The weighted average of rectified emg activity has been found by Lippold[16] to be linearly related to muscular activity, i.e., the activity of the force generator in the muscle model. The apparatus for recording this is briefly described below.

Two surface emg electrodes were taped about an inch apart on the belly of the muscle whose emg activity was to be recorded. A large, common electrode was taped to the subject's neck. These three electrodes served as a balanced input to a Grass preamp with gain = 1000. The balanced output from the preamps was fed into a full-wave rectifier followed by a low pass filter.

The output at this point is given by

$$\overline{e(t)} = \int_{-\infty}^{t} |emg(t-\sigma)| \, e^{-\frac{\sigma}{T}} \, d\sigma$$

where T, the time constant of the low pass filter, is 30 m sec. The signal was further amplified by a Philbrick amplifier and recorded with a portable Sandborn heat recorder. Sample records are shown in Fig. 6.2.

2. MCT Apparatus

Impulsive torque disturbances were inserted into the PCS, and its response was measured with the MCT (motor coordination tester) shown in Fig. 6.1. Subjects were instructed to grasp the handle. Their elbow was anchored, and they were not allowed to see the falling pendulum which would deliver the disturbance to the shaft and subject. It should be noted that for this experiment the shaft becomes part of the PCS, contributing inertia which adds to the inertia of the hand (evaluated in Chapter II). Concentric masses could be added to increase the inertia of the PCS.

Subject position (i.e., shaft position), θ, and pendulum position, θ_p, were monitored by recording e_1 and e_2 (Fig. 6.2). Sample records are shown in Fig. 6.2. An evaluation of the impulse delivered by the pendulum is presented in Appendix B.

B. EMG EXPERIMENTS

In the experiments which are described and interpreted below, emg activity of the pronator teres muscle and the extensor digitorum communis muscle was recorded. The primary function of the pronator teres, as its name implies, is that of causing the wrist to pronate or resist superination-causing disturbances. The extensor digitorum communis, on the other hand,

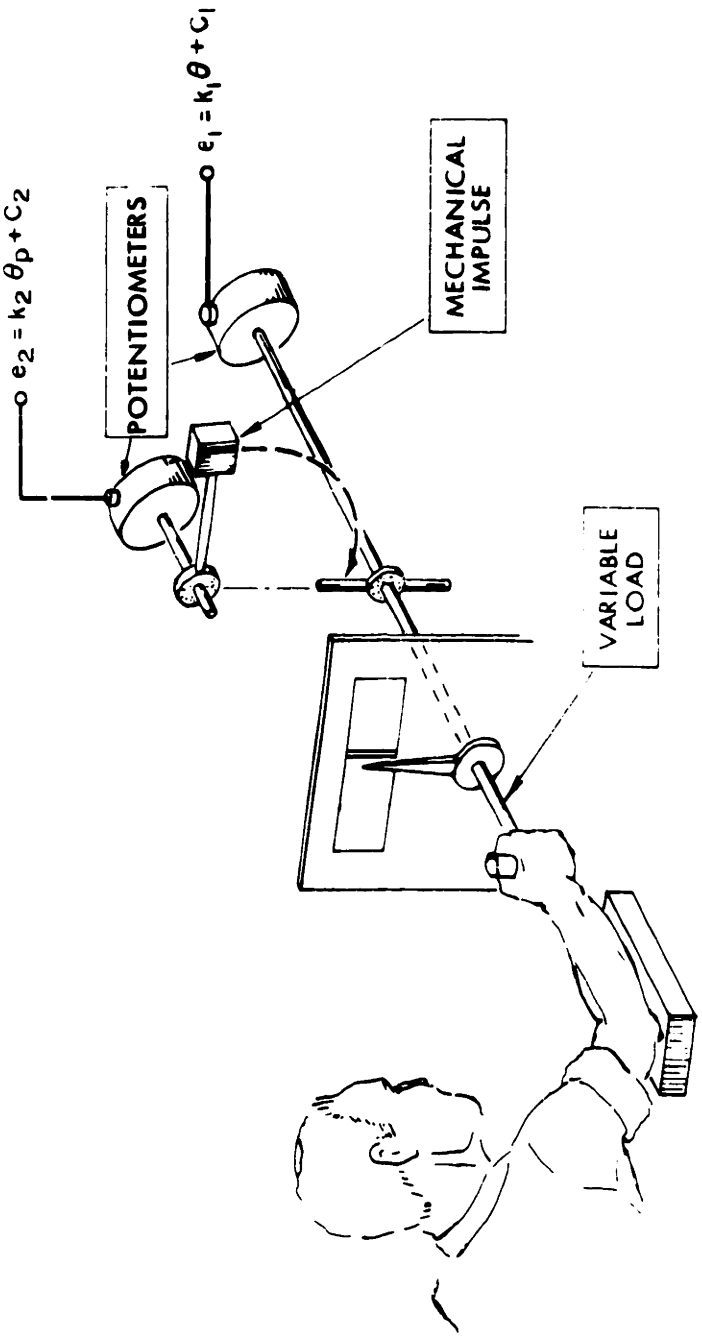

Fig. 6-1 THE MCT (MOTOR COORDINATION TESTING) APPARATUS

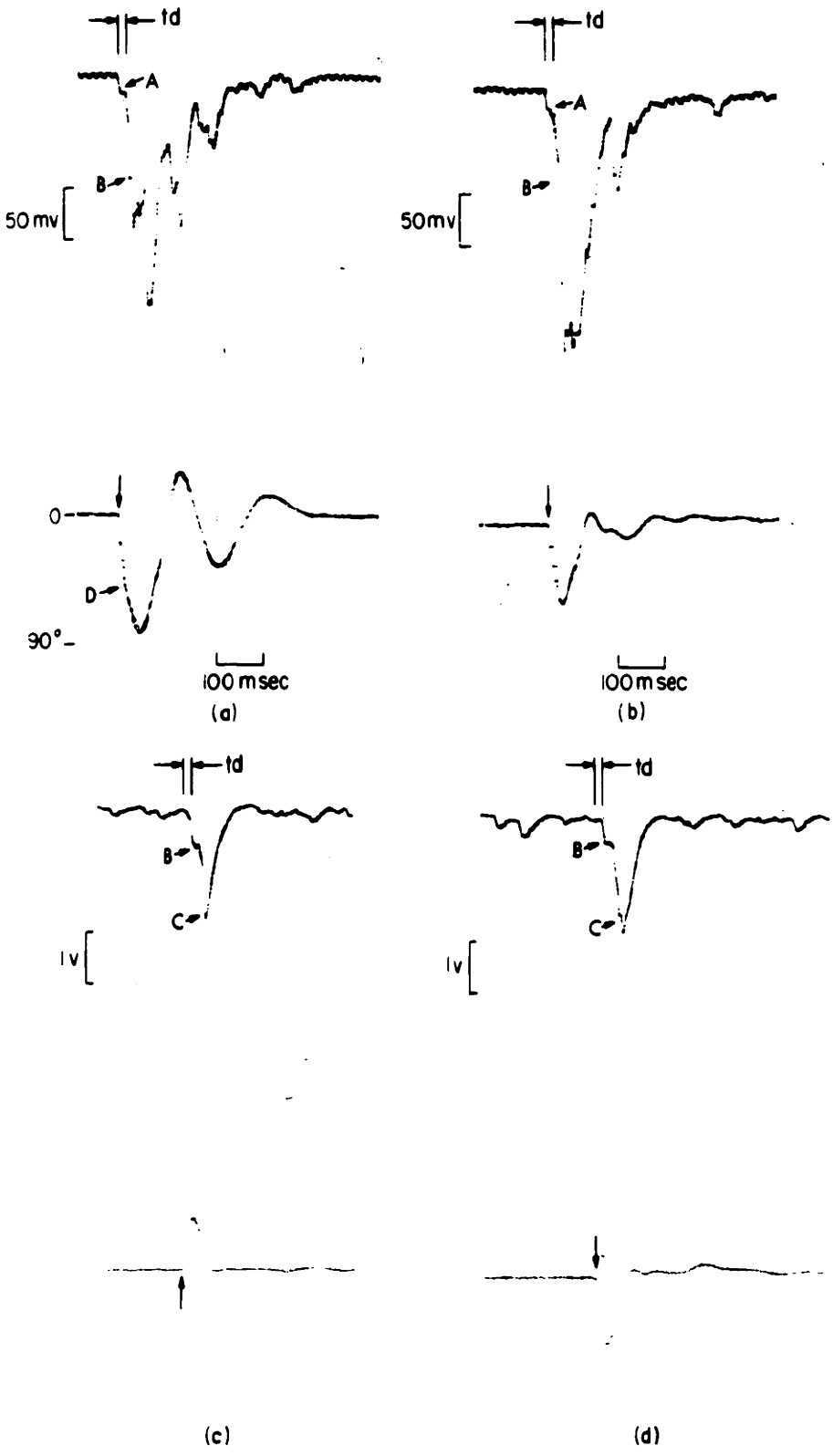

Fig. 6-2 ELECTRO-MYOGRAPHIC (EMG) ACTIVITY DURING IMPULSE DISTURBANCES. Electrodes on belly of Pronator Teres ((a) and (b)) and Extensor Digitorum Communis ((c) and (d)). (Pronation is down) (See text)

plays no direct role in wrist rotation. Its excitation causes dorsi flexion of the wrist or extension of fingers or both. Additionally it plays a part in the grasping reflex and acts to stiffen the whole forearm both of which actions are of interest here. When a subject prepares for a pendulum disturbance, he tightens his grasp on the handle to prevent slipping, and he stiffens his whole forearm musculature which perhaps adds damping to the PCS. The comparison of the emg activity of these two muscles will prove to be interesting.

1. Proprioceptive Loop Delay

In Chapters IV and V the delay to a signal traversing the neural part of the proprioceptive loop was approximated from empirical considerations to be 15-20 m sec. The experiments below serve to (1) verify this value of delay time and (2) prove that this simple monosynaptic pathway is, at least in this experimental situation, responsible for the stretch reflex. Hammond's[8] evidence for believing higher centers are responsible for the stretch reflex will be discussed.

An impulsive disturbance to the PCS causes an almost discontinuous change in θ. It was thought that this type of stimulus to a relaxed hand would elicit a clearly defined volley of nerve pulses from the spindles followed by more less-synchronous activity. The time delay, t_d, around the proprioceptive loop could therefore be determined by measuring the time interval between stimulus and initial emg activity.

Figure 6.2 shows the results of this experiment. The top trace represents emg activity; the bottom trace is wrist position. Onset and direction of stimulus are indicated by the vertical arrows. An artifact, "A",

A, due to movement of the electrodes is present in (a) and (b); it is not noticeable in (c) and (d) since the amplification of emg activity was less and more background activity of this initially tense muscle is present. In all of the records t_d, proprioceptive loop delay, was between 15 and 20 milliseconds.

Hammond[8] found about the same delay for this monosynaptic loop; however, his records showed no change in tension until 50 m sec after the onset of his stimulus. He therefore concluded that this initial volley was ineffectual in counteracting the disturbance and credited higher centers in the brain as producing the stretch reflex. Careful inspection of $\theta(t)$ in Fig. 6.2 (a) (see point (D)) reveals that a sudden change in slope of the impulse response occurs simultaneously with this initial emg activity. This evidence is present in all the records, and is particularly noticeable in (a). Moreover, record (b) shows that $\theta(t)$ reverses direction in less than 30 m sec. after the disturbance concurrent with a very large emg activity in the pronator teres. It is quite certain, therefore, that a stretch reflex with a time delay of about 20 m sec is responsible for resetting the wrist to its former position following an impulsive disturbance. Hammond was driving the system open loop, i.e., forcing the system, with step disturbances of velocity, a rather drastic disturbance. It is quite probable that the stretch reflex was being inhibited by "danger" signals from the tendon organs.

Comparison of records (a) and (b) demonstrates that the loop gain increases with increasing forearm tonus. When the subject is instructed

to tense his arm, there is no noticeable increase in the activity of the pronator teres. However, record (b) shows that the emg response to an impulse disturbance which causes about the same deflection of the wrist as in (a) is greatly enhanced. This increase in loop gain with increased muscle tonus has also been noticed by Granit.[25]

The pronator teres did not respond to negative impulses until the second peak of the oscillations of θ occurred. This corresponds with its suggested role of functioning only as a pronator. The extensor digitorum communis, on the other hand, responds equally to both positive and negative impulses (Fig. 6.2 (c) and (d)). This is consistent with its role of functioning neither as a pronator or a supinator. Point (B) of the response in both cases corresponds to the time when θ makes its first change of direction, a peak value of acceleration. The extensor has probably been called upon to strengthen the subject's grasp on the handle to eliminate the possibility of the handle slipping when the reversal of direction is performed.

Point (C) of the same responses corresponds, again in both cases, to a time when θ is subject to a very rapid damping to its zero position. Perhaps the extensor has been called upon both to strengthen the grip for the sudden stop and also to, by making the whole forearm stiffer, increase the damping at this critical moment.

The latter two paragraphs call attention to the extreme intricacy of control which probably implements the muscular control system. They remind us that an approach to the muscular control problem which considers only single, or, in the case of this thesis, double, channels of control

may be severely limited. Nevertheless, since it is the simplest, this approach should be investigated for validity.

2. Origin and Degree of Forearm Tone

The origin and degree of possible tension, or tone, in the forearm was investigated by comparing the maximum isometric activity of a muscle with its activity during conditions of maximum forearm tone. Maximum isometric activity occurred for the pronator when the shaft was clamped in its zero position and the subject was instructed to exert maximum effort in pronation. For the extensor it occurred when the subject was instructed to exert maximum flexion effort in his wrist which was maintained in a horizontal position. Maximum tone occurred in both muscles when the subject was instructed to tense his arm as much as possible.

Tone of the forearm recruitted 30% of the maximum possible activity of the extensor digitorum communis muscle, but only 2% of the maximum possible activity of the pronator teres. One might hypothesize that an increase in forearm tone stiffens the arm only by the increased activity of muscles not envolved in wrist rotation. Concurrently the reflex gain of wrist rotating muscles is increased. The former may add a coulomb friction to the joint, the node where torques are summed in the PCS model. Since no further evidence was available, this possibility has been neglected. The increase in loop gain will help to explain the change in the PCS impulse response which occurs with a change in forearm tone.

3. Maximum Rise of EMG Activity

The ability of the central nervous system to effect a step change of emg activity was investigated by clamping the shaft at a central position and measuring emg activity of the pronator teres as the subject is instructed to

suddenly change from rest to maximum pronation. Figure 6.3 shows that the time constant of rise may be as small as 15 m sec. which, indeed, is less than the 30 m sec time constant of the low pass filter. This suggests that the central nervous system is capable of inserting not only steps, $f_a(t)$ in Fig. 6.4, but also inputs such as $f_b(t)$ which help overcome any lag effects in the efferent-muscle pathway. However, without actually monitoring the input to the alpha motor neurons, it is not possible to ascertain the existence or non-existence of small lags in the transmission from neuron to muscle. Nevertheless, we may be reasonably certain that no dynamics with time constants which would appreciably influence the overall performance of the PCS (i.e., with time constants greater than 10 m sec) are present in this pathway. Wilkie[13] arrived at the same conclusion on different theoretical grounds.

C. IMPULSE DISTURBANCE EXPERIMENTS

Impulse disturbances were inserted into the PCS under six experimental conditions and the time course of θ was recorded as the output (Fig. 7.9). The emg responses to impulse disturbances are submitted as evidence that the proprioceptive loop is responsible for the human subject's response to the disturbance (see experiments and discussion in Section B). Thus we are assured that it is the PCS itself, and not higher centers in the nervous system which were not included in the PCS and its model,which is being experimented upon and analyzed.

The records in Fig. 7.9 show the subject's impulse response under three conditions of forearm tone. The condition, "tense", is that of near maximum tone; "relaxed" is that of a completely relaxed forearm but

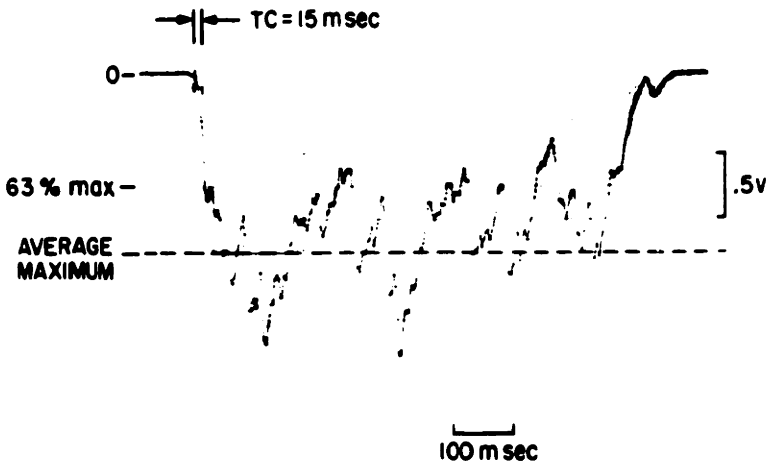

Fig. 6-3 EMG ACTIVITY DURING A SUDDEN APPLICATION OF ISOMETRIC TORQUE.

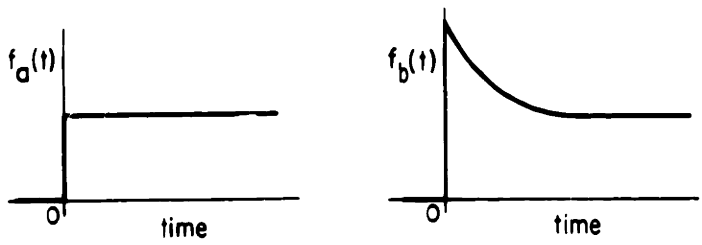

Fig. 6-4 A POSSIBLE COMPENSATING INPUT TO THE ALPHA MOTOR NEURON (see text).

nevertheless alert subject; and "moderate" is that of a moderate tone somewhere in between the former two. The subject seemed to be able to judge his state of tone well enough so that results were consistent without devising a method for monitoring tone.

In Fig. 7.9 (d), (e) and (f) the MCT apparatus was loaded with additional inertia which was more than ten times the normal inertia of the forearm. In records (a), (b), and (c), however, the inertia of the MCT was reduced to 1/2 the calculated inertia of the wrist and forearm. This corresponded very closely to the natural situation of a completely unloaded forearm.

In all of the impulse responses, except perhaps in the case of the tense, unloaded forearm, the responses suggest that the PCS behavior is dominated by a pair of complex poles; i.e., the response is very much like that of a second-order, underdamped system where the impulse response may be given by

$$h(t) = A e^{-\sigma t} \sin \omega t$$

Investigation of the movement of this dominant pair of poles, as tone or inertia is varied, provides a convenient means of evaluating the PCS performance; pole movement is illustrated in Fig. 6.5 . The attenuation factor, σ, was evaluated from the equation

$$\sigma = \frac{\ell n \frac{A_1}{A_2}}{t_2 - t_1}$$

where A_1 is the first amplitude peak which occurs at time t_1, and A_2 is the second amplitude peak which occurs at time t_2. The angular velocity, ω, was evaluated from the first half period in the case of the unloaded arm

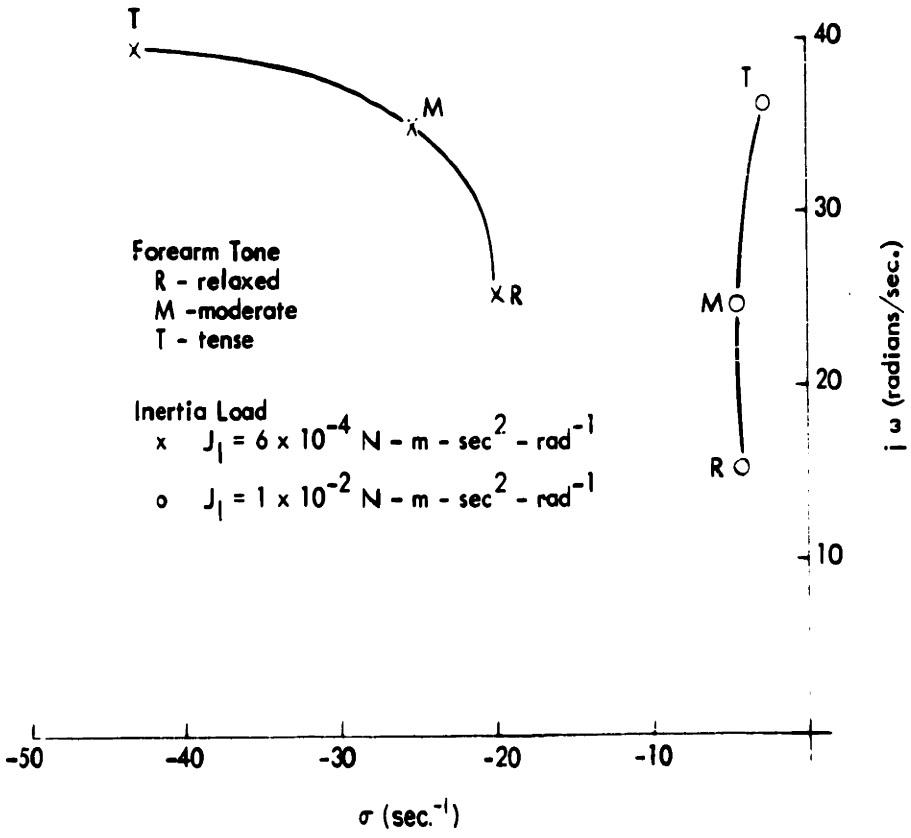

Fig. 6-5 MOVEMENT OF DOMINANT POLES OF IMPULSE RESPONSES ACCOMPANYING FOREARM TONE

and from the first full period in the case of the loaded arm. The plot and associated impulse responses are for the subject J.H. only; similar results have been found for other subjects.[36]

D. SUMMARY

EMG experiments on the PCS have:

1. Established that the monosynaptic stretch reflex is responsible for the PCS response to impulsive disturbances.
2. Evaluated the time delay caused by neural elements in the proprioceptive loop to be 20 m sec.
3. Suggested some of the diverse roles that forearm muscles may play in muscular controlled movements.

Impulse disturbance experiments have been performed on the PCS under various states of forearm tone and inertial loading. These responses will be compared with those of a linear model of the PCS in the following chapter.

CHAPTER VII

A LINEAR MODEL OF THE POSTURAL CONTROL SYSTEM

The need for a rather simple model of the PCS for conceptual understanding and initial studies was discussed in Chapter V. Appropriate assumptions will now be made to reduce the nonlinear model of the PCS to a linear model suitable for analytic work and simulation on an analog computer. The unknown gain factors and spindle time constants will then be approximated by comparing simulated impulse responses with the subject's impulse responses under the six experimental conditions which were discussed in Chapter VI.

A. LINEAR REDUCED MODEL (LRM) OF THE POSTURAL CONTROL SYSTEM

Linearization

Four nonlinearities are present in the PCS model of Fig. 5.1.

1. The equivalent torque producing muscles are unilateral devices which may be biased at different levels of muscle tone.
2. The apparent viscosity, B^*, of each muscle is a function of excitation and angular velocity.
3. The isometric torque of the equivalent muscles varies with θ.
4. A no-memory nonlinearity is present in each spindle.

Quasi-linear approximations to each nonlinearity will be considered, but first muscular tone in the model must be discussed.

When a subject tenses his forearm, he allows his agonist muscles to work against his antagonist muscles. If these torques are carefully balanced against each other, no rotation of the wrist results,

but, rather, the muscular tone of the whole forearm is increased. The degree to which each of the two known pathways from the CNS (central nervous system) participates in establishing tone has not been clearly established; however, most qualified investigators favor the gamma pathway. In either case we may note that the presence of the stretch reflex is necessary to stabilize the system in the presence of noisy or slightly incorrect neural instructions. Without its position feedback a small unbalance of torque would drive the system to saturation.

If tone is inserted via the gamma route, both spindles become biased at a point of increased incremental gain of the spindle squarer. This causes an increase in incremental loop gain in the proprioceptive loop. Increased loop gain for increasing tone was suggested by both the emg experiments and impulse experiments of Chapter VI. Therefore, because of the consistency of its implications, the postulate that tone is inserted via the gamma route by biasing the spindles will be adopted.

Next we would like to postulate that a single, bilateral muscle will adequately represent the two opposing unilateral muscles in the prototype model. The greatest obstacles to this postulate are the radical changes in gain that occur as the system passes from a region where both muscles are in operation (the force of one decreasing while the force of the other is increasing) to a region where one is inoperative (due to the fact that a muscle cannot push). Figure 7.1 illustrates how a change in gain may or may not occur, depending on whether tone is or is not present. Let us assume identical spindles and gains in both proprioceptive loops. Figure 7.1(a) shows that, if the spindles are biased at zero gamma input, the two unilateral muscles work together perfectly to provide a bilateral muscle with constant gain in all regions

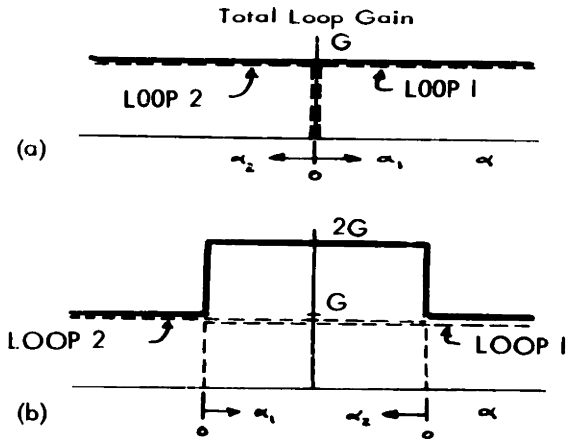

Fig. 7-1 THE EFFECTIVE INCREASE IN GAIN DURING MUSCULAR TONE. G is the gain of a single proprioceptive loop; a_1 and a_2 are the neural signals present in loop 1 and loop 2; a is the neural signal for the additive combination of both loops. (a) no tone; (b) tone present.

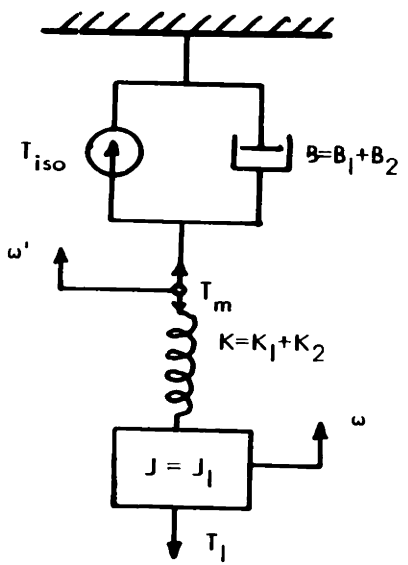

Fig. 7-2 THE EQUIVALENT, QUASI-LINEAR, BILATERAL MODEL OF MUSCLE

of operation. If, however, gamma inputs bias both loops at some constant output, then, since the loops are additive, in the region where both loops are operative the total loop gain is twice as large as it is in a region where only one loop is operative (Fig. 7.1(b)). In the LRM a constant gain factor between G and 2G will be selected based upon the level of muscular tone, i.e., gamma bias.

Reference to Figs. 2 through 10 will help the reader to realize that the effects of viscous elements and springs in the two muscles are additive, therefore giving rise to components in the equivalent bilateral muscle with values which are sums of the individual muscle values. The equivalent, bilateral muscle model is shown in Fig. 7.2. The average value which B assumes in the course of an experiment has been substituted for its nonlinear behavior in the PCS model. α now assumes both positive and negative values.

For small variations about $\theta = 0$ the isometric torque of a muscle remains reasonably constant. Its constancy is assumed in the LRM.

The incremental gain of the spindle nonlinearity at the level of gamma bias corresponding to the simulated muscle tone was chosen as a linear approximation to its gain. The neural gain factors, the spindle gain factors, and any additional gain due to the equivalent bilateral muscle approximation were considered together as the single gain factor, k.

Block Diagram of the LRM

The equations of motion for the equivalent bilateral muscle are

$$T_m(t) = \alpha(t)(T_{iso} - B\,\omega'(t)) \tag{1}$$

$$T_m(t) = K \int_{-\infty}^{t} (\omega'(t) - \omega(t))dt \tag{2}$$

$$T_m(t) - T_L(t) = J_L \frac{d\omega(t)}{dt} \tag{3}$$

If the Laplace transform of these three simultaneous equations is taken, an expression for ω in terms of the two inputs, α and T_L, may be obtained algebraically.

$$\omega(s) = \frac{T_{iso}\alpha(s) + T_L(s)\left(\frac{B}{K}s + 1\right)}{\frac{JB}{K}s^2 + Js + B} \tag{4}$$

Employing the above simplification to the PCS model of Fig. 5.1 and the two transmissions to ω given by Eq. 4 the block diagram of the LRM may be constructed as in Fig. 7.3. The values of the parameters in rationalized mks units which relate 7.3 to the wrist control system are

$J = 1 \times 10^{-2}$ (loaded) or 6×10^{-4} (unloaded)

$K = 20$

$0 < B < 2.0$ (depending on muscular activity)

$t_d = 0.02$

The parameters k, η, and T are to be determined from comparisons between impulse experiments and simulations.

B. SOME INTERESTING SYSTEM CHARACTERISTICS

Before proceeding on to the task of analog simulation and curve fitting, it will be instructive to investigate a few inherent system characteristics. Transition from a relaxed to a tense state of muscular tone is accompanied by an increase in B, the viscous term in the quasi-linear muscle model. These variations in B have a profound effect on the pole positions of the transfer function which models the muscular system (Eq. 4). The denominator of Eq. 4 has been set equal to zero to solve for

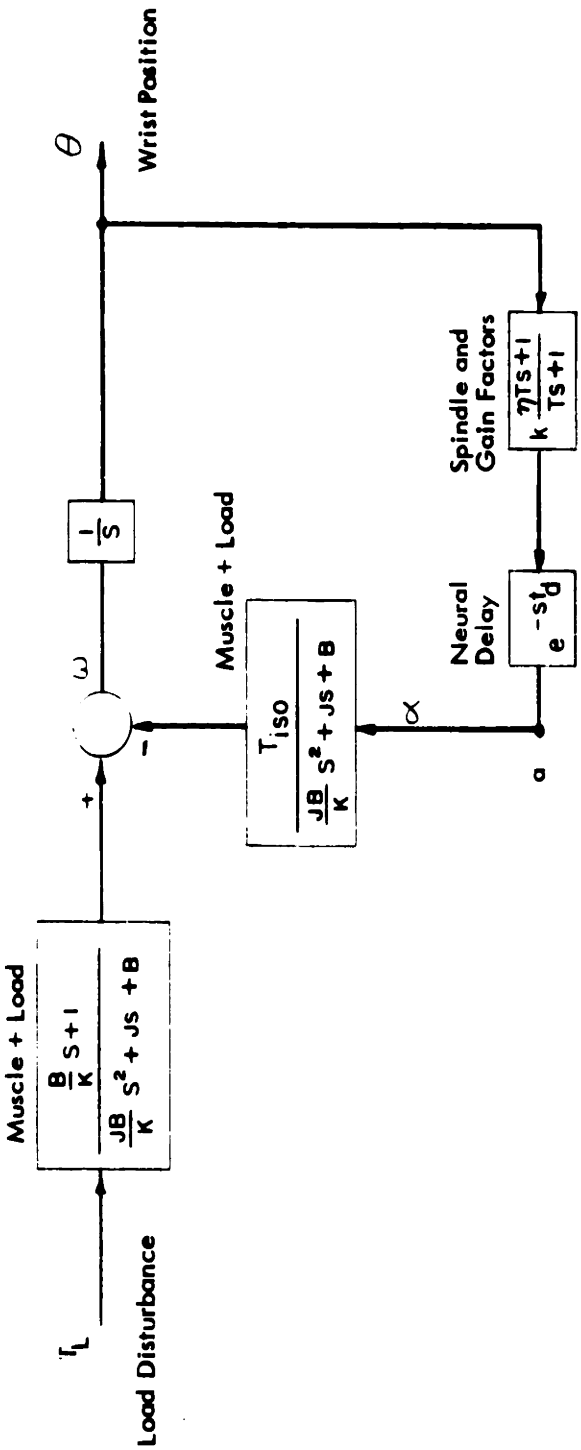

Fig. 7-3 BLOCK DIAGRAM OF THE LINEAR REDUCED MODEL OF THE PCS.

the transfer function's poles and rearranged to standard second order form in Eq. 5.

$$s^2 + \frac{K}{B} s + \frac{K}{J} = 0 \qquad (5)$$

It is particularly interesting to note that increasing values of B lead to less damping which is quite opposite the behavior of most second order systems. Figure 7.4 illustrates the pole movement accompanying increases of B for two values of load inertia. As B increases the poles approach each other along the real axis, meet, and leave the real axis at $\omega_0 = \sqrt{\frac{K}{J}}$ to become complex, oscillatory poles. These radical movements will have a profound effect on system characteristics.

The emg investigations of the degree of muscular tone (Chapter VI, Section B) indicate that only 2 - 30% of the maximum muscular activity possible is present in the maximum state of forearm muscular tone. The larger percentage was found in an extensor which experiences little change in length during wrist rotation; hence contributing relatively little towards the total equivalent viscosity of the muscular system. The lower percentage was found in a pronator which makes a relatively large contribution to the total equivalent viscosity. 5% was selected as a weighted average of muscular activity in the tense forearm. Since B has been modeled as a linear function of muscular activity, 5% of the maximum viscosity will represent the value of B in the tense forearm. This amounts to $B \leq 0.1$ N-m-sec^2-rad^{-1}. The lower limit to B for impulse disturbances into the relaxed hand was somewhat arbitrarily selected to be 0.01 which corresponds to an average muscular activity of 0.5% maximum. Rough calculations based on the emg responses to impulses showed this estimate to be reasonable.

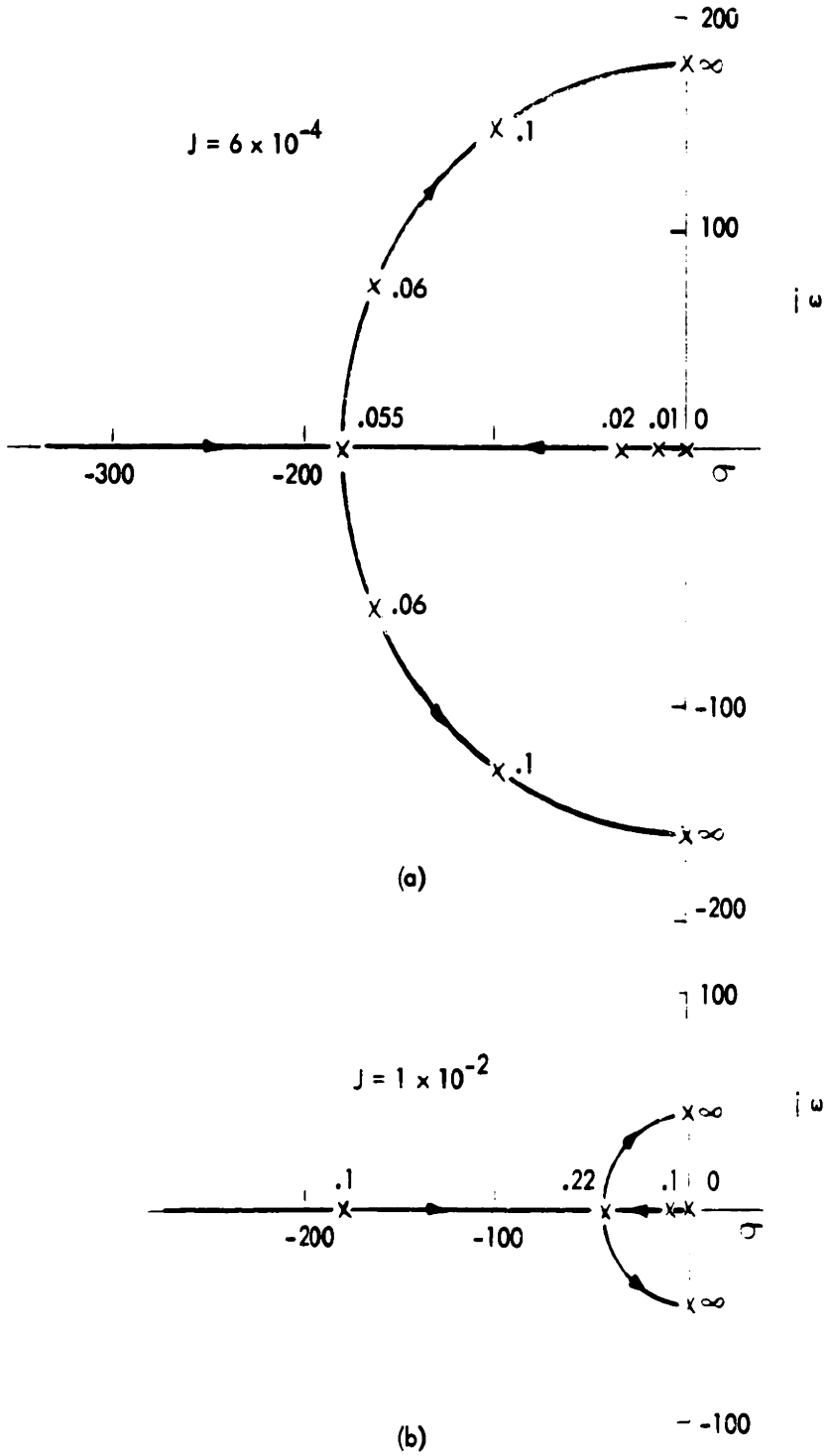

Fig. 7-4 THE MOVEMENT OF MUSCLE POLES WITH VARIATIONS OF APPARENT VISCOSITY. Arrows indicate increasing values of B, the parameter accompanying each calculated pole position.

Let us now consider the spindle as a compensating network whose break frequencies will be defined later. We would like to investigate the system without compensation to determine what effect movement ofmuscle poles has on its characteristics. The transfer function around the feedback loop (Fig. 7.3) is given by

$$G(s) = \frac{k e^{-st_d}}{s} \quad \frac{T_{iso}}{\frac{JB}{K} s^2 + Js + B} \tag{6}$$

where the lead network has been eliminated. The transfer function relating wrist position to load disturbance may then be written as

$$\frac{\theta(s)}{T(s)} = \frac{G(s)}{1+G(s)} \quad \frac{e^{st_d}}{kT_{iso}} \quad (\frac{B}{K} s + 1) \tag{7}$$

The last factor may be neglected since its break frequency, $\frac{K}{B}$, occurs at frequencies of 200 radians/sec or greater and will have negligible effects on the system. The terms e^{st_d}/kT_{iso} have no effect on system dynamics. Therefore the dynamical behavior of the system is determined essentially by the relation

$$W(s) = \frac{G(s)}{1+G(s)} \tag{8}$$

W(s) may be approximated from Bode plots of a $G(j\omega)$ (e.g., Fig. 7.5) by the following procedure.

1. Multiply $|G(j\omega)|$ by a constant such that $|G(j\omega)| = 1$ when $< G(j\omega) = -150°$. This will yield a damping ratio of approximately 0.2 (observed in the experimental responses of Fig. 7.9) for the second order fit to the closed loop system response.

2. If $|G(j\omega)| >> 1$, then $W(j\omega) \simeq 1$; if $|G(j\omega)| << 1$, then $W(j\omega) \simeq G(j\omega)$. The asymptotic approximation for an arbitrary $|W(j\omega)|$ is shown in Fig. 7.5.

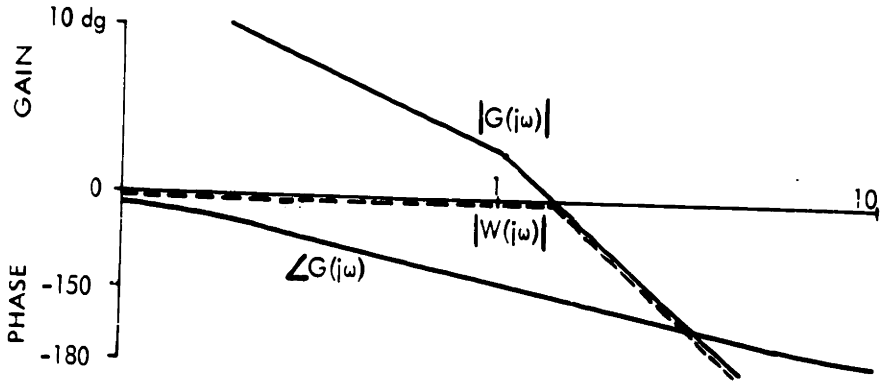

Fig. 7-5 ASYMPTOTIC APPROXIMATION OF CLOSED LOOP FREQUENCY RESPONSE FROM OPEN LOOP BODE PLOTS

This approximation is a conceptual tool which allows one to visualize the closed loop response of a unity feedback system from an inspection of its open loop Bode plot.

The Bode plots of Fig. 7.6 (solid line) show the approximate gain and calculated phase characteristics of $G(j\omega)$ for relaxed and tense conditions with two values of load inertia. An increase in B moves the lower break frequency of the muscle transfer function to greater values of ω. The 150° phase-lag point is also moved to a higher frequency. Using the conceptual tool discussed above we may visualize that the frequency response of the closed loop system has been improved by increasing forearm tone (increasing B). The above postulated improvement of frequency response is evident from the experimental records in Fig. 7.9. The impulse responses in the tense state are definitely faster than those in the relaxed state.

Increasing J, the inertial load on the system, moves the muscle poles towards lower frequencies. Similar reasoning suggests that the frequency response will be damaged by this additional inertia. That this is the case is clearly shown again by the records in Fig. 7.9. The responses of the loaded system are much slower.

Movement of muscle poles as K is varied has not been investigated quantitatively since it cannot be directly altered by either the subject or the experimenter. Inspection of Eq. 5 does reveal, however, the importance of a stiff series elasticity to a fast muscular coordination system. Lower values of K would both move the poles towards the origin, thus decreasing the frequency response, and, in situations where the poles are complex, decrease damping.

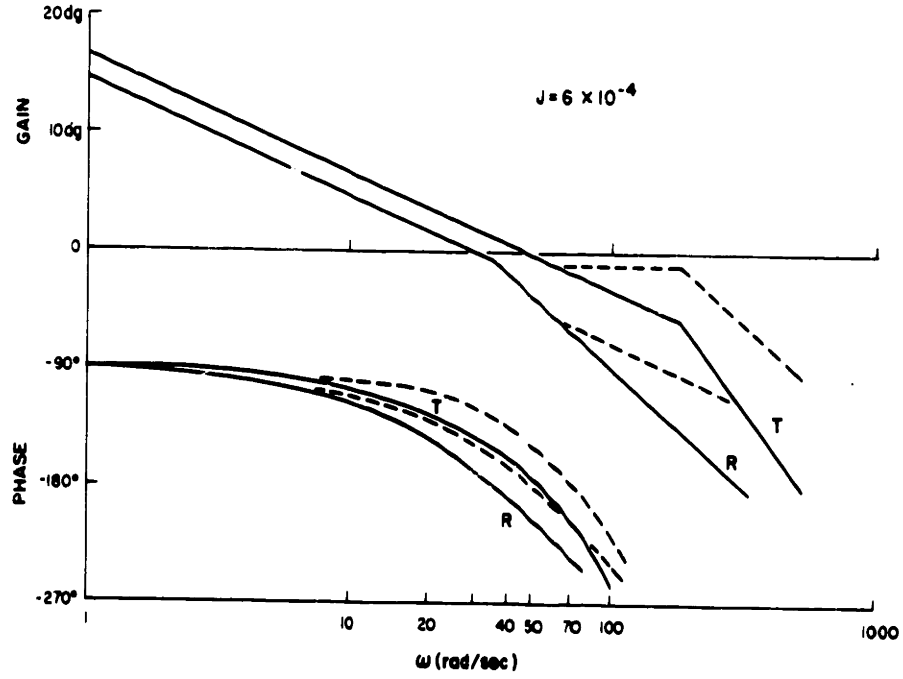

(a)

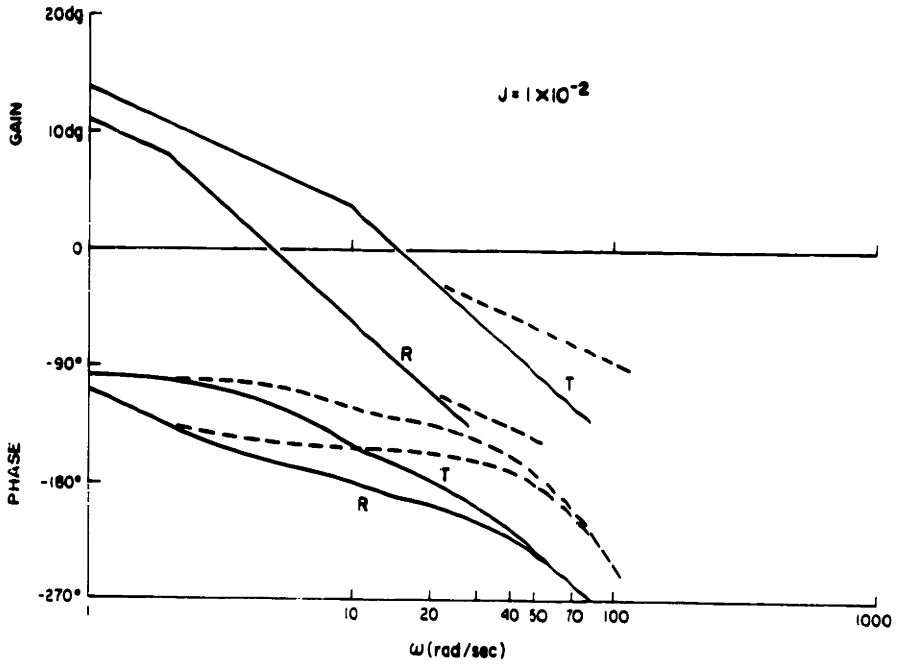

(b)

Fig. 7-6 APPROXIMATE GAIN AND CALCULATED PHASE vs. FREQUENCY PLOTS FOR THE OPEN LOOP UNCOMPENSATED LRM. T = tense forearm; R = relaxed forearm. Loop gain has been arbitrarily set to unity at the point where phase is -165°. Dotted lines show modification due to spindle lead filter.

The above results suggest that the CNS is capable of adjusting the loop gain factor, k, so as to insure an approximate damping ratio of 0.2 regardless of forearm tone and inertial loading. The feasibility of this postulate may be investigated by evaluating the steady state loop gain.

$$\lim_{s \to 0} G(s) = \lim_{s \to 0} \frac{k T_{iso}}{B s}$$

For very low frequencies G(s) acts like an integrator with a gain factor,

$$G_l = \frac{k T_{iso}}{B} \tag{9}$$

where T_{iso} is constant, k is the neural gain factor, and B is the viscosity of muscle. Increases in B, tend to reduce loop gain; therefore, variations in k will also have to counteract the variations in loop gain due to changes in B. It should be recalled that the development of the LRM in Section A indicated that an increase in gamma bias (initiator of the tense state) resulted in an increase in the loop gain factor. The effects of these two considerations tend to cancel each other; however, since adjustment of loop gain is quite critical, intervention by the CNS may be necessary for sharp regulation of k.

These approximate system characteristics suggest that the spindle lead filter is probably playing the conventional role of lead compensation frequently exemplified in linear control theory. Its introduction of phase lead near the uncompensated 180^{o} phase crossover point would move this crossover out further and allow an increased frequency response of the closed loop system. The analog simulations will illustrate this compensatory effect on transient responses.

C. ANALOG SIMULATION OF IMPULSE DISTURBANCES

The LRM shown in Fig. 7.3 was simulated on the REAC analog computer, Electronic Systems Laboratory, M.I.T. Since in a linear system the order of operations may be reversed, the integration which changes ω to θ may be carried out before inputs are fed into the two transmissions due to muscle and load dynamics. Therefore an impulse disturbance of T_L now becomes a step input to the muscle and load dynamics; a step is a much easier input to provide for the computer.

The time delay was represented by the second order Pade approximation,

$$\frac{y(s)}{x(s)} = \frac{\frac{1}{12} t_d^2 s^2 - \frac{1}{2} t_d s + 1}{\frac{1}{12} t_d^2 s^2 + \frac{1}{2} t_d s + 1} \simeq e^{-t_d s} \qquad (6)$$

The approximation is valid up to about 180^o of phase lag which is adequate for these simulations, and, since it is a rational parameter model, simulation presents no problems.

It was desirable to begin by fitting responses of the unloaded forearm since it is the more natural state for the subject. Whether or not the responses of the loaded arm could be fitted without again altering the spindle parameters would then be a good question to ask because alteration of the spindle parameters would require an adaptive intervention by the central nervous system, another level of complexity which teleogically seems objectionable. That some adaptive process must be present will be shown.

Reference to the phase characteristics of the unloaded LRM without spindle (Fig. 7.6 (a) and (b)) indicates that phase lead compensation would be helpful in the frequency range 30 - 100 radians/sec.; i.e. $\frac{1}{\eta T}$, the

lower break of the lead filter, should be placed at about 30 rad/sec. The value of η which was found in both of the analyzed responses (Chapter III) was 5, and,if adhered to, leads to $T = \frac{1}{150}$ sec^{-1}.

It is not possible to achieve both the speed of response and degree of damping present in the response of the tense PCS (Fig. 7.9(a)) by altering solely the gain of the uncompensated system (Fig. 7.7(a)). Moreover insertion of lead compensation at the break points suggested above results in responses which possess either a slowly decaying exponential component or insufficient damping depending on loop gain (Fig. 7.7(c) and (d)). A lead compensator for which

$$\eta T = \frac{1}{60} \quad ; \quad T = \frac{1}{300}$$

will replicate the PCS impulse response quite well (Fig. 7.7(b)).

Root locus plots of closed loop pole movement for increasing loop gain will facilitate understanding the above results. The root locus for the uncompensated system demonstrates that it is not possible to obtain rapid and highly damped responses without compensation (Fig. 7.8(a)). The rather pronounced change in root locus accompanying only 20 m sec. time delay in the proprioceptive loop is also illustrated. The strange system behavior when the lead filter is placed too low in frequency is due to a dominant pole on the real axis (see arrow in Fig. 7.8(b)). When the compensator is moved further out in frequency, although the real axis pole is still dominant, its rapid time constant of decay is no longer objectionable (Fig. 7.8(c)). The spindle lead filter does indeed improve system response.

Moderate and relaxed responses of the unloaded forearm were matched by varying loop gain at various B values less than its value

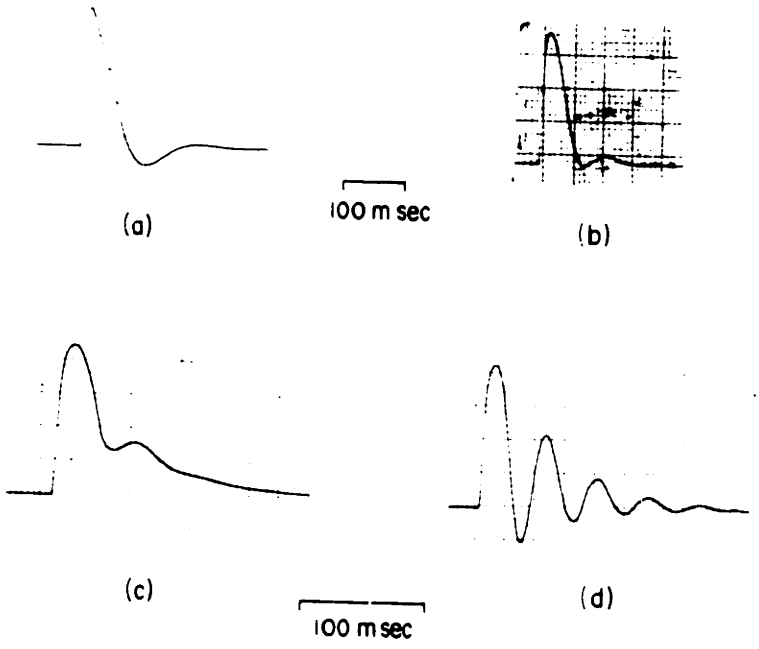

Fig. 7-7 IMPULSE RESPONSES OF THE LRM SIMULATING THE TENSE FOREARM (B = 0.1), UNLOADED (J = 6×10^{-4}) PCS. The uncompensated response (a) is greatly improved (b) when the spindle lead filter is added ($T = \frac{1}{300}$, $T = \frac{1}{60}$). The response becomes worse, (c) and (d), if the filter is placed too low in frequency ($T = \frac{1}{150}$, $T = \frac{1}{30}$).

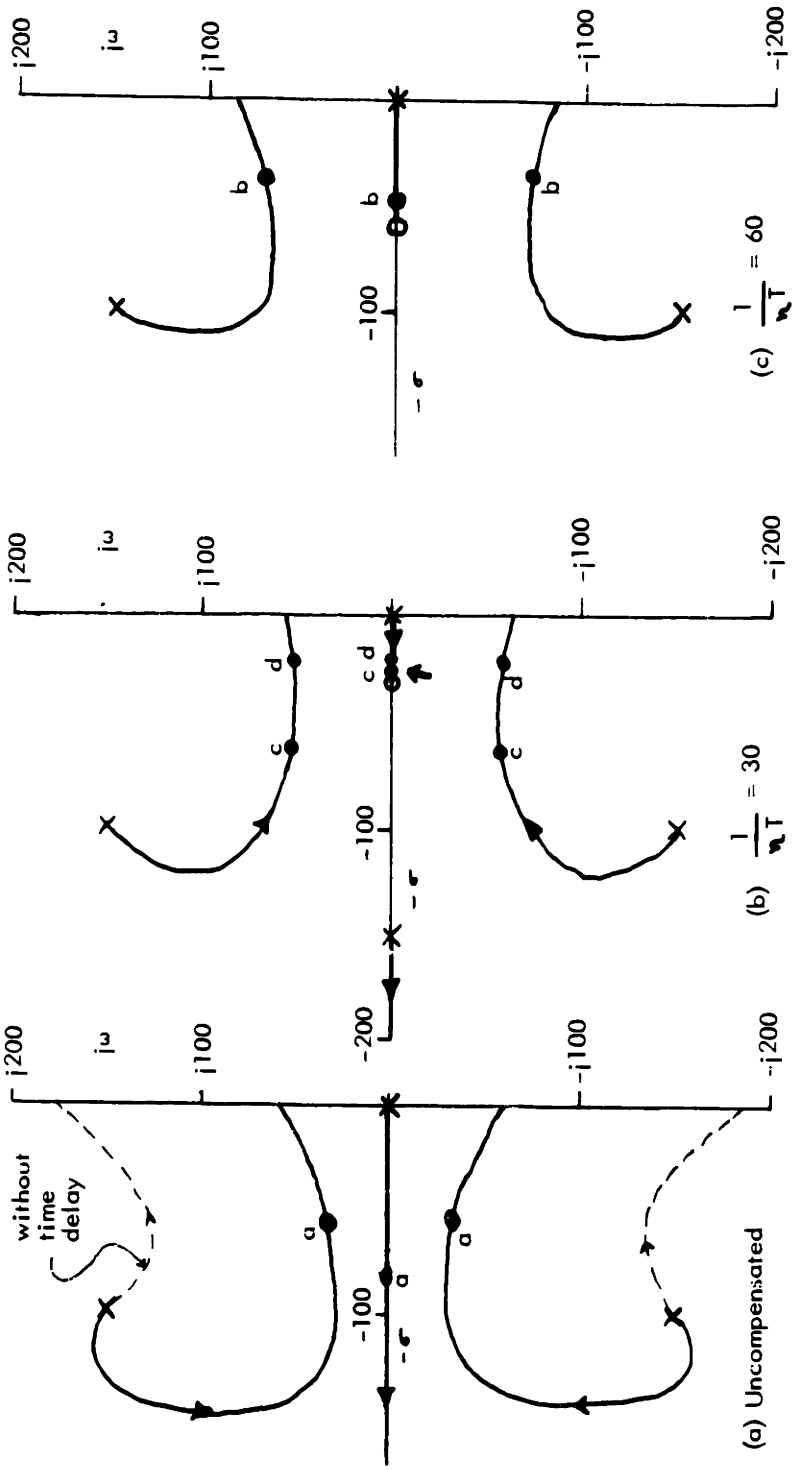

Fig. 7-8 APPROPRIATE ROOT LOCUS DIAGRAMS OF THE LRM (TENSE, UNLOADED FOREARM). Arrow is in the direction of increasing loop gain. a, b, c, and d are the operating points for the responses in Fig. 7-7.

for the tense arm (0.1 N-m-sec^{2}-rad^{-1}). The simulated responses were deemed a good match if the time between zero crossings and decay rate of the simulated responses corresponded reasonably well with those of the experimental responses (Fig. 7.9 (c) and (d)). Since the magnitude of the impulses delivered to the PCS had not been determined (see Appendix B), no attention was paid to the magnitudes of response during the matching process (a rough comparison is given in Appendix B).

The root locus of the model in the relaxed state (B = 0.02) indicates that the pole movement is radically altered when muscle poles begin on the real axis (Fig. 7 - 10). The real axis pole which caused a simple exponentially decaying behavior in the tense forearm is no longer dominant. Damped oscillations similar to those of a second order system result. This behavior will be prevalent in the remaining responses.

Given the fixed elements and their parameters as constraints and the spindle time constants and gain as variable parameters, the impulse response of the LRM which matched the experimental response under analogous conditions represented the optimum model response as judged by general speed and damping criteria. This evidence of optimization in a linear sense by a biological control system is interesting. Optimization is not as apparent in the situations of moderate and relaxed forearm tone. These responses could have been improved upon had the time constants in the spindle been increased.

An expectable slowing of response accompanies loading the system with inertia since this additional inertia moves one of the muscle poles to a lower break frequency (Fig. 7.4). The uncompensated Bode plots of the loaded system (Fig. 7.6(b)) reveal the reduced frequency

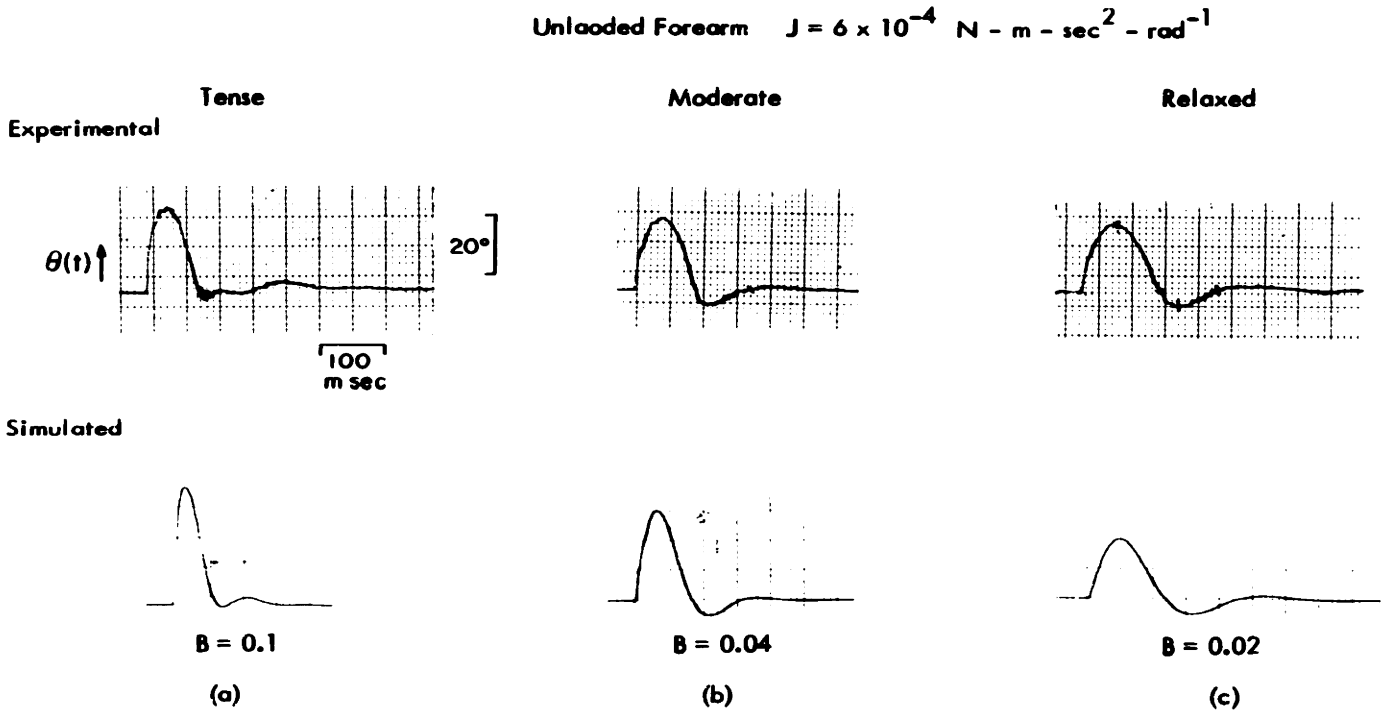

Fig. 7-9 COMPARISON BETWEEN EXPERIMENTAL AND SIMULATED IMPULSE RESPONSES. Zero crossings and decay rate were matched; amplitudes were not considered.

(continued on next page)

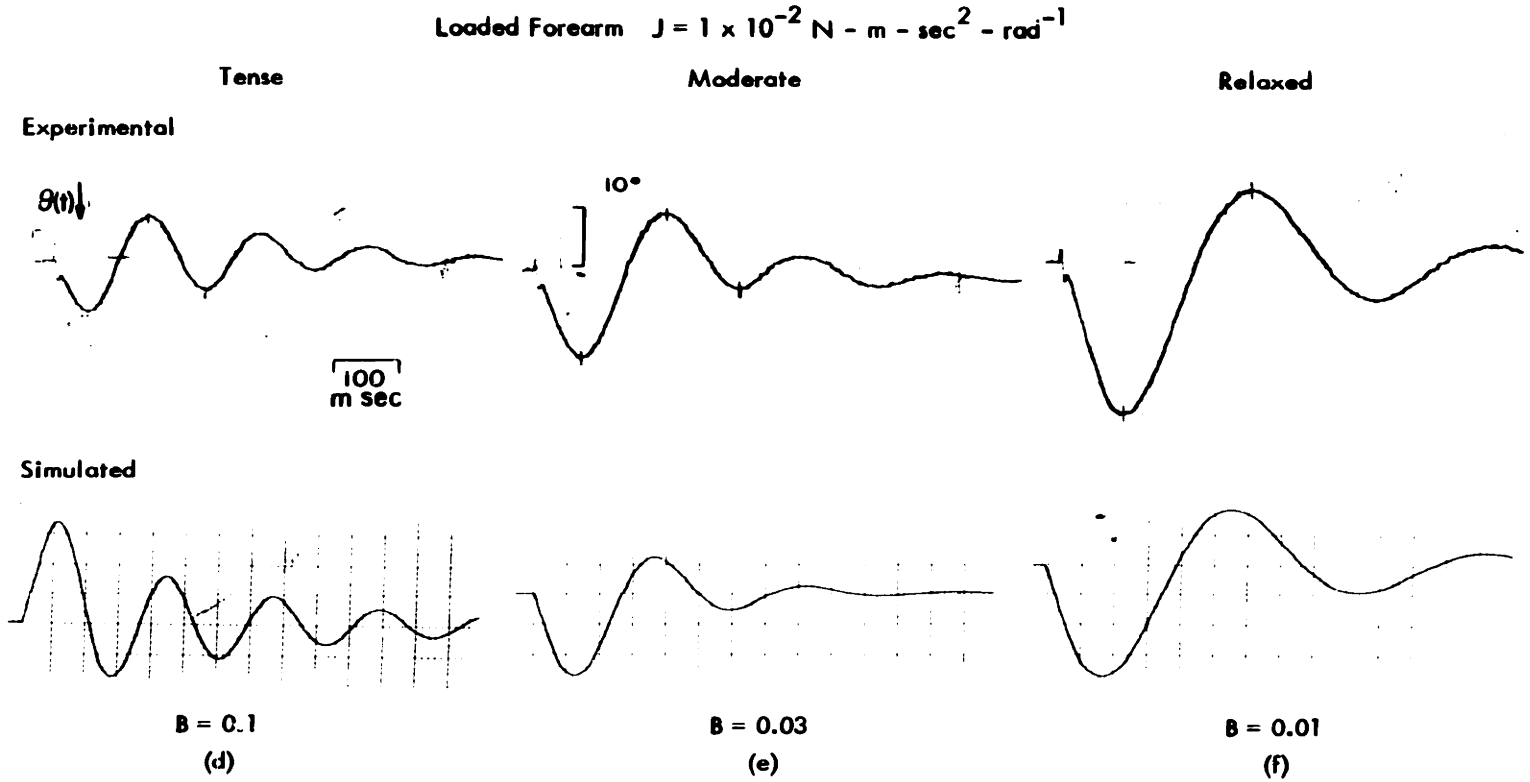

Fig. 7-9 COMPARISON BETWEEN EXPERIMENTAL AND SIMULATED IMPULSE RESPONSES. Zero crossings and decay rate were matched; amplitudes were not considered.

(continued from previous page)

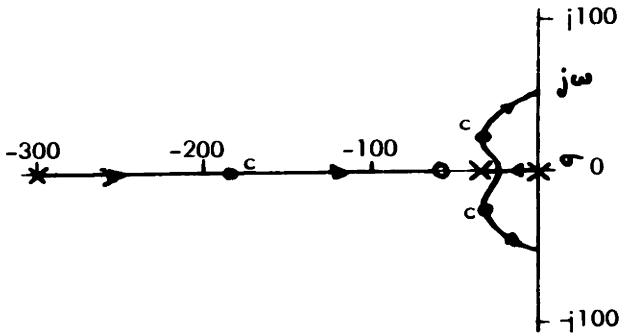

Fig. 7-10 APPROXIMATE ROOT LOCUS OF THE RELAXED (B = .02), UNLOADED ($J = 6 \times 10^{-4}$) LRM. Pole movement is much different than that illustrated in Fig. 7-8 because a muscle pole has moved to the right of the zero.

response and lower 180° crossover point of the system which results from this pole movement. Even with lead compensation, a slower oscillatory response can be predicted.

If the spindle time constants are maintained at the values which were predicted from the responses of the unloaded forearm, experimental responses cannot be matched by the slower simulated responses (Fig. 7 - 11(b)). However, when the lower break frequency of the lead filter is lowered to 20 radians/sec, the responses may be successfully matched. This may be accomplished by any of the combinations of η and T given below.

1. $\frac{1}{T} = 100$; $\frac{1}{\eta T} = 20$ (Fig. 7 - 11(c))
2. $\frac{1}{T} = 300$; $\frac{1}{\eta T} = 20$ (not illustrated)
3. $\frac{1}{T} = 200$; $\frac{1}{\eta T} = 20$ (Fig. 7 - 11 (d))

Their equivalent action suggests that the response of the system to frequencies above one hundred radians/sec. is negligibly small in all three cases.

Responses of the moderate and relaxed forearm were easily matched with the spindle constants given above by varying loop gain and progressively reducing B (Fig. 7 - 9(e) and (f)).

All three responses could have been improved upon (in the sense of speed and damping) if the zero of the spindle compensator had been moved to a lower frequency. That the response is not better suggests a limitation to the possible adaptation of spindle time constants. This was apparent when greater inertial loading was imposed on the arm. The origin of spindle adaptation deserves speculation which may be based on the physiological model of spindle presented in Chapter III.

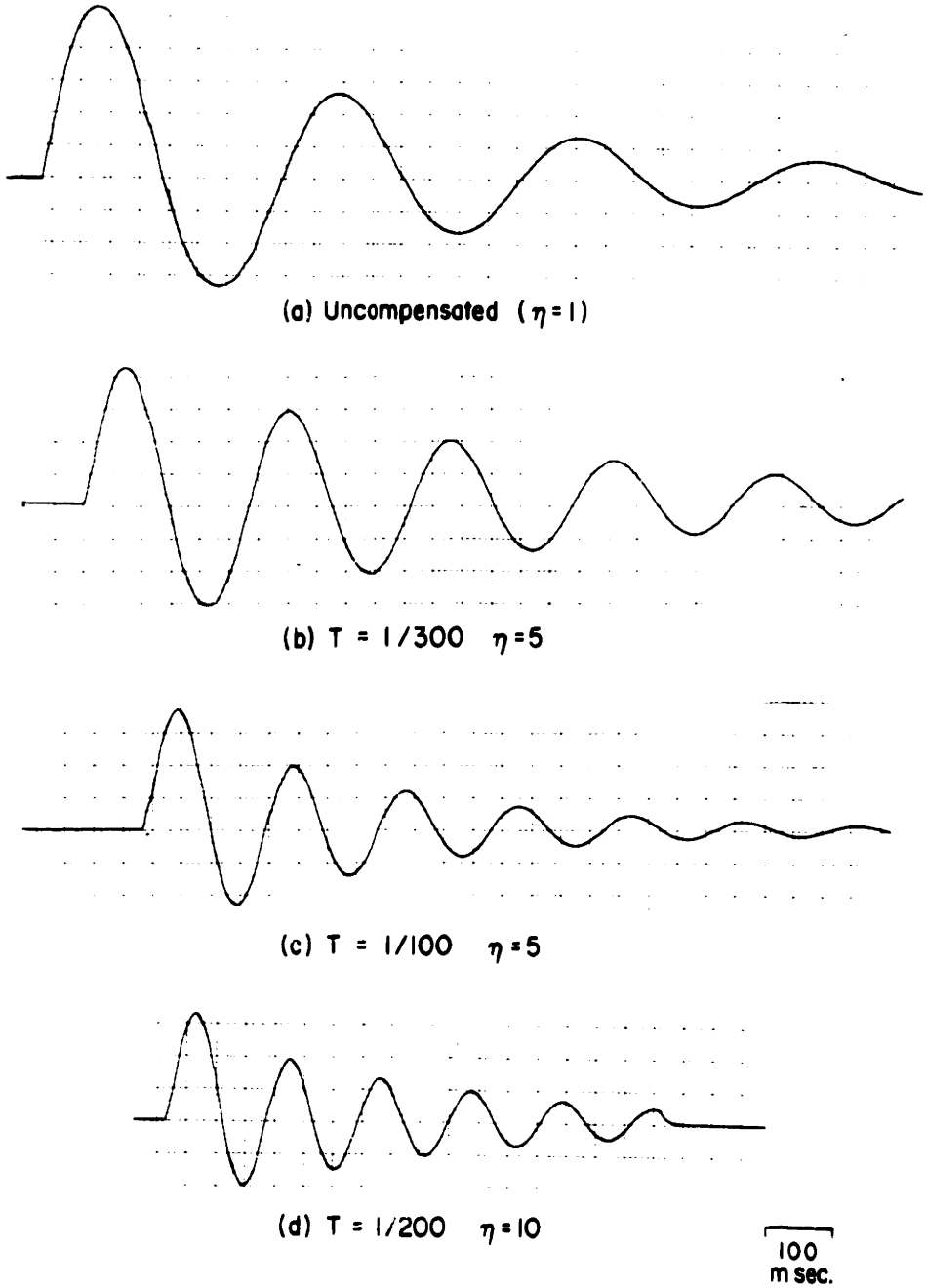

Fig. 7-11 RESPONSES OF THE TENSE (B = 0.1), LOADED (J = 10^{-2}) LRM ILLUSTRATING NEED FOR SPINDLE ADAPTATION.

The overshoot factor, η, is determined in the model by the ratio of the number of primary nerve endings to the number of secondary nerve endings. It is conceivable that the central nervous system has control over the numbers of each type of afferent fibers that make effective connections to the alpha motor neurons, thus exerting direct control over the factor η and permitting adaptation of spindle parameters. With this hypothesis one would predict that adaptation is not immediate but, rather, successive impulse responses to the PCS, after suddenly increasing its inertial loading, would exhibit successive improvements in response similar to the improvement of record 7 - 11(d) over that of 7 - 11(b). Time has not allowed checking this prediction.

An alternative hypothesis is that the spindle paramter, $T = \frac{B_f}{K_b}$ (Chapter III, Eq. 10), has been increased. It was found in Chapter II that the apparent viscosity of extrafusal muscle fibers increased with the fiber's activity. The same behavior is probably true of the intrafusal muscle fibers serving the spindle. Large increases in gamma activity might increase B_f sufficiently to decrease T by a factor of 3; moreover an increase in loop gain would accompany increased gamma activity. (Two factors contribute to increased gain: 1) biasing of unilateral muscles (see Fig. 7.1) and 2) operation around a point of higher gain on the nonlinear component of the spindle model (see Fig. 3.7)). The fact that the loop gain, given by Eq. 9, did increase threefold for all matched responses of the loaded arm adds plausibility to this hypothesis. However, increased gain due to gamma bias is difficult to explain in the case of the initially relaxed, loaded hand. Also, the adoption of this hypothesis leads to decreasing values of

T with muscle tone which is quite opposite to that which would be necessary if something close to optimum performance is expected. Decreasing T moves the spindle break frequencies to lower values, a movement which is opposite in direction to that of the muscle break frequency when tone is increased. For optimum performance the movements of spindle break frequencies should follow those of the muscle. (See Fig. 7 - 8 and associated discussion).

The most favorable hypothesis seems to be:

1. Relatively little intrafusal fiber activity is required to stretch K_b and bias the spindle. Therefore changes in gamma bias are accompanied by only relatively small changes in B_f, and hence, T.

2. Spindle adaptation results from direct intervention by the central nervous system which senses changes in inertial loading and correspondingly adjusts η.

Assuming, then, that $T = \frac{1}{300}$, the model of spindle demands that $K_b = 300\ B_f$, which is a rather large difference in magnitude of these mechanical elements. However, a single bundle of intrafusal fibers represents approximately 1% of the cross sectional area of a muscle. Since the viscosity of a muscle is made up of the sum of the viscosities of its fibers, the maximum value of the parameter B_f should be about 1% of muscle viscosity, of the order of magnitude 0.1 N-sec.-m^{-1} (from Wilkie[13]). Its value for submaximal stimulation might be 0.01 N-sec-m^{-1}. A rough estimate of the parallel elasticity in a muscle fiber is 1 N-m^{-1} (from Houk and Stark[37]). The nuclear bag would probably be somewhat stiffer, let us say 3 N-m^{-1}. These estimates yield

$$T = \frac{1}{300} \text{ seconds}$$

as a reasonable time constant. The values of these parameters, when other models of spindle are considered, are discussed by Houk and Stark[37].

It must be emphasized that the speculations discussed above are only weakly supported by physiological findings and are presented here only as interesting consequences forced on the spindle model by the results of these simulation studies.

Values of LRM loop gain which were necessary to match simulated responses to experimental responses are presented in Table 7.1 for the six conditions which were studied. The neural gain factor, k, also given in Table 7.1, was calculated from Eq. 9. The evident rise in neural

Table 7.1

Comparison of Gain Factors For Six Experimental Conditions

Inertial Load	$J = 6 \times 10^{-4}$			$J = 1 \times 10^{-2}$		
Forearm Tone	T	M	R	T	M	R
G_l	24	27	27	26	40	90
k	0.14	0.06	0.03	0.15	0.08	0.05

gain with increasing forearm tone has been suggested several times earlier in this thesis. In Chapter III two experimental findings of Granit[25] which indicated that neural loop gain increases with muscular tone were used in supporting a nonlinear, no-memory component of the spindle model. The EMG response of the PCS to impulse disturbances showed an increased neural gain for the tense arm (Chapter VI). In Section B of this chapter it was pointed out that gamma bias, the initiator of musclar tone, would increase the gain factor, k, as much as twofold because of the unilateral arrangement of the muscle system (also see Fig. 7.1). Any further increases in k would have to be accounted for by the neural gain constants and the spindle no-memory transformation. Control of k by the CNS is suspected.

D. SUMMARY

The mathematical model of the PCS presented in Chapter V has been reduced to a linear model with situation varying parameters (Linear Reduced Model) by making appropriate simplifications and assumptions. Spindle and gain parameters were predicted as those values which were found necessary to match simulated impulse responses with the experimental impulse responses discussed in Chapter VI. The hypothesis that the central nervous system exerts adaptive influence over the PCS

1. by regulating the neural loop gain and
2. by adjusting the spindle time constant

was advanced from the results of the simulation and analytic studies on the LRM.

CHAPTER VIII

A DISCUSSION OF MUSCULAR CONTROL

A. A SUMMARY OF PREVIOUS CHAPTERS

The subsystem of a mammalian muscular control system which is responsible for the stretch reflex has been defined, termed the "postural control system (PCS)", modeled, and simulated. The PCS was modeled by interconnecting individual models of each of the physiological components which participate in PCS activities. Muscle, the system's actuator, was modeled as a force generator acting in parallel with a nonlinear viscous element against a load inertia through a series elastic element (Chapter II). Spindle receptor, the system's length transducer, was modeled as a lead filter, based on postulated mechanical properties of its morphology and input-output data, followed by a nonlinear, no-memory transformation, based only on experimental input-output data (Chapter III). The alpha motor neuron, the system's only processor, was modeled as a summing node with variable attenuation (Chapter IV). Finally, nerve fibers, the system's active transmission lines, were modeled as delay lines (Chapter IV). Wherever neural signals appeared they were treated as continuous signals representing instantaneous frequency of firing averaged over the ensemble of all nerve fibers with a common function.

The integrated model of the PCS was then treated as an engineering control system (Chapter VII). The two unilateral proprioceptive loops which appeared were collapsed into a single bilateral loop with variable

gain. All nonlinearities were then linearized about an operating point, and a block diagram of this linear reduced model (LRM) was constructed. Simulation studies of the LRM were compared with responses of the PCS to impulsive disturbances under various conditions of muscular tone and inertial loading. Time constants and gains of the LRM varied, depending on the condition being simulated. Their values were determined from measurements on the system and engineering reasoning. The particular system which was employed in the experimental-simulated comparisons was that of wrist or forearm rotation in the human.

The fundamental conclusions and hypotheses which have resulted from the above summarized work are listed below.

1. It has been concluded that the postural control system is responsible for the rapid responses of a human subject to transient load disturbances.

2. The hypothesis has been put forth and supported that the postural control system may be adequately characterized by linear differential equations whose constants which vary with experimental conditions are, for the most part, physically meaningful.

3. The simulation studies (Chapter VII) lead one to hypothesize that the lead characteristics of mammalian spindle may exhibit adaptive behavior. As the inertial loading on the PCS increases, the lower break frequency of the spindle lead filter decreases. This adaptive behavior improves the PCS's responses to transient disturbances.

4. The hypothesis that an adaptive regulation of the neural gain constants is mediated by the CNS was also advanced.

B. IMPLICATIONS OF THE MODEL TOWARD OTHER STUDIES OF MUSCULAR CONTROL

One of the rewards of a system model based on models of its components is its gross versatility with regard to application. Because the autonomy of each of the PCS components has been maintained, this model may be applied to any of the experiments which have been performed on the system and may even suggest crucial experiments which have not, as yet, been conceived. One need only choose the pertinent input and output and open appropriate loops to investigate new experimental arrangements. In this section the model will be applied to several muscular control studies which have been carried out by other investigators.

1. Tracking Studies

The performance of the human subject in following a moving target has been the subject of many experimental studies. A visual indication of target position or target error is usually given as an input to the subject who processes this information in his brain after which commands are sent to a muscular system, thus effecting following movements of a pointer or some other indicator. The muscular system represents the final component in this complex control system. The nervous system's commands may reach it by either or both of two possible pathways, the direct path to the alpha motor neuron (the alpha pathway) or the slower route along the gamma efferent nerve (the gamma pathway). (See Fig. 5.1) The dynamic characteristics of both pathways will be illustrated.

a. The Alpha Pathway. Node "a" in the proprioceptive feedback loop of Fig. 7.3 will represent the summing node at the alpha motor neuron if the delay due to the alpha efferent nerve, t_A, is subtracted from the total

delay, t_d, and moved to the other side of node "a". (See the integrated model in Fig. 5.1.) Commands to the PCS via the alpha pathway are inserted at this point. Whether or not the proprioceptive loop is closed during voluntary control tasks has not been established; therefore, the PCS dynamics for both cases will be discussed.

Comparison will be made with the data of Stark, Iida, and Willis[1] since their studies were conducted on the same system that was examined in this thesis (wrist rotation). Their coordination testing apparatus had an inertia somewhat less than the loaded MCT, and muscular tone in their subjects during tracking was somewhat less than maximum (personal discussion). The non-negligible pole contributed by the muscle system must, therefore, have a break frequency no lower than 10 radians/sec. The spindle lead filter may be represented by

$$F(s) = \frac{\frac{1}{30}s+1}{\frac{1}{200}s+1}$$

where values of the choosen time constants lie within the range shown to be possible in Chapter VII. Their data shows that the voluntary control system has a negligible response to frequencies above 30 radians/sec.; therefore the following transfer functions will be evaluated only for frequencies below this cut-off.

The PCS will present the transfer function given in Eq. 1 as a cascaded element of the entire control system if the proprioceptive loop is open during its operation.

$$\frac{\theta(s)}{a(s)} = \frac{e^{-st_A}}{s} \quad \frac{T_{iso}}{\frac{1}{10}s+1} \qquad (1)$$

θ is the output wrist position; and α is the neural input to the alpha motor neuron.

The PCS will present the transfer function given in Eq. 2 if the proprioceptive loop is closed (valid for $s = j\omega < 30$ radians/sec).

$$\frac{\theta(s)}{\alpha(s)} = \frac{1}{k} e^{-st_A} \tag{2}$$

where k is the neural gain factor in the proprioceptive loop (shown to be about 0.1 in Chapter VII).

b. The Gamma Pathway. Commands via the gamma pathway enter the PCS at the spindle receptor (Fig. 5.1). Gamma commands will not reach the muscular system if the proprioceptive loop is not closed. Therefore only the closed loop system need be investigated. The PCS presents an almost identical transfer function to gamma inputs (Eq. 3) as it did to alpha inputs in the closed loop configuration

$$\frac{\theta(s)}{\gamma(s)} = C_z e^{-st_d} \tag{3}$$

C_2 is a constant proportional to the maximum isometric force of the bundle of intrafusal fibers in the spindle.

c. Discussion of Tracking. The role of the postural control system in compensatory tracking is illustrated in Fig. 8.1. The pure time delay in the forward path may be measured as the reaction time to a transient input of target position, θ_T. The wrist rotation system has a 200 m sec reaction time.[36] The central nervous system processes the error signal and sends a correction signal to the PCS. Let us investigate what processing

is necessary for each of the three choices of PCS inputs if stable performance is to prevail.

If the PCS operates open loop (Eq. 1), the CNS has the problem of controlling a pure integrator, a difficult control task which requires prediction to compensate for the large time delay if stable operation is to be realized. The wrist compensatory tracking system has been found to operate with unity gain out to frequencies of 6 radians/sec.[1] The time delay presents about 70° phase lag at this frequency, the integrator 90°, and the lag element about 15°. This makes a total of about 175° of phase lag at the break frequency and a large overshoot in the closed loop response would be seen at this frequency if no phase lead were inserted by the CNS. Excessive tremor due to noisy signals at the motor neuron or neuromuscular junction would also be expected if the PCS were operating open loop.

Since for closed loop operation (Eqs. 2 and 3) the PCS presents no phase lag, the control task becomes much easier; this alternative will be postulated. (Navas has recently proposed an intermittent operation of the proprioceptive loop[44].) We are left with two possible control routes, gamma and alpha.

Gamma commands are mediated by the extrapyramidal system, a morphologically old and functionally slow system. Alpha commands, on the other hand, are mediated by the pyramidal system characterized by direct pathways of rapid nerve fibers from the cerebral cortex, its control center, to alpha motor neurons. The 200 msec reaction time undoubtedly characterizes the latter pathway. The much longer delay in the gamma route makes it unlikely as the primary control pathway.

However, the alpha route possesses a definite disadvantage which may be realized from the PCS model in Fig. 5.1. If a step change in position is

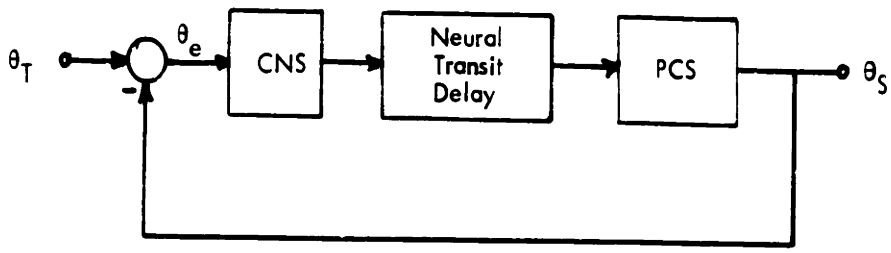

Fig. 8-1 BLOCK DIAGRAM OF COMPENSATORY TRACKING. θ_T represents target position, θ_s subject position, and θ_e error.

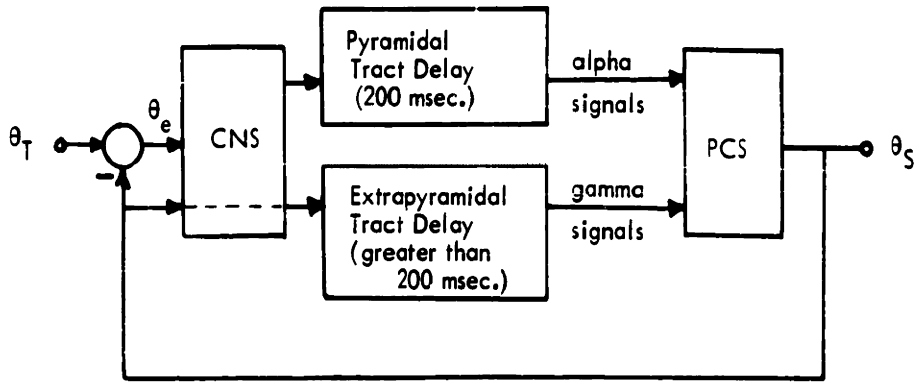

Fig. 8-2 POSTULATED ORGANIZATION OF COMPENSATORY TRACKING. Long term variations are mediated by the gamma system to conserve muscular energy. Transient variations are mediated by the much faster alpha system.

commanded via the alpha route, both muscles must remain active to counteract the restoring effects of the stretch reflex, even after the new position has been maintained for some time. This represents a considerable waste of muscular energy and, furthermore, is known not to occur.

Commands for step changes in position mediated via the gamma route would reset the zero levels of the spindles such that when the desired position is attained their outputs settle back to zero. The muscular system is thus able to relax while still being ready to counteract any disturbances tending to move it from its new position.

The advantages of both pathways could be realized if the control system were topologically arranged as suggested in Fig. 8.2. Here the gamma system is being continually, although slowly, reset to the subject's average wrist position while the alpha system performs rapid control tasks. The model should be helpful in designing experiments which would test this hypothesis.

2. Servo-analysis Studies of the Stretch Reflex

A number of investigators have driven the PCS with sinusoidal, transient, and random forcing functions. Johnson[9] inserted random torque disturbances into the wrist flexion-extension system and measured wrist position as his output. He found the transfer function $\theta(s)/T(s)$ to be constant out to about 300 radians/sec. The closed loop response of the tense, unloaded forearm was computed from the LRM for comparison. $\theta(s)/T(s)$ was found to be constant at 10 dg. out to about 60 radians/sec. where it began to drop -10 dg per decade. At 200 radians/sec, where the gain was down about 6 dg, it began to drop -30 dg per decade. The

approximate transfer function is given by Eq. 4.

$$\frac{\theta(s)}{T(s)} = \frac{\frac{1}{kT_{iso}}}{\left(\frac{1}{60}s+1\right)\left(\frac{1}{200}s+1\right)^2} \qquad (4)$$

The PCS looks like a stiff spring out to about 60 radians/sec, and kT_{iso}, the product of the neural gain factor and maximum isometric torque, is analogous to a torsional spring constant. Johnson's conclusions were similar.

Other investigators have constrained a postural control system to follow sinusoidal changes in position and have measured either resisting force or neural activity as their output.[7, 43] This type of forcing function opens the proprioceptive loop by brute force. Position, velocity, and acceleration of the system are constrained to follow the input which, therefore, must overcome inertia, apparent viscosity, and forces due to proprioceptive feedback. Generally the claim of these investigators is that they have been studying only the proprioceptive loop where, in reality, they were studying the summated effects of all three terms.

The LRM was used to determine the transmissions, $T(s)/\theta(s)$, due to each factor (Fig. 8.3). The asymptotic Bode plot for the tense, loaded PCS (Fig. 8.4) illustrates that the transmission due to inertia would be negligible up to about 300 radians/sec if these experiments were performed on the forearm system. Below 10 radians/sec the spring constant contributed by the stretch reflex (proprioceptive loop) would dominate in the production of torque. However, these trends are not generally applicable, but, rather, depend greatly on the preparation being tested. In Chapter VII it was reported that the lower break in the spindle lead filter could occur at a

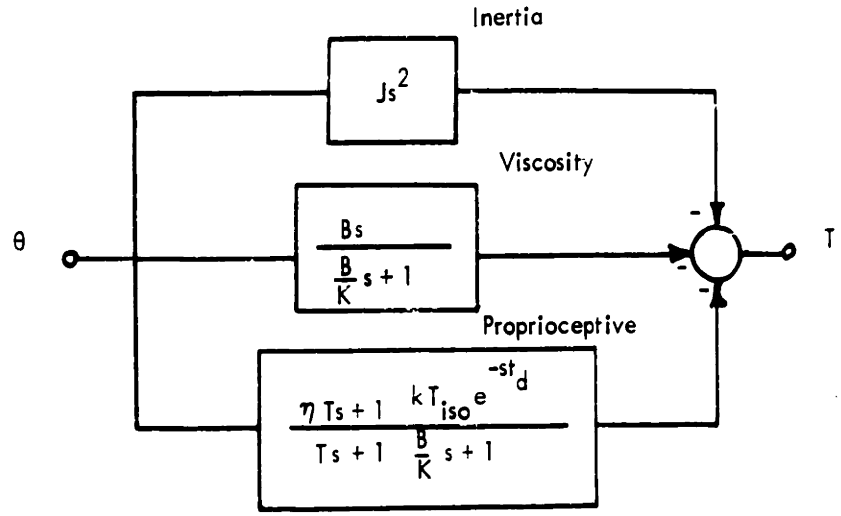

Fig. 8-3 LINEAR MODEL REPRESENTING OPEN LOOP ANALYSIS OF THE PCS.

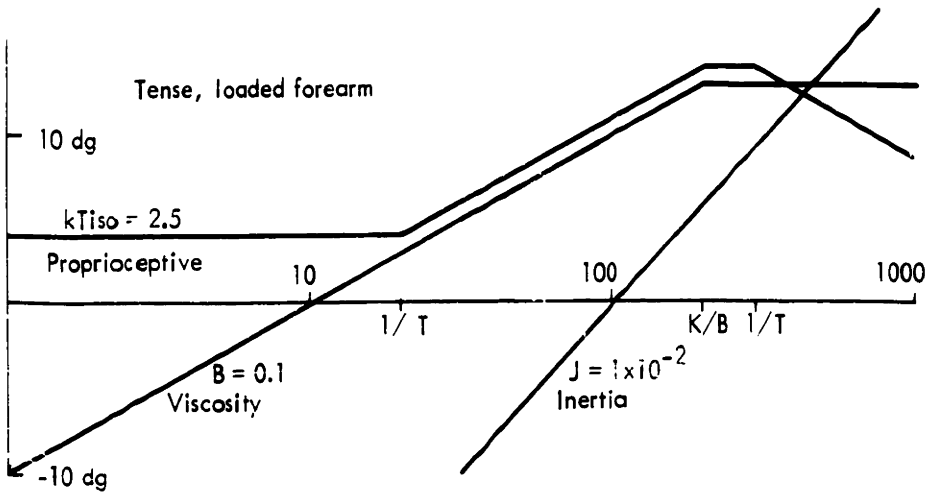

Fig. 8-4 ASYMPTOTIC BODE PLOTS OF EACH TRANSMISSION, $T(s)/\theta(s)$, IN FIG. 8-3.

much lower frequency than the $\frac{1}{\eta T}$ = 20 radians/sec frequency found in the forearm system. If preparations with these characteristics were being tested, the response of the stretch reflex would dominate provided the inertia of the stretching device was kept reasonably small. Such experiments turn cut to be just another way of studying spindle receptor assuming, of course, that any dynamics added by neurons in the spinal cord are negligible. Moreover, one must now be careful not to force the system too violently if complication due to participation of the tendon organ signals is to be avoided. Indeed, violent stretching is perhaps a means of studying tendon organ signals.

Partridge and Glaser's[7] stretch responses of gastrocnemius and soleus muscles in spastic cats indicate that only the stretch reflex was being studied in their sinusoidal analyses. However, their step responses have a sharply rising and falling component attributed by them to a general "mechanical origin", which quite probably was due to inertia. They did not publish typical lower break frequencies where the magnitude of the response began to increase with frequency although they did stress this effect.

Lippold, Redfearn, and Vuco,[43] working with various hind leg muscles in cats and dogs, avoided the problem of inertial and viscous contributions to their responses when they recorded neural activity before it reached muscle. This amounted to a measurement of the transfer function

$$\frac{a(s)}{\theta(s)} = k e^{-st_d} \frac{\eta T s + 1}{T s + 1}$$

Their results indicate that $\frac{1}{\eta T} \simeq 2$ radians/sec and $\frac{1}{T} \simeq 50$ radians/sec.

C. SUGGESTIONS FOR FURTHER RESEARCH

The work of this thesis suggests topics for further research in three separate disciplines; engineering, physiology, and clinical neurology.

Further engineering studies would determine the limitations of the linear representation for the PCS which was proposed and supported in Chapter VII. The effects of the nonlinearities inherent in the PCS could be investigated by simulating the nonlinear model which was presented in Chapter V. The hypothesis that the proprioceptive loop is closed during voluntary tracking tasks could be tested by artificially opening the visual feedback loop as Young[45] did in his eye movement studies.

In the field of physiology experimental studies of mammalian spindle receptors within the framework of its proposed model would be particularly interesting. Without a model, which represents a theory to be tested, descriptive efforts are sluggish and arduous. Presently there exists no quantitative representation of spindle in terms of its two independent inputs.

Many common neurological disorders are frequently attributed to peripheral aspects of muscular control systems. The model should be helpful in testing these notions, in locating the source of the disorder more exactly, and in suggesting corrective measures.

GLOSSARY

CNS	Central Nervous System
PCS	Postural Control System
LRM	Linear Reduced Model
a	Normalized neural signal
B	Apparent viscosity of muscle
K	Series elasticity of muscle
s	The Laplace operator
T_{iso}	Maximum isometric torque of equivalent muscle
ω	Angular velocity of forearm
θ	Angular position of forearm

APPENDIX A

BIOSIM

A self-interpretive program for dynamic simulation of biological systems.

INTRODUCTION

BIOSIM is a binary program deck for an IBM 709 or 7090 computer to be used within the framework of the MIT Computation Center Fortran Monitor System. The dynamic system to be simulated is specified by DATA cards in a form in which each card specifies a single block out of the block diagram representation of the system. Nonstandard blocks can be simulated by compiling special subroutines in either FORTRAN or FAP. Simulation output is also specified by Data cards. BIOSIM can be run either as a main program or as a subroutine controlled by a separate FORTRAN program.

No prior knowledge of computing techniques is required to use BIOSIM in its basic form. An elementary knowledge is needed if special functions are required. A more complete description of BIOSIM can be obtained from Kipiniak's report.[42]

NODE VARIABLES

Summers and Summing-integrators, referred to as integrators, are provided as the standard blocks in BIOSIM. The output of an integrator will be called a state variable and the output of a summer will be called an auxiliary variable. Collectively these are the node variables.

Y(I) are node variables. $T_j(I)$ is the transmission into node I from any other node or combination of nodes.

State variables compute:

$$Y(I) = \int_{-\infty}^{t} \{ \sum_j T_j(I) \}\, dt$$

Auxiliary variables compute:

$$Y(I) = \Sigma T_j(I)$$

TRANSMISSIONS:

A number of convenient operations can be performed on the output of one node as it is transmitted to the input of another node. These operations are called transmission blocks. The nine transmission blocks presently provided in BIOSIM are listed below.

$$T_k(i, t, y_j) = C_k y_j(t) \qquad T_k(i, t, y_j) = C_k |y_j(t)|$$

$$T_k(i, t, y_j) = C_k y_j(t - C'_k) \qquad T_k(i, t, y_j) = C_k \log_e(C'_k y_j(t))$$

$$T_k(i, t, y_{j_1}, y_{j_2}) = C_k y_{j_1}(t) y_{j_2}(t) \qquad T_k(i, t, y_j) = C_k \exp(C'_k y_j(t))$$

$$T_k(i, t, y_{j_1}, y_{j_2}) = C_k y_{j_1}(t)/y_{j_2}(t) \qquad T_k(i, t, y_j) = C_k \exp(C'_k + C''_k / y_j(t))$$

$$T_k(i, t, y_j) = \begin{cases} C_k \beta_k & \text{if } C'_k y_j(t) \geq \beta_k \\ C_k C'_k y_j(t) & \text{otherwise} \\ C_k \alpha_k & \text{if } C'_k y_j(t) \leq \alpha_k \end{cases}$$

SPECIAL BLOCKS

Nonstandard blocks, called special functions, are used 1) to perform operations which cannot be formed by some combination of summers, integrators, and the transmission blocks provided, and 2) to provide input signals for the simulation problem. A FORTRAN statement of the desired operation is compiled and added behind the BIOSIM binary deck. The simulation program refers to it as a subroutine.

EVALUATION

There are certain restrictions which limit the complexity of the simulated biological system.

Auxiliary variables compute:

$$Y(I) = \Sigma T_j(I)$$

TRANSMISSIONS:

A number of convenient operations can be performed on the output of one node as it is transmitted to the input of another node. These operations are called transmission blocks. The nine transmission blocks presently provided in BIOSIM are listed below.

$$T_k(i,t,y_j) = C_k y_j(t) \qquad T_k(i,t,y_j) = C_k |y_j(t)|$$

$$T_k(i,t,y_j) = C_k y_j(t-C'_k) \qquad T_k(i,t,y_j) = C_k \log_e(C'_k y_j(t))$$

$$T_k(i,t,y_{j_1},y_{j_2}) = C_k y_{j_1}(t) y_{j_2}(t) \qquad T_k(i,t,y_j) = C_k \exp(C'_k y_j(t))$$

$$T_k(i,t,y_{j_1},y_{j_2}) = C_k y_{j_1}(t)/y_{j_2}(t) \qquad T_k(i,t,y_j) = C_k \exp(C'_k + C''_k/y_j(t))$$

$$T_k(i,t,y_j) = \begin{cases} C_k \beta_k & \text{if } C'_k y_j(t) \geq \beta_k \\ C_k C'_k y_j(t) & \text{otherwise} \\ C_k \alpha_k & \text{if } C'_k y_j(t) \leq \alpha_k \end{cases}$$

SPECIAL BLOCKS

Nonstandard blocks, called special functions, are used 1) to perform operations which cannot be formed by some combination of summers, integrators, and the transmission blocks provided, and 2) to provide input signals for the simulation problem. A FORTRAN statement of the desired operation is compiled and added behind the BIOSIM binary deck. The simulation program refers to it as a subroutine.

EVALUATION

There are certain restrictions which limit the complexity of the simulated biological system.

BIOSIM presently has provision for no more than 32 node variables. No more than 16 special functions may be used. Also, no more than 64 transmission blocks other than CON are provided.

Digital simulation through BIOSIM of the biological system considered exhibits definite advantages over analog simulation techniques. Nonlinearities can be accurately represented by quite simple FORTRAN programs. In fact most nonlinearities encountered are already provided for by the standard transmission blocks. Desired nonlinearities are often difficult to obtain with analog computers. However, pertinent parameters cannot be adjusted as the experiment is being run. Frequently many runs are needed before realistic parameters can be approximated.

APPENDIX B

CALCULATION OF THE AMPLITUDE OF THE PENDULUM-DELIVERED IMPULSE

The amplitude of the pendulum-delivered impulse disturbance to the PCS is to be calculated from energy considerations. An elastic collision with the load and no loss of energy in the pendulum due to friction will be assumed.

A schematic diagram of the pendulum is shown in Fig. B.1. θ_i is the initial angle at which the pendulum is released; θ_f is the maximum angle to which the pendulum rebounds after impact with the load. The other parameters are tabulated below.

ρ = linear density of rod = 0.58 Kg/m

M = mass of hammer = 0.05 Kg

ℓ_1 = 0.43 m.

ℓ_2 = 0.42 m.

The energy lost by the pendulum is given by

$$E = m g \Delta h$$

where m is mass, g is the acceleration due to gravity, and Δh is the change in elevation of m. Δh may be calculated from the angles θ_i and θ_f.

$$\Delta h = \ell(\cos \theta_f - \cos \theta_i)$$

where ℓ is the radius of swing of m. The energy lost by M is therefore

$$E_2 = M g \Delta h_2 = 0.205\, k$$

where $k = \cos \theta_f - \cos \theta_i$. The energy lost by the rod may be calculated by integrating the energy lost by differential segments of mass along ℓ.

$$dE = g \Delta h\, d(m) = g \ell k \rho\, d(\ell)$$

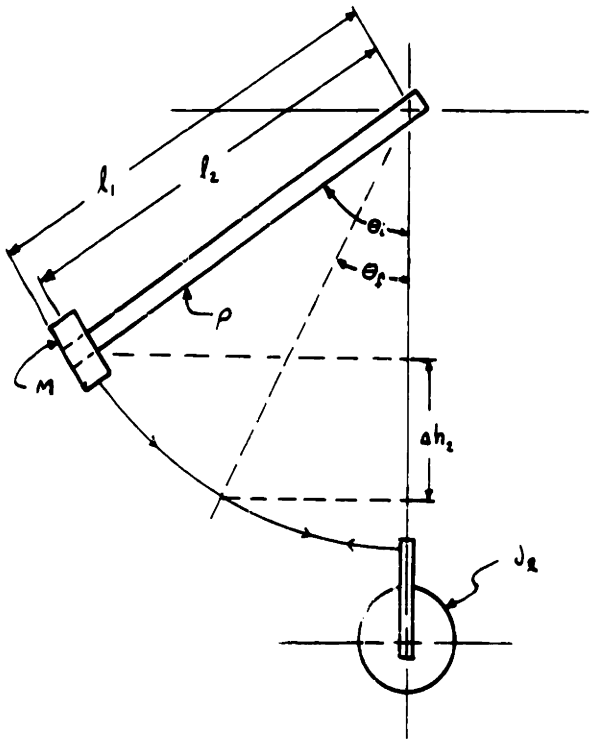

Fig. B-1 DIMENSIONS OF IMPULSE DELIVERING PENDULUM

$$E_1 = g k \rho \int_0^{\ell_1} \ell_1 \, d(\ell_i) = \frac{1}{2} g k \rho \ell_i^2$$

Substituting the values of ρ and ℓ_1 from above and $g = 9.8$ m-sec^{-2}, one obtains

$$E_1 = 0.525 \, k$$

The total energy lost by the pendulum is therefore

$$E_p = 0.73 \, k \tag{B.1}$$

Now, when the pendulum collides, an impulse of torque is inserted into the load. Initially, the unbalanced torque is absorbed by the inertia, thus causing an impulse of acceleration to the load given by

$$T = T_o U_o(t) = J_L \frac{d(\omega_L)}{dt} \tag{B.2}$$

This causes an initial step change in the angular velocity of the load, ω_L. Integration of Eq. B.2 illustrates this.

$$T_o U_{-1}(t) = J_L \omega_L(t) = J_L \omega_L(0) U_{-1}(t) \tag{B.3}$$

We now have an expression for the magnitude of the impulse in terms of the initial velocity.

$$T_o = J_L \omega_L(0) \tag{B.4}$$

The energy delivered to the load may also be calculated from the initial velocity.

$$E_L = \frac{1}{2} J_L \omega_L^2(0) \tag{B.5}$$

From our assumption of an elastic collision $E_L = E_p$, and B.5 may be solved for $\omega_L(0)$ and substituted into B.4.

$$T_o = \sqrt{2 E_p J_L}$$

In terms of the pendulum angles which may easily be recorded

$$T_o = \sqrt{1.46\, J_L (\cos \theta_f - \cos \theta_i)} \qquad (B.6)$$

The validity of the original assumptions was checked by loading the MCT, having a known J_L and negligible friction, with a known torsional spring K. A pendulum impulse was delivered, and energy lost by the pendulum was compared with the energy in the load before appreciable damping of its oscillatory response had occurred. The results showed that only 5% of the energy lost by the pendulum was being delivered to the load. The major cause of this tremendous loss of energy was thought to be due to coulomb friction at the pivot point of the pendulum. Unfortunately this result was not anticipated, and as a result was discovered too late to correct and repeat the experiments. Comparison between the absolute value of the response of the prototype and the PCS model, consequently, can only be carried out on a relative basis since it is by no means certain that the 95% loss of energy will remain constant under varying experimental situations.

Amplitudes were compared by defining

$$a = C \frac{A_1}{T_o}$$

where A_1 is the amplitude of the first peak, T_o is the estimated value of the delivered impulse, and C is a normalizing constant adjusted such that $a_e = 1$ for the tense, unloaded experimental response, and, in computing

From our assumption of an elastic collision $E_L = E_p$, and B.5 may be solved for $\omega_L(0)$ and substituted into B.4.

$$T_o = \sqrt{2E_pJ_L}$$

In terms of the pendulum angles which may easily be recorded

$$T_o = \sqrt{1.46\, J_L(\cos\theta_f - \cos\theta_i)} \qquad (B.6)$$

The validity of the original assumptions was checked by loading the MCT, having a known J_L and negligible friction, with a known torsional spring K. A pendulum impulse was delivered, and energy lost by the pendulum was compared with the energy in the load before appreciable damping of its oscillatory response had occurred. The results showed that only 5% of the energy lost by the pendulum was being delivered to the load. The major cause of this tremendous loss of energy was thought to be due to coulomb friction at the pivot point of the pendulum. Unfortunately this result was not anticipated, and as a result was discovered too late to correct and repeat the experiments. Comparison between the absolute value of the response of the prototype and the PCS model, consequently, can only be carried out on a relative basis since it is by no means certain that the 95% loss of energy will remain constant under varying experimental situations.

Amplitudes were compared by defining

$$a = C\,\frac{A_1}{T_o}$$

where A_1 is the amplitude of the first peak, T_o is the estimated value of the delivered impulse, and C is a normalizing constant adjusted such that $a_e = 1$ for the tense, unloaded experimental response, and, in computing

the same measure for the simulated responses, such that $a_s = 1$ for the tense, unloaded simulated response. The factor, a, is a measure of the system's ability to limit the maximum displacement caused by a standardized impulse disturbance, smaller values indicating superiority in this respect.

Table B.1

AMPLITUDE COMPARISON OF PCS AND LRM IMPULSE RESPONSES

Forearm Tone	Relaxed	Moderate	Tense
Inertia	$J_L = 6 \times 10^{-4}$		
Experimental	1.7	1.2	1
Simulated	4	3	1
Inertia	$J_L = 1 \times 10^{-2}$		
Experimental	2.0	1.3	.7
Simulated	.48	.35	.29

The poor comparison indicates that the experimental inpulse responses should be repeated with particular attention paid to input and output amplitudes. However, it is apparent that both increased inertial loading and increased forearm tone improve the system's ability to limit maximum displacement following disturbances.

REFERENCES

1. Stark, L., Iida, M. and Willis, P.A., "Dynamic Characteristics of the Motor Coordination System in Man," Biophysics Journ. 1: 234, 1961.

2. Elkind, J. and Green, D., "Measurement of Time-Varying and Nonlinear Dynamic Characteristics of Human Pilots," Technical Report, Bolt, Beranek, and Newman, 1961.

3. Sheridan, T.B., "Time-Variable Dynamics of Human Operator Systems," Dynamic Analysis and Control Laboratory, M.I.T.

4. Roig, R., "Nonlinear Adaptation in Manual Control Systems," Electronic Systems Laboratory, ESL-7420-R-4, M.I.T., 1960.

5. Merton, P.A., "Speculations on the Servocontrol of Movement," The Spinal Cord, A Ciba Foundation Symposium, p. 247, 1953.

6. Adolph, A., "An Application of Feedback Analysis and Stochastic Models to Neurophysiology," Bulletin of Math. Biophy. 21:59.

7. Partridge, L.D. and Glaser, G.H., "Adaptation in Regulation of Movement and Posture. A Study of Stretch Responses in Spastic Animals," J. Neurophysiol. 23:257, 1960.

8. Hammond, P.H., "An Experimental Study of Servo Action in Human Muscular Control," Third International Conference on Medical Electronics, London, 1960.

9. Johnson, A.R., "The Servo-Analysis of Postural Reflexes," Ph.D. Thesis, M.I.T., 1960.

10. Stark, L., "Biological Organization of the Control System for Movement," Quarterly Progress Report No. 61, Research Laboratory Electronics, p. 234, 1961.

11. Hill, A.V., "The Dynamic Constants of Human Muscle," Proc. of Royal Soc. B., 128:263, 1940.

12. Hill, A.V., "The Heat of Shortening and the Dynamic Constants of Muscle," Proc. of Royal Soc. B., 126:136, 1938.

13. Wilkie, D., "The Relation Between Force and Velocity in Human Muscle," J. Physiol., 110:249, 1950.

14. Fenn, W.O. and Marsh, B.S., "Muscular Force at Different Speeds of Shortening," J. Physiol. 85:277, 1935.

15. Katz, B., "The Relation Between Force and Speed in Muscular Contraction," J. Physiol., 96:45, 1939.

REFERENCES (continued)

16. Lippold, O.C.J., "The Relation Between Integrated Action Potentials in a Human Muscle and Its Isometric Tension." J. Physiol., 117:492, 1952.

17. Bigland, B. and Lippold, O.C.J., "The Relation Between Force Velocity, and Integrated Electrical Activity in Human Muscles," J. Physiol., 123:214, 1954.

18. Hammond, P.H., Merton, P.A. and Sutton, G.G., "Nervous Gradation of Muscular Contraction," British Medical Bulletin, 12:214, 1956.

19. Mason, S.J. and Zimmermann, H.J., Electronic Circuits, Signals, and Systems, John Wiley and Sons, 1960.

20. Wilkie, D.R., "Facts and Theories About Muscle," Prog. in Biophysics and Biophysical Chem., v. 4, p. 288, 1954.

21. Barker, D., "The Innervation of the Muscle Spindle," Microscopial Science, v. 89.

22. Barker, D. and Ip, M.C., "The Primary and Secondary Endings of the Mammalian Muscle Spindle," J. Physiol., 153:8.

23. Granit, R., "Some Problems of Muscle-Spindle Physiology," Hong Kong Symposium on Muscle Receptors, 1961.

24. Lippold, O.C.J., Nicholls, J.G. and Redfearn, J.W.T., "Electrical and Mechanical Factors in the Adaptation of a Mammalian Muscle Spindle," J. Physiol., 153:209, 1960.

25. Granit, R., "Neuromuscular Interaction in Postural Tone of the Cat's Isometric Soleus Muscle," J. Physiol., 143:387, 1958.

26. Houk, J.C., Sanchez, V. and Wells, P., "Frequency Response of a Spindle Receptor," Quarterly Progress Report No. 67, Research Laboratory of Electronics, Mass. Inst. of Technology., 1962.

27. Harvey, R.J. and Matthews, P.B.C., "The Response of De-efferented Muscle Spindles In the Cat's Soleus to Slow Extension of the Muscle," J. Physiol., 157:370.

28. Janson, J.K.S. and Matthews, P.B.C., "The Central Control of the Dynamic Response of Muscle Spindle Receptors," J. Physiol., 161: 357, 1962.

29. Brindley, G.S., Physiology of the Retina and the Visual Pathway Chapter III, London, Edward Arnold (publishers) LTD, 1960.

REFERENCES (continued)

30. Rushton, W.A.H., "Peripheral Coding in the Nervous System," Chapter 10, Sensory Communication, Edited by W.A. Rosenblith M.I.T. Press, 1962.

31. Arden, G.B. and Söderberg, U., "The Transfer of Optic Information Through the Lateral Geniculate Body of the Rabbit," Chapter 27, Sensory Communication, see Ref. 30 for further information.

32. Ruch, T.C. and Fulton, J.F., Medical Physiology and Biophysics, 18th Edition, W.B. Saunders Company, 1960.

33. Boyle, D.R., "A Neuron Model Which Performs Analog Functions," San Diego Symposium for Biomedical Engineering, La Jolla, California, 1962.

34. Hill, A.V., "The Series Elastic Component of Muscle," Proc. of the Royal Soc., B., 137:275, 1960.

35. del Castillo, J., "The Transmission of Excitation from Nerve to Muscle," Neuromuscular Disorders, v. 38, Res. Publ. Assoc. New Ment. Dis., 1960.

36. Houk, J., Okabe, Y., Rhodes, H., Stark, L. and Willis, P.A. "Transient Responses of Human Motor Coordination System," Quarterly Progress Report No. 64, R.L.E., p. 315, 1962.

37. Houk, J.C. and Stark, L., "An Analytical Model of a Muscle Spindle Receptor for Simulation of Motor Coordination" Quarterly Progress Report No. 66, R.L.E., M.I.T. p. 384, 1962.

38. Chestnut, H. and Mayer, R.W., Servomechanisms and Regulating System Design, Volume I, John Wiley and Sons, 1959.

39. Truxall, J.G., Control System Synthesis, McGraw-Hill, 1955.

40. Fulton, J.F. and Pi-Suñer, J.A., "A Note Concerning the Probable Function of Various Afferent End-Organs in Skeletal Muscle," Am. J. of Physiol., 83:554, 1928.

41. Katz, B., "Depolarization of Sensory Terminals and the Initiation of Impulses in Muscle Spindle," J. Physiol., 111:261, 1950.

42. Kipiniak, V.W., "BIOSIM" Neurology Section Report ESL, MIT.

43. Lippold, O.C.J., Redfearn, J.W.T. and Vuco, J., "The Effect of Sinusoidal Stretching Upon the Activity of Stretch Receptors in Voluntary Muscle and Their Reflex Response," J. Physiol., 144:373, 1958.

REFERENCES (continued)

44. Navas, F., "Sampling or Quantization In the Human Tracking System," B.S. Thesis, Electrical Engineering, M.I.T., January, 1963

45. Young, L.R., "A Sampled Data Model for Eye Movements," Sc.D. Thesis, Aeronautical Engineering Department, M.I.T., June, 1962.

GENERAL BIBLIOGRAPHY

Brown, A.C., "Analysis of Myotatic Reflex," Ph.D. Thesis, University of Washington, 1959.

Eldred, E., "Posture and Locomotion," Handbook of Neurophysiology, Vol. II, Chapter 41.

Hill, A.V., "The Effect of Series Compliance on the Tension Developed in a Muscle Twitch," Proc. of Royal Soc., 138:325, 1951.

Jansen, J.K.S., Matthews, P.B.C., "The Effects of Fusimotor Activity on the Static Responsiveness of Primary and Secondary Endings of Muscle Spindles in the Decerebrate Cat," Acta Physiol. Scand. (1962) 55:376.

Lippold, O.C.J., Redfearn, J.W.T. and Vuco, J., "The Effect of Sinusoidal Stretching Upon the Activity of Stretch Receptors in Voluntary Muscle and Their Reflex Responses," J. Physiol. 144:373; 1958.

Ritchie, J.M. and Wilkie, D.R., "The Dynamics of Muscular Contraction," J. of Physiol. 1958, Vol. 143, p. 104.

Stark, L., Houk, J., Willis, P.A. and Elkind, J., "The Dynamic Characteristics of a Muscle Model Used in Digital-Computer Simulation of an Agonist-antagonist Muscle System in Man," Quarterly Progress Report No. 64, R.L.E., p. 309, 1962.